DESIGNING, BUILDING, AND TESTING A SOLAR THERMOELECTRIC GENERATION, STEG, FOR ENERGY DELIVERY TO REMOTE RESIDENTIAL AREAS IN DEVELOPING REGIONS

By

Yacouba Moumouni

Bachelor of Engineering - Electrical and Computer Engineering
Federal University of Technology, Minna
2002

Masters of Science in Engineering - Mechanical Engineering
University of Nevada, Las Vegas
2012

A dissertation submitted in partial fulfillment
of the requirements for the

Doctor of Philosophy - Electrical Engineering

Department of Electrical and Computer engineering
Howard R. Hughes College of Engineering
The Graduate College

University of Nevada, Las Vegas
December 2015

UNLV | GRADUATE COLLEGE

Dissertation Approval

The Graduate College
The University of Nevada, Las Vegas

November 10, 2015

This dissertation prepared by

Yacouba Moumouni

entitled

Designing, Building, and Testing a Solar Thermoelectric Generation, Steg, for Energy Delivery to Remote Residential Areas in Developing Regions

is approved in partial fulfillment of the requirements for the degree of

Doctor of Philosophy in Engineering – Electrical Engineering
Department of Electrical and Computer Engineering

R. Jacob Baker, Ph.D.   Kathryn Hausbeck Korgan, Ph.D.
Examination Committee Chair   *Graduate College Interim Dean*

Yahia Baghzouz, Ph.D.
Examination Committee Member

Rama Venkat, Ph.D.
Examination Committee Member

R.F. Boehm, Ph.D.
Graduate College Faculty Representative

Abstract

New alternatives and inventive renewable energy techniques which encompass both generation and power management solutions are fundamental for meeting remote residential energy supply and demand today, especially if the grid is quasi-inexistent. Solar thermoelectric generators can be a cost-effective alternative to photovoltaics for a remote residential household power supply. A complete solar thermoelectric energy harvesting system is presented for energy delivery to remote residential areas in developing regions. To this end, the entire system was built, modeled, and then validated with LTspice simulator software via thermal-to-electrical analogy schemes. Valuable data in conjunction with two novel LTspice circuit**s** were obtained, showing the achievability of analyzing transient heat transfer with the Spice simulator. Hence, the proposed study begins with a comprehensive method of extracting thermal parameters that appear in thermoelectric modules. A step-by-step procedure was developed and followed to succinctly extract parameters, such as the Seebeck coefficient, electrical conductivity, thermal resistance, and thermal conductivity needed to model the system. Data extracted from datasheet, material properties, and geometries were successfully utilized to compute the thermal capacities and resistances necessary to perform the analogy. In addition, temperature variations of the intrinsic internal parameters were accounted for in this process for accuracy purposes. The steps that it takes to simulate any thermo-electrical system with the LTspice simulator are thoroughly explained in this work. As a consequence, an improved Spice model for a thermoelectric generator is proposed. Experimental results were compiled in the form of a lookup table and then fed into the Spice simulator using the piecewise linear (PWL) command in order to validate the model. Experimental results show that a temperature differential of 13.43°C was achievable whereas the simulation indicates a temperature gap of 9.86°C, with the higher error being

associated with the hot side. Also, since the analytical method of transient heat transfer analysis is cumbersome, an LTspice model of a real-world solar thermoelectric generation system was investigated. All the physical parameters were converted into their electrical equivalences through the thermal-to-electrical analogy. Real site direct normal insolation was fed into the Spice model via PWL in order to capture the true system's thermal behavior. Interestingly, two distinct analogies result from this study: 1) an RC analogy and 2) another analogy similar to an N-type doped semiconductor material's carrier density dependence with temperature. The RC analogy is derived in order to demonstrate how thermoelectric generation systems respond to square wave-like solar radiation. This analogy is utilized to measure temperature variations on the cold side of the Spice model; it shows 80% accuracy. The N-type analogy is intended to help analyze the actual performance of a LTC3105 converter. However a few of the problems to be solved remain at the practical level. Despite the unusual operation of the thermoelectric modules with the solar radiation, the measurements and simulation were in good agreement, thus validating the new thermal modeling strategy.

Acknowledgements

I would like to express my deepest gratitude to my mentor and academic advisor Dr. R. Jacob Baker, for his excellent guidance, patience, caring, and providing me with an adequate technical and financial atmosphere for doing research. I learned a lot from Dr. Baker about all aspects of engineering, and also about my personal attitude towards life in general, and education in particular. Indeed, working under his supervision has been a gigantic milestone in my life.

On behalf of all the researchers in the Center for Energy Research, I also want to thank Rick Hurt, who not only provided me with some guidance at the early stage of my research, but also let me utilize some of their research facilities for a period of a year and half. Additionally, I would like to thank all the crew in the mechanical shop who assisted me with measuring, cutting, welding, polishing, and mounting some of the physical parts required to build the STEG energy harvesting system.

I would like to thank Dr. Yahia Baghzouz, Dr. R. F. Boehm, and Dr. Rama Venkat for being part of my committee and teaching me what I know today.

In addition, I would also like to thank, from the bottom of my heart, all my colleagues for their continuous support and help in so many ways. Each one of them taught me something meaningful one way or another and gave me valuable ideas and comments.

Finally, words alone cannot express the thanks I owe to all my family members for their ceaseless encouragement and assistance. Thank you anyway!

Dedication

This dissertation is dedicated to my deceased parents for bringing me up. My dedication also goes to my wife, Ramatou Hassimi Djibo, for her continual support and assistance, especially during hardships.

Table of Contents

List of Tables

List of Figures

List of Abbreviations and Acronyms
ABVS = Arbitrary Behavioral Voltage Sources
Al = Aluminum
Al HEX = Aluminum Heat Exchanger
Al_2O_3 = Alumina
Bi_2Te_3 = Bismuth Telluride
Cd = Cadmium
CER = Center for Energy Research
DC-DC = Direct Current input - Direct Current output
DEG = Dispersed Energy Generation
DES = Dispersed Energy Storage
DNI = Direct Normal Insolation
DOD = Depth of Discharge
GUI = Graphical User Interface
HEX = Heat Exchanger
HEX = Heat Exchanger = Heat Sink
IEA = International Energy Agency
LAB = Lead Acid Battery
LDO = Low Dropout
LED = light Emitting Diode
LFP = Lithium Iron Phosphate
LHS = Left Hand Side
Li-Ion = Lithium-Ion
LTO = Lithium Titanate Oxide
NiMH = Nickel-Metal-Hydride
NiOOH = Nickel Hydroxide
NTP = Normal Temperature and Pressure
PC = Personal Computer
PUR = Polyurethane Insulation foam
PV = Photovoltaic
RE = Renewable Energy
Re-Alk = Reusable Alkaline
RH = Relative Humidity
RHS = Right Hand Side
RMS = Root Mean Square
SoC = State of Charge
STC = Standard Test Conditions
STEG = Solar Thermoelectric Generator
TEG = Thermoelectric Generator
TEM = Thermoelectric Module

TV = Television
VRLA = Valve Regulated Lead-Acid batteries

Chapter 1: Introduction to the Problem

Across the nations, around one and half billion people lack consistent access to electrical energy [1]. The vast majority of those people dwell in rural and/or remote areas where the electrical grid is either practically inexistent or sometimes technically difficult and expensive to transmit power through standard ways. The lack of access to this basic component of modern civilization is even more acute and commonplace in developing regions, such as countries in Africa and Asia. Furthermore, not having this vital resource has hindered any economic development up to date in remote and developing regions, and is considered to be one of the sources of continued poverty in those areas. Although electrical energy alone is not enough for initiating the conditions for economic growth, it is still certainly essential and plays a most important part. The number of people accessing electricity is one of the most clear and sound indications of a country's energy poverty status. The ambitious millennium goals that have been set forth to eradicate extreme poverty in the World can never be fully achieved without confronting and resolving this fact. Thus, the existent inequality gap that has persisted over centuries between the West and the East, on one hand, and the urban and rural areas, on the other hand, can certainly be explained by means of the aforementioned electrical energy scarcity issues. At the same time, the inequality between the Western and Eastern civilizations keeps widening even more because of the lack of serious and strong electrical energy policies in the East.

Conversely, electronic gadgets, such as smart electronic devices, mobile phones, and computers are becoming more popular in the cities as well as the remote villages [2]. As a direct consequence, the electricity to operate and recharge those devices remains a serious challenge.

Countless articles have been written on the subject of sustainable and affordable energy, but few have approached it, specifically, from the perspective of emerging economies.

A good understanding of a sovereign country's energy consumption is important for the country's long term development of its economy. A reliable energy supply is an important component for economic achievement and is needed for most aspects of social promotion, happiness, security, comfort, and a mobility that is unprecedented to human history [3]. Developing nations need to be self-sufficient in terms of both food and energy in order to enjoy the benefits of modern life and a high standard of living. Hence, energy plays a central and crucial role for the sustainability and the improvement of the current level of living in developing regions. Energy has become an important commodity to the communities in the developing countries; it directly affects the economies of the nations and has had a tremendous impact on the environment [4].

However, it is worthy to point out that the major portion of today's energy supply in the World is not regenerative in nature and is destined to be depleted in the near future. In this era, humanity finds itself confronting a colossal energy challenge. The latter possesses at least two critical dimensions. It has been evidenced that current patterns of energy usage are neither environmentally friendly nor sustainable in the long run. The overwhelming dependence on fossil fuels, in particular, threatens to modify the Earth's climate to a point that could have irreversible consequences on the integrity of both the eco-system and the human race. Additionally, with respect to that alarming depletion rate of the non-renewable energy sources, if government policy makers, engineers and scientists altogether put their gut intuition and human ingenuity forward, the appropriate solutions to this issue would be sufficient and capable of solving the global energy crisis for decades to come.

Unfortunately any energy policy that produces improvements in the short term is often one that destroys the environment in the long run. It is a universal truth that no exponential growth will last forever. In other words, the global net impacts have heavy consequences on the entire planet's inhabitants. Also, as stated above, the Earth is running out of fossil fuel-based resources that are neither self-regenerative nor replenished at a much faster rate on a human scale.

As every illness has a cure, there exist alternative solutions to bring electricity to remote residential regions. These solutions include micro-grids and distributed energy generations (DEG) at smaller scale. In fact, the former has the advantage of being the complete and permanent solution to the problem. In contrast, a micro-grid has not only a higher capital investment cost, but also requires a specialized workforce [5][6]. The latter supplies only a sufficient amount of electricity for basic household needs, such as charging electronic devices, light emitting diodes (LEDs) for lighting, and fans for household interior comfort. This technology is uncomplicated and inexpensive; it requires no expertise to setup and operate. Besides, it will have a tremendous impact on the lives and the economy of the people in those areas [7].

Indeed, a vast array of methods of producing electrical energy does exist today although some of the technologies are still rudimentary. They all operate for the benefit of the rural inhabitants and are completely independent of the grid infrastructure. Such alternative resources are: 1) solar photovoltaic (PV); 2) wind power; 3) geothermal; and 4) thermoelectric generators (TEG). As stated in [8], TEG can be utilized to supply electricity to power either main units or ancillary devices by directly converting any sort of thermal energy or renewable energies, such as solar energy (electromagnetic waves) and geothermal energy to electrical energy. Hence, solar

thermoelectric generation (STEG) technology is the main focus of the present research and will be given a comprehensive consideration.

Many researchers have been concentrating their efforts towards photovoltaic (PV) energy. Solar energy, however, is a broader concept than just energy delivered by PV system. For example, thermoelectric generators (TEG) can also use solar energy, in the form of heat, to generate electrical power. It is possible for TEGs to directly convert as much solar energy into electrical energy as their fellow PVs do. This conversion of energy from solar radiation to electricity is done via the Seebeck effect, named for the discovery made in 1821 by the German physicist, Thomas J. Seebeck. TEGs are versatile heat controlled solid-state pn junction devices that have no moving parts and emit zero greenhouse gases (GHG) into the environment during the course of their operation [9]. In addition, they can be used for cooling, heating or energy generation. In contrast to PV, TEGs' heat sources could be derived directly from the sun, a radioisotope reaction or waste heat from any sort of conventional plant [10].

When one side of the TEG is subjected to heat while the other side is at a lower temperature, caused by a highly conductive heat exchanger, an electromotive force (ΔV) is generated proportional to the Seebeck coefficient of the TEG semiconductor material as discussed in [11]:

$$V = \alpha \cdot (T_H - T_C) \tag{1}$$

Where, T_H and T_C represent the hot and cold side temperatures respectively

The literature abounds with works related to a Spice thermal-to-electrical modeling of TEG devices [12], [13], and [14]. As opposed to the study performed in [12], which deals only with one DC-DC converter (LTC3105), we propose to investigate the outcome of an additional DC converter (LTC3525). This work also suggests taking full advantage of the free and abundant

solar energy by conducting a real-world test, whereby the only heat source is composed of solar electromagnetic waves. As a direct consequence, the variability in the incoming solar energy due to weather events may affect the way TEG systems perform in the real-world environment. Therefore, during cloudy weather days, the TEG power output changes suddenly by responding instantaneously to the fluctuations of sunlight. The output power issues related to the variability are addressed in this study. It should also be mentioned that the DC-DC converter's primary function is to boost the low DC output voltage up, and then stabilize the power output ripples due to intermittencies. Otherwise, the sensible appliances would malfunction and would be detrimental to their respective life spans.

It can be hypothesized that the major drawbacks due to the relatively low overall efficiency of thermal electric generators could be overlooked under certain circumstances. Since the TEGs' advantages outweigh their disadvantages, this technology can compete with photovoltaic once the appropriate design is laid out, followed by the proper building and testing of the correct systems. We also hypothesize that for STEG to be able to compete with PV in order to benefit rural inhabitants in arid regions, additional external circuitries are needed. The external circuitries (DC-DC boost converter and a battery charge-controller system) could make the design ideal, fit, and comparable to PV systems as an alternative and/or a variety in terms of systems' stability, reliability, and efficiency. Finally, we hypothesize that the transient heat transfer analysis in TEG by means of the numerical electrical analogy method utilizing an LTspice simulator would yield better estimates and insights than the analytical procedures.

Hence, some of the main objectives this work seeks to accomplish are as follows:

- Understanding the challenges associated with the probable increase in the overall efficiency of the STEG in order to accomplish the intended task.

- Developing a unique sense of understanding the physics and theory behind the Seebeck, Peltier, and Thompson effects through the device physics and the electronics principles. As a matter of fact, it will be advantageous to also investigate the different heat transfer modes and the energy losses associated with each one of the effects for overall system efficiency improvement purposes. In order to achieve that, we have to not only properly design and implement the proper engineering practices, but also to account for the assumptions and simplifications made early in the energy-harvesting model during the testing and analysis phases.

- To efficiently construct the STEG system to be electrically and mechanically sound. The various integral components that will be either interacting and/or physically tied to one another are: solar reflectors, the five (5) TEG modules, two thermocouples, one solar flux sensor, a DC-DC boost converter, two heat sinks, one battery charge controller, a battery bank, wires, insulation materials, and a data-logger.

- Applicability of such a system mainly in rural areas would be of a tremendous benefit when it comes to alleviating people's daily energy needs. But it has to emerge from the designed structure itself by being a cost-effective system that would be unbeatable as compared to other counterparts.

- The final objective of this proposed study is to be able to run a computer simulation of the designed energy-harvesting system based on the aforementioned standards. In essence, the aim is to develop a Spice compatible thermal-to-electrical equivalent circuit of the entire STEG system. This analogy greatly simplifies the TEG's transient heat transfer analysis by means of the LTspice simulator in comparison to traditional

analytical methods. Thus, all the physical parameters (non-electrical processes) are described in terms of their electrical analogies, as can be seen in Sec. 3.2.

1.1 Motivation

Comparatively to what Antoine L. Lavoisier stated about chemical reactions in which "matter is neither created nor destroyed," energy in its various forms cannot be created or destroyed, but rather transformed. In producing electricity, no new energy is being created. In reality one form of energy is changed to another kind [15]. In light of this statement, the primary source of renewable energy, emitting energy in the form of electromagnetic radiation at a relatively constant rate in the entire universe, remains the sun. Although the global tendency of the Earth's current consumption of fossil fuel resources is unsustainable, the sun is undeniably a renewable and dependable source of energy for humanity. Furthermore, the theoretical solar energy potential striking the Earth's surface in 1 ½ hours (480EJ[68]) is greater than the worldwide energy demands in one year, with all sources combined (430EJ[67]) [16]. Consequently, the energy crisis the world is consistently facing lately resides at a transformation level rather than a reserve level. Hence, since the vast majority of the twenty-first century's technology is geared toward accommodating more energy-efficient appliances and/or harvesting the new and renewable sources of energy across the globe, time has come to shift from a state of skepticism to a more optimistic state about the future. Recently, various PV technologies—monocrystalline, polycrystalline, thin film, and triple junction—have been proven to harvest this free and abundant solar energy for the sake of global sustainability. Another silent and reliable pn junction semiconductor device utilized to harvest the above mentioned infinite source of energy is the thermoelectric generator. TEGs are more dependable when it comes to working in a harsh and arid weather conditions, and have the potential of harvesting all kinds of waste heat.

The design of a solar thermoelectric generation (STEG) system for reliable energy delivery to remote residential areas in emerging economies remains a technically important and challenging task. New alternatives and inventive renewable energy techniques, which encompass both generation and power management solutions, are fundamental for meeting remote residential energy supply and demand today, especially where the grid is quasi-inexistent.

Hence, according to the international energy agency (IEA), the availability of modern energy services is vital to human well-being and to a country's economic growth. Yet, globally over 1.3 billion people are without access to an electric power supply. It is very unfortunate that more than 95% of these people are either residents of sub-Saharan Africa or emerging Asia; 84% of those left-out of the modern world are in rural areas. Conversely, affordable and renewable energy sources do not always require a standard transmission system. This kind of system could be the first step out of poverty for individuals in rural areas who persistently need electricity.

It is very unfortunate that most TEG manufacturers do not provide real data for output power and output voltage versus differential temperature, which procure significant and valuable information to designers of solar thermoelectric energy harvesters. They often provide the standard testing condition (STC) parameters, which include the maximum operating voltage, V_{MAX} and current, I_{MAX} for a specific TEM.

Therefore, the primary motivations for this research are to: 1) investigate a real-world solar environment energy-harvesting system since most of the TEG technologies, thus far, were laboratory based experiments; 2) examine and propose a new transient heat transfer analysis method, utilizing LTspice software in conjunction with the thermal-to-electrical analogy theory; 3) explore new ways to supply cheap and dependable electricity to improve the living standards of the inhabitants of remote residential areas in developing regions; 4) as a final motivation, to

investigate through a cost comparative study, the feasibility of a real STEG system competing with photovoltaic systems.

1.2   Background

Solar energy is one of the most abundant and cleanest renewable sources in the universe, because it is free from any greenhouse gas (GHG) and other harmful environmental pollutants. It also requires no incursion upon the natural habitats of wild animals if harnessed with environmentally-friendly semiconductor devices, such as photovoltaics (PV) and thermoelectric generator (TEG). In fact, solar energy's immensity, year round availability, and benign effect on the climate, have made it the most appealing energy source on Earth. In spite of the versatility and abundance of solar energy, very little of it is directly utilized to power human activities. If solar energy is to become a concrete alternative to fossil fuels, efficient ways to convert photons into electricity and useful heat must be engineered [17]. However, problems with solar renewable energy include variability due to weather events and the nocturnal absence of the sun [18]. Since most of the time solar energy is stochastic in nature, there is a great need for energy storage. As a result, it is noteworthy to point out that energy storage can be utilized to mitigate renewable system transients[19].

Primarily, TEGs were exclusively assigned for outer space applications. Soon after that, they were applied, as stated throughout the literature, to many waste heat recoveries. Among these applications, TEGs have been proposed for woodstoves [20]; body heat powered watches [21]; car seat cooling/heating for passenger comfort by the major car manufacturers, including, but not limited to, Toyota, GM, Nissan, Ford, and Range Rover [22]; bio-sensors [23]; industrial waste heat recovery to power ancillary devices [24]; vehicular waste heat recovery to enhance fuel economy [25]; and harvesting micro-power for low power applications, such as wireless and

mobile sensors [26].. It should be pointed out that currently, TEG applications move beyond the above mentioned areas. Hence, solar thermoelectric generators (STEG) are irrefutably one of the most recent applications as reported by Crabtree et al. [17], whereby the energy from the sun is concentrated on the TEG in order to generate electrical power by means of the Seebeck theory.

Despite the advantages of thermal electric devices being solid, reliable heat energy converters, silent during the course of their operation, and lacking of any mechanical moving parts [27], their low energy conversion efficiency (5%) has limited their applications to specialized situations as stated above [28]. It is worthy of note that TEG is such a versatile technique capable of harnessing heat from naturally occurring sources of energy, such as solar, geothermal, ocean thermal, and waste heat from micro to macro devices [29]. However, their potential of power generation through the utilization of all sorts of heat (ranging from solar radiation to manmade heat sources, along with their maintenance free operation) causes TEGs to become technically attractive [30]. In contrast to PV systems, TEGs do not rely on solar radiation only. They are reliable and scalable quantities required in green technology, applicable in harsh and arid environments, such as Southwest United States (US) and Sahel in Africa, etc.

Previous studies mentioned rural electrification and domestic applications of TEG technology for lighting, heating, and ventilating [12], [31], [32], [33], and [34]. However, not many of these studies have looked into the thermal-to-electrical analogy which utilizes the LTspice simulator to analyze the transient heat transfer as is suggested in this study.

The proposed model is based on the internal parameter fluctuations, such as the Seebeck coefficient, parasitic inductance (*L*) and capacitance (*C*), and the internal resistance of the TEG. In addition, the proposed system is a real-world environment solar energy harvester mounted on a dual-axis tracker. It is important to specify that the values of the parasitic *C*, and *L* were

borrowed from a previous work reported in [35] because they cannot be determined with the equipment available to us.

This study defines and determines keys concepts for a reliable energy delivery to remote residential areas in developing nations. More than a century after the light bulb was invented, most of the developing countries are still in the dark after nightfall. Somewhere in Africa or Asia, people often cannot read after twilight, businesses are dependent on gas lamps, and clinics cannot refrigerate vaccines. In such an economically hostile environment, industries are rudimentary, hampering any potential commercial growth. In fact, around thirty countries in sub-Saharan Africa, as reported by the World Bank, are facing a severe electricity crisis evidenced by continuing electric power shortages and/or total blackouts. Despite the African continent being naturally well endowed with renewable resources, there is a potential need to not only transform these resources, but also to reach out with reliable energy supplies to the remote locations. The manner in which electrical power is unevenly distributed throughout the continent continuously creates exacerbating crisis as well as windfall profits for some countries. The remote residential areas are naturally factored out from this vicious economic game. In order to attain any short or long term development, they need to have both a renewable and dependable energy supply. Additionally, a summary of some of the key issues in Africa's energy sector are: 1) low access and insufficient capacity; 2) poor reliability with enterprises experiencing frequent power outages; and 3) high cost/kWh consumed with an average tariff of USD 0.13/kWh.

Thus, this work proposes to design, build, and test a STEG energy-harvesting system for energy delivery to remote residential areas in developing regions.

1.3   Outline of the Dissertation

This work proposes an innovative concept of a solar thermoelectric generation system (STEG). The proposed STEG is a real-world environment energy-harvesting system for electrical power delivery to remote residential areas in developing regions. In order to acquaint ourselves with the theory and the physics behind TEM technology, the research was first divided and conducted in two separate but interrelated steps. The preliminary study was conducted in a laboratory in order to develop a thorough understanding of both Seebeck and Peltier phenomena. The idea was to accustom ourselves with the technology before the in-depth real-environment STEG system's implementation. In addition to that, the second and most challenging complete solar energy-harvesting system was then designed, built, and tested, whereby the only input to the system, in the form of heat, was the solar electromagnetic radiation. Furthermore, the first step was to investigate the true performance of commercial solar TEGs under arid weather conditions comparable to the Southwest of the US or the Sahel in Africa. Then, due to the intermittent nature of solar energy in general and STEGs in particular, this study investigated the optimal power solutions by means of DC-DC converters for output stability and enhancement purposes. The TEG devices were mounted on a solar tracker. The reflectors on the tracker were positioned in such a way that the sun is concentrated four times on the devices. The second part of this research consists of computing the electrical parameters (resistance, capacitance, and inductance) of all the physical parts from both device geometries and properties and then accomplishing the novel electrical analogy of the whole STEG system utilizing the LTspice simulator. The novel transient heat transfer approach, through the thermal-to-electrical analogy schemes, intends to simplify the analysis. Hence, this dissertation is divided into five separate chapters: 1) chapter one gives a general introduction to the recurrent problem of energy in the

world and presents the main objectives this work seeks to accomplish; 2) chapter two reviews the current state-of-the-art in the field of TEGs; 3) chapter three emphasizes the proposed design methodology, electrical parameter extraction, the Spice modeling schemes, and some of the energy storage technology followed by a brief economic analysis; 4) chapter four details the experimental verification of the work and then gives the results; 5) and finally, the last chapter concludes this work by summarizing concisely the main findings, discussing them succinctly, and briefly suggesting the future course of research.

Chapter 2: Literature Review

Much of the solar resources on Earth are inversely related to electrical load centers. Thus far, significant motivations prevail for developing new stand-alone energy-harvesting technologies. These technologies, such as PV, STEG micro-grid, and the like, can not only autonomously convert the incoming solar radiation into DC power, but can also deliver reliable power to remote residential zones where the grid is quasi-absent. Hence, TEGs are gaining a great deal of research attention in this area since they have proved to perform well in harsh and remote locations. Also, they have the advantage of not possessing moving parts, thus less maintenance is required. Figure 1 illustrates the most common categories of papers surveyed during the course of this work. As can be seen, the articles treating the thermal-to-electrical analogy concept that utilize the family of spice simulator software, were given a higher priority, as they are the most frequently cited papers throughout this work. A thorough literature survey, divided into a general and specific review, is attempted with emphasis on the latter section. The Spice modeling of TEGs based on the thermal-to-electrical analogy using LTspice software is the core piece of this study. In a nutshell, a bottom-up fashion survey is methodically organized in the two subsequent sections in order to address, through a step-by-step scheme, all the research gaps that would be of interest to the current and future potential research works.
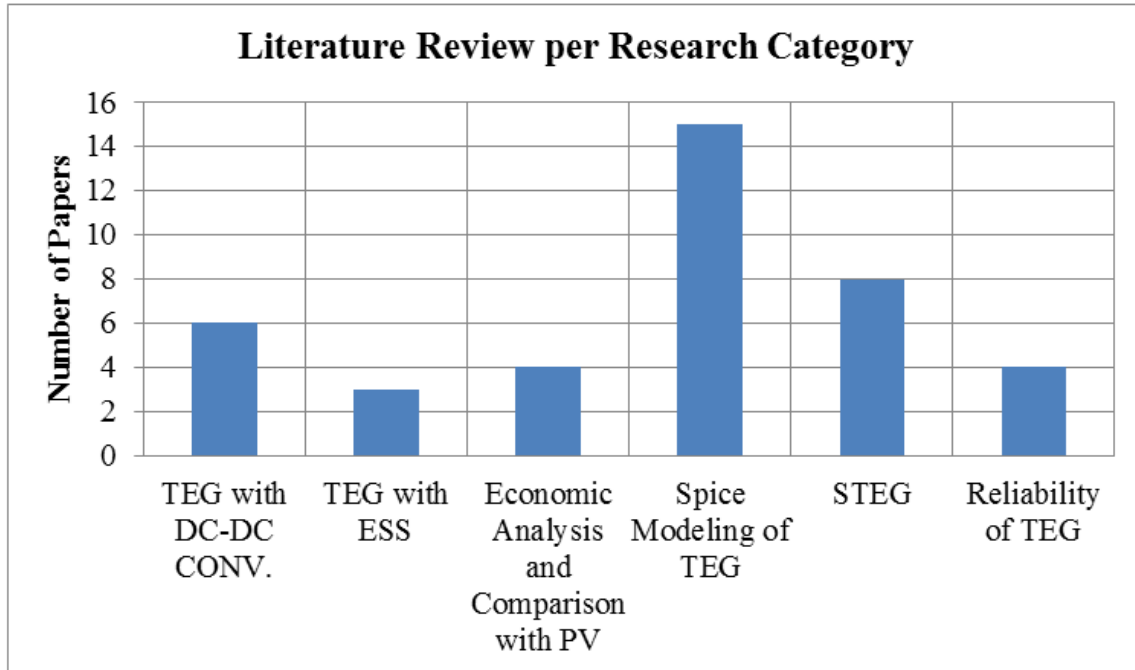
Figure 1 – The most frequent research areas surveyed

2.1 General Review

During the last century, the population on Earth escalated at a much faster rate than ever seen before. In a similar fashion, the human race has attained the highest possible level of technological development, leading mankind to taste a certain flavor of happiness, joy, and well-being. Hence, there are two important concepts worthy of note here: one is the major breakthroughs in all matters of Science and Engineering and the second is mankind's ability to apply these breakthroughs to their benefit. This is especially true with respect to the use and harnessing of all sorts of energy and waste heat to improve mankind's well-being.

Unfortunately, any energy policy that produces improvements in the short term is usually one that destroys the environment in the long term. It is a universal truth that no exponential growth will last forever. In other words, the global net impacts have heavy consequences on the

entire inhabitants of the planet. There is, in fact, a global tendency to run out of energy resources that are either non-regenerative or not replenished at a fast enough rate on a human scale. In essence, the major portion of our energy supply is not renewable in nature and is destined to be depleted in the near future.

On the other hand, with respect to this alarming depletion rate of the non-renewable energy sources, if the government policy makers, in combination with engineers, and scientists work together, the appropriate solutions to this issue would be sufficient and capable of solving the global energy crisis for decades to come.

The sun is inarguably the primary source of energy; it is at the center of all surface phenomena and living beings on Earth and beyond. This tremendous amount of energy, in conjunction with the global atmospheric greenhouse effect, provides the means for the prosperity of the immensely diverse forms of life found on Earth [36]. The greenhouse effect has made life possible on Earth by averaging the global temperature to 18°C. That averaged temperature has increased during the past century by about 0.7°C. It has been speculated that most of the increase is attributable to the manmade greenhouse effect due to the release in the air of not only the major GHG in general, but particularly to the millions of tons of carbon dioxide emitted when fossil fuels are burned to produce energy on a daily basis. For instance, the US alone emits 2.2 billion tons of CO_2 per annum to produce electricity, which corresponds to approximately 40% of the national total gas emissions [37]. Hence, the relative raise of the average temperature above the pre-industrial level has led to the relatively new concept of *global warming*. Consequently, methods need to be found in order to solve this global temperature increase through curbing global warming in order to better improve people's lives with clean air and clean water. Also, methods must be found for reducing a reliance on fossil fuels, while

increasing at the local, regional, and global levels an investment in clean and renewable energy. It is noteworthy that the latter is continuously and sustainably replenished at a human scale and that it comes from natural sources. Furthermore, green jobs and smarter energy solutions need to be found that will contribute to a global economy boost for the benefit of the whole of mankind [37].

This literature survey is intended to demonstrate the urgent need for finding new long term alternative renewable sources to replace the existing fossil fuel-based sources that may be depleted in the near future. Furthermore, scientists and those in the field of energy came to a valid conclusion in the early 18th century, at the dawn of the industrialization era, that fossil fuel was not a perpetual energy source [38]. Therefore, many new renewable technologies have been investigated to either firmly supplant fossil fuel-based sources or to provide an alternative to them.

The thermoelectric module (TEM) is considered to be one of the best generators of renewable energy because of its extreme reliability. Furthermore, the TEM has no moving parts. Thermoelectric generators can use solar energy, in the form of heat, for the generation of electrical power. It is possible for TEGs to directly convert as much solar energy into electrical energy as their fellow PVs do. This conversion of energy from the sun to electricity is done via the Seebeck effect, named for the discovery made in 1821 by the German physicist Thomas J. Seebeck. TEM's main drawback, when compared to other renewable resources, is lower efficiency. As reported in [29], a TEM is only about five to six percent efficient. Even with this low efficiency, the TEM can utilize the abundance of free thermal energy resources for conversion into electrical energy for the benefit of mankind [28]. Thermoelectric solid-state devices directly convert thermal heat into electrical energy or vice-versa. In other words, not

only can TEMs be used to convert the energy from the sun or any kind of wasted heat into electricity, but they also have the potential to transform electrical energy into heating/cooling [39]. How much of the energy is being converted from one form to the other is solely dependent upon the figure-of-merit which is often called the *goodness factor, (GF)* [40].

$$ZT = \alpha^2 \cdot \delta \cdot \frac{T}{K} \tag{2}$$

Where, α, δ, k, and T are the Seebeck coefficient, electrical conductivity, thermal conductivity, and absolute temperature in Kelvin, respectively.

A key factor to note in Eq. (2) is that the thermal conductivity needs to be lowered for the goodness factor *ZT* to be increased, and thus the efficiency of the TEM to be improved. A summary of the important ZT achieved that has so far been found in the literature is illustrated in Figure 2.
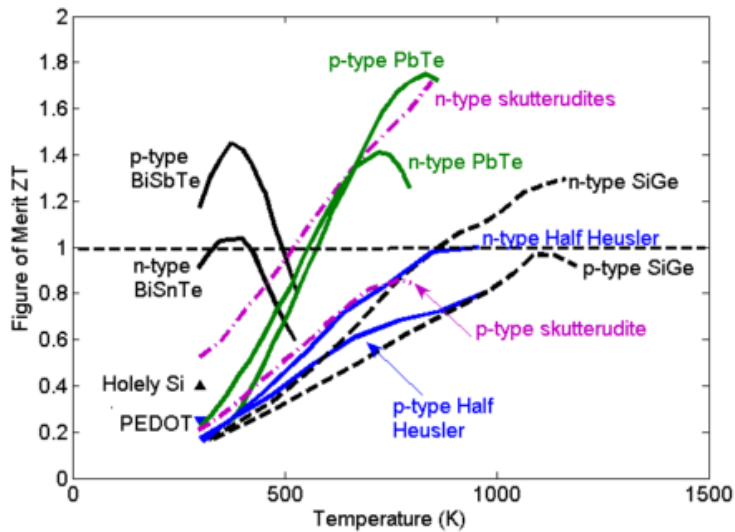
Figure 2 – Reported ZT values across the literature [41]

One of the pioneering works in this field was done by Telkes in 1954 [42] before the first oil crisis in the world. Utilizing the best alloys available at that time, she was able to improve the TEGs efficiency by 3.35 percent. Though the study set the foundation of TEG technology, no real solar energy application was attempted. Years later, right at the time of the crisis, Suleebka [43] studied a sintered Si-Ge alloy TEG with three different high temperature solar absorbers. Despite the fact that the efficiency has been increased nearly by five times as reported, a major drawback was the assumption that the TEGs were receiving a constant solar flux, which was not the case in reality, since the weather changes constantly. A decade passed by before David Rowe, in 1981, investigated the theoretical performance of a solar-powered TEG [44]. His work dealt with fine-grained TEM material fabrication for electricity generation. The maximum efficiency of the device at the STC was in excess of 12 percent. Some limitations were obviously noticeable, as the experiment was not allowed to be exposed to real-environment test conditions, because the cold side temperature was fixed at 300K. In 1998, this same author evaluated the power generation performance of a TEG in terms of its efficiency and reliability [45]. He found that an optimization mechanism was necessary for the TEGs to deliver maximum output power. Thereafter, Meneewan et al. in 2004 applied TEGs in order to enhance indoor air movement in hot regions [46]. The aim of their work was to develop a thermoelectric roof solar collector. Though the ventilation rate was induced in order to reduce the heat transfer from the roof to indoors, it is important to point out that the experiment was lab-scale based, and may not give the sought output in a real life experiment. One year later, Vatcharasathien et al. [47] built and analyzed a STEG system, where they attempted a comparative design. The project effectively

19

demonstrated the feasibility of a combined TEG with conventional solar thermal collectors by minimizing system cost and seasonal adjustment of the slope angle between 0 and 30 degrees.

In the year 2008, a group of MIT material scientists demonstrated a possible increase of the electrical conductivity and a decrease of the thermal conductivity in bulk nano-materials. Hence, the GF, as discussed earlier, of the Bi_2Te_3 based material was quite enhanced from 1 to 1.4. [48]. On the other hand, it is worthy to note that the predicted efficiencies are not only hard to achieve in real TEG applications, but also are always higher than the real material ones because of the effects of parasitic losses. This latter point is further developed in chapter three.

In contrast, two concomitant but slightly different studies were carried out in 2009. First, Juanico and Renalde investigated a comparative economic analysis between TEG and PV for rural isolated homes [49]. They found that the load factor of the PV was 10 percent, as compared to 100 percent for the TEG. The direct implication is that the TEG system not only presented a better performance in all cases, but also could improve the sustainability of firewood stoves in rural households. The second study by Eswaramoorthy and Shanmugam, evaluated rural residential energy demand utilizing TEG systems [32]. Their results showed that the payback period was one year and one month and the electrical grid dependence was tremendously reduced. Another STEG economic analysis utilizing parabolic concentrator for micropower was performed in 2010 by Amatya and Ram [50]. They discovered that the STEG's peak power price was $1.67/Wp, as compared to $4/Wp for the PV module.

In the following year, Rinalde et al. investigated the use of TEG for rural electrification, where they designed an energy-harvesting prototype for isolated households [31]. In this same year 2010, Zhang et al. evaluated the performance of a solar micro-energy harvester based on TEG in conjunction with latent heat effects [51]. Their device was sensitive to seasonal

variations in solar radiation and wind patterns, which makes it a good candidate for building wireless applications. Also, in 2010, Champier et al. attempted to improve rural communities' living standards by incorporating TEG to a cooking stove for electricity generation in developing regions. The only drawback to their study was that a thermo-coax electric heater was used, rather than a real stove, to provide a continuous power of 150W [33]. Recently in 2011, two important research works were conducted. Kraemer et al. analyzed the real performance of Flat-panel STEGs with a high thermal concentration at an AM1.5, equivalent to 1kW/m^2. The latter value is too ideal for real STEG testing to yield any meaningful result. Nevertheless, their model achieved a peak efficiency of 4.6 percent [52]. Finally, Meng et al. suggested a numerical and comparative study of a TEG with multi-irreversibilities [53]. All the major inner effects, such as Seebeck, Fourier, Joule and Thomson, were considered in the novel model. Unfortunately, accuracy may be lost in the results because the capacitances of the various elements were completely ignored.

It should be mentioned that TEM technology, as per the abundance of literature, consists of n- and p-type semiconductor materials connected electrically in series and thermally in parallel. When one side of the TEG is subjected to heat while the other side is at a lower temperature because of a thermal resistance heat exchanger, an electromotive force (ΔV) is generated proportional to the Seebeck coefficient of the TEG semiconductor material as discussed in [11]:

$$V = \alpha \cdot (T_H - T_C) \tag{3}$$

Where, T_H and T_C represent the hot and cold side temperatures respectively.

On the other hand, if an electrical current flows in the junction, this generates a thermal difference between the two sides of the device. This phenomenon is referred to as the Peltier

effect [54]. One side of the junction will absorb heat (Q), while the other side dissipates heat to the surroundings, depending on the amount and the direction of the current flow as in Eq. (4).

$$Q = \alpha \cdot T \cdot I \tag{4}$$

Where, *I* represents the current that flows in the device.

Although some of the aforementioned works described remote application of TEGs, none of those studies have looked into the thermal-to-electrical analogy utilizing the LTspice simulator to model a complete energy-harvesting system, as investigated in this study.

2.2   Specific Review

A chronological literature survey is attempted in this section. The work aims to emphasize how the idea of LTspice modeling of transient heat transfer analysis, utilizing thermal-to-electrical analogy, evolves over time.

One of the originators of transient heat transfer analysis utilizing Spice simulator in conjunction with TEGs is Chavez et al. in 2000 [55]. This study sought to analyze and propose a three port Spice model of a Peltier cooler by using the electrical analogy of the thermal system. Four years later, Lineykin and Ben-Yaakov presented a Spice compatible circuit of a TEM [56]. The following year, the same authors investigated ways to model and analyze, utilizing Pspice software, thermoelectric modules (TEMs) [57]. Comparable to the previous work, their objective was to develop a Spice compatible equivalent circuit of a TEM. In the following year (2006), Chen et al. analyzed the transient behavior of a TEG through an Electro-thermal scheme utilizing Spice [13]. Although the model was able to reflect the thermo-electric coupled multi-field system effect of TEG by considering the finite heat transfer rate at the interface (TEG - thermal ambient), the results could be much better if T_h and T_c were not idealized to be constant. In

reality the Seebeck coefficient is dependent on the above mentioned temperatures, as demonstrated in [62] and [63].

Again, in 2007,, Lineykin et Ben-Yaakov aimed to develop a Spice compatible equivalent circuit of a TEM [14]. This study showed that the modeling of the thermoelectric cooler (TEC) and the TEG was about the same. Consequently, the same circuit can be utilized to simulate both behaviors, providing that the current direction is reversed. In addition, the TEG parameters were simply extracted from the datasheet. Unfortunately, there was a major drawback to that approach. There was not enough precision in the results because not only was the thermal resistance of the aluminum plates assumed to be negligibly small, but also the thermal capacitance of the isolation chamber was neglected. These assumptions surely affected the accuracy of the overall results. As opposed to the original, previous works, in 2008, Mirocha and Dziurdzia proposed an improved electro-thermal model of a micro TEG system utilizing the Spice simulator [60]. Their version introduced the Peltier module's dependence of the internal resistance (R_{int}) variation with respect to temperature changes, since R_{int} fluctuations have an impact on the actual performance of TEG. Nevertheless, a better accuracy was achieved in the range of small temperature gradients.

As a final review, in the years 2012 and 2013, respectively, Mihail Cernaianu [61] and Gontean and Cernaianu [12] proposed a TEG energy-harvesting system's analysis by means of the LTspice simulator. Their improved model was solely based on the thermal-to-electrical modeling schemes. They investigated the variation of the parameters, such as the Seebeck coefficient, internal resistance, and thermal conductance, as heat was being transferred from the hot to the cold side. Furthermore, a DC-DC converter (LTC3105) was introduced to boost the TEG's output voltage to a desired level needed to charge the battery. In both studies, the authors

did use current-dependent sources rather than voltage-dependent sources. They claimed that the former proved to solve different convergence problems that may appear in simulations due to the large number of variables. The drawback of these energy-harvesting systems was that they were limited to laboratory experiments. Therefore, they did not have as significant an impact as if they were conducted in an open environment to harvest the free and abundant solar energy.

2.3   Conclusion

There is a generous endowment of solar, wind, geothermal and other renewable resources on Earth.   With the current technological development attained, mankind is consistently inventing new ways to improve the existing electrical power generation mix. Learning how to harness these infinitely important renewable resources to replace the traditional fossil fuel energy sources would untangle the current worldwide economic model that is based on fossil fuel.

This work reviews succinctly the state-of-the-art technologies in the field of thermoelectric generation. Since STEG systems recently gained more popularity in terms of real solar energy-harvesting applications, the survey is split into two main parts: 1) a general review, as a whole, treating the concepts and most important applications of TEGs; and 2) a specific review elaborating on the electrical modeling of any thermal system in a chronological manner.

The survey highlights the recurrent and absolute necessity for finding new methods for energy delivery to remote residential regions. Also, this review reveals a gap in terms of transient heat transfer analysis of a real-world STEG system utilizing thermal-to-electrical analogy in conjunction with LTspice software.

Chapter 3: Proposed Design

A popular saying goes like this: "No one is truly a scientist if [his/her] research confirmed all [his/her] ideas, as [s/he] is not stepping into the unknown". In line with this quotation, the initial research expectations were set high so as to gradually reach a common ground, whereby theory and practice mutually meet each other. For a better understanding of the four major effects that normally occur in any TEM, an experiment was first initiated in the laboratory in order to characterize the device. This also allowed us to familiarize ourselves with it for future, more elaborate real-world solar experiments. Having experimented with real thermal behavior, in terms of device true performance and limitations, of the TEG elements under non ideal testing conditions, the major research goal was adjusted accordingly. The new solar energy-harvesting system must be designed to withstand severe and arid weather conditions, but also must be robustly designed to supply electricity to remote residential households, so long as is needed. Both the indoor and the real-environment TEG experiments were put together following a similar methodology, as their inner heat transfer functionalities remain mostly identical.

3.1   Design Methodology

This work proposes to design, build, and test a solar thermoelectric generator system. Possible methods to enhance its efficiency, understand its functionality, and optimize its performance, i.e. the heat transfer capabilities between the top and the bottom surfaces, will be investigated. The thermal to the electrical analogy scheme was adopted to simulate the designed energy-harvesting model by means of the LTspice simulator software. Experimental and simulated results were then analyzed.

This study is twofold. The first step was to investigate the performance of a commercial solar TEG under arid weather conditions comparable to the Southwest of the US or the Sahel in Africa. The TEG devices were chosen to be five in number and were mounted on a solar tracker. The reflectors on the tracker were positioned in such a way that the sun is concentrated four times on the semiconductor devices. The second step of the project was to not only compute the electrical parameters from both the datasheet and device's geometries and properties, but also, and most importantly, to perform the electrical analogy of the whole system with the Spice simulator. A lookup table of real experimental data (temp hot side, T_H and temp cold side, T_L) was fed into the circuit to improve simulation speed. The LTspice's built-in piecewise linear (PWL) command was utilized in order to achieve the goals. Due to the complexity of the geometry of the system and the corresponding longer simulation time, some assumptions were required. The thermal capacitance of the insulation material utilized may be neglected for simplicity in the approach. The thermal resistance of the heat transfer grease was assumed to be $0.45K.W$ [58]. The necessary temperature values used to simulate the real behavior of the TEG are organized in a table and stored for the simulation in a text file, as already stated above. Afterward, both the experimental and simulated energy harvested were analyzed and compared. Stated differently, the real experimental data served to validate the simulated results by plotting them in the same graph.

Finally, the amount of energy harvested, in relation to the real-environment solar experiment, was stored in rechargeable batteries for a later usage, such as in the case of powering light emitting diodes (LED) in homes. Furthermore, the LED system may be equipped with USB ports to charge cell phones, since people in remote areas today depend on them for exchanging news and money as well as education and health services. The performance and characteristics of

the major battery technologies are thoroughly addressed. As a result, the best battery technology in terms of functionality and cost-effectiveness are chosen to fit the current needs.

3.2 Parameter Extraction

An indoor experiment was first conducted to first characterize the device (TEG) parameters from: 1) datasheet, 2) device geometries, and 3) material properties. Furthermore, the indoor test was to not only understand how the TEG operates in real environment which is different from the STC, but also to get accustomed to it before the main part of the work. Afterward, a complete solar energy-harvesting system was then set up on the roof of the TBE-B building at UNLV.

3.2.1 TEG Basic Principles

As reported in [14] and [57], several physical phenomena take place in a thermoelectric device. Therefore, only the most significant of them will be mentioned that are of particular relevance in this research.

Convection and Radiation - heat transfers through three thermally possible transport mechanisms. The predominant mechanisms in a TEM are convection and radiation [62]. The former, is the transfer of internal energy, generally in the form of heat, through fluids by obeying the natural laws of diffusion. The latter, i.e., electromagnetic radiation, is the continuous emission of energy from all substances due to their molecular, atomic, and sub-atomic agitations.

Joule heating - another name for this thermo-electrical phenomenon is resistive heating. It is known to be the process by which the passage of a current through a conductor emits heat. The amount of heat, Q, released due to Joule heating is proportional to the square of the current flow times the resistance ($R = \rho \cdot l/A$) as seen in Eq. (5).

$$Q = I^2 \cdot R \tag{5}$$

Where ρ, Q, I, l, and A are the resistivity of the material (Ω.m), the Joule heating (Watts), the current (Amperes), the length of the material (meters, m), and the surface area (m^2) respectively.

Peltier cooling/heating - this particular effect is of great interest when the TEM is run as a cooler. The Peltier effect supplies power to the thermoelectric module with a resultant cooling of one side and heating of the other.

Finally, the *Seebeck power generation* - as detailed in [63], the Seebeck effect occurs when two dissimilar metals are looped together. They develop an electromotive force (emf) when the two junctions are kept at different temperature.

The *Thompson effect* - is explicitly neglected at this stage due to its smaller contribution in terms of cooling as reported in [56].

3.2.2 Extraction from Datasheet

The parameters were extracted from the manufacturer's datasheet and utilized in conjunction with the internal parasitic components to derive the proposed model [44]. The following values were provided by *Custom Thermoelectric* web site [63]: the maximum power, $P_{max} = 21.6$ *W*; the maximum voltage, $V_{max} = 7.2$ *V*; the maximum current, $I_{max} = 3$ *A*; Thermal Conductivity, $k = 2.18$W/$m{\cdot}K$, and the optimal efficiency of the module, $\eta = 6.5\%$. The following values were then computed and succinctly utilized toward the final goal, which is the electrical analogy.

3.2.2.1 Electrical Resistance

The electrical resistance of the module, R_{Elect}, can be estimated by Eq. (6).

$$R_{Elect} = \frac{(V_{max})^2}{P_{max}} = 2.4\ \Omega \tag{6}$$

3.2.2.2 Seebeck Coefficient

The computation of the Seebeck coefficient, α, is done by means of Eq. (7).

$$\alpha = 2 \cdot \frac{Vmax}{Th-Tc} = 0.0534 \ V/K \tag{7}$$

3.2.2.3 Thermal Resistance of the Module

The thermal resistance of the module, R_{Ther}, is computed by Eq. (8).

$$R_{Ther} = 2 \cdot \Delta T \cdot \eta \cdot (2 - \eta) \cdot \frac{R_{Ther}}{(\Delta T - \eta \cdot Ta)^2 \cdot \alpha^2} = \frac{0.6365K}{W} \tag{8}$$

3.2.2.4 Thermal Resistance of the Insulation Foam

The resistance of the thermal insulation, R_{Insul} as reported by Jan et al. [64] can be calculated as follows based on the experimental data gotten after steady state conditions had been reached within 32 minutes [63], i.e. $T_H = 324.89$K; $T_C = 311.46K$, as can be seen from Eq. (9).

$$R_{Insul} = \frac{\alpha^2 \cdot R_{Ther}^2 \cdot (Tc + Th + 2.273)^2}{(T_C - T_H)^2} \cdot$$

$$\frac{(Tc - Troom)}{(2R_{Elect} + \alpha^2 \cdot R_{Ther} \cdot (Tc + Th + 2.273))}$$

$$= 5.9K/W \tag{9}$$

Where, T_{room} represents the normal temperature of a living room.

3.2.3 TEM Modeling Steps

Modeling a TEM system with SPICE as done in [63] could be ambiguous as it hasn't been clearly explained up to this point. The following are the seven (7) major steps that it takes to simulate any thermo-electrical system with an electronic SPICE simulator, such as LTspice.

1) Identify the physical components

2) Calculate their *Biot* number as explained thoroughly in [64]; its value determines the approach to adopt in the analysis. Should that value be much less than unity, the lumped capacitance method is solely recommended for accuracy in the results. If it isn't much less than, then some sort of numerical discretization method should be considered.

3) Calculate the thermal resistances and capacitances of all the mechanical parts mentioned in [63] by splitting them into smaller parts. The nature of the material and other properties such as density and volume should be accounted for in calculation.

4) A further step in the design is to not only define, but also draw the electrical parts that will encompass all the parasitic elements such as *R*, *L*, and *C*. The latter point is not important at this stage in the research, but will be given a further consideration in the second part dealing with real-environment solar energy-harvesting design, where the goal is to utilize a DC-DC converter for accuracy in the results.

5) Express the electrical equivalence of the thermal parameters. Table 1 lists the most commonly used thermal-to-electrical analogies as presented in [65].

Table 1 - Thermal-to-electrical equivalence

Thermal		Electrical	
Temperature	T [°C]	Voltage (source)	V [V]
Heat flow/power	Φ [W]	Current (source)	I [A]
Heat resistance	R [°C/W]	Resistance	R [Ω]
Heat capacitance	C [J/°C]	Capacitance	C [F]
Fourier's law	$\Phi = \dfrac{\Delta T}{R}$	Ohm's law	$i = \dfrac{V}{R}$
Heat capacitance equation	$\Phi = C \cdot \dfrac{dT}{dt}$	Capacitor equation	$i = C \cdot \dfrac{dV}{dt}$
Ambient Temperature		Ground	0 [V]

6) Then connect these analogy blocks in series and/or parallel in order to reconstruct the actual system.

7) Finally, the TEM is ready to be modeled in LTspice, provided the right codes were written.

3.2.4 Parameters Computations

Some of the material properties that turned out to be helpful in this study were mentioned on website of *Custom Thermoelectric* [66]. Hence, Table 2 depicts the most relevant values. The TE modules were specified by the manufacturer to be bismuth telluride (Bi_2Te_3) and that the ceramic substrates or faces were made of alumina (Al_2O_3).

Table 2 – TEM properties

Material	$\rho[kg/m^3]$;	c [$J/kg \cdot K$];	$\kappa[W/m \cdot K]$
Aluminum	2770	875	177
Alumina	3570	837	35.3
Bi_2Te_3	7530	544	1.5

In which, ρ is density, c is specific heat, and κ is conductivity.

3.2.4.1 Aluminum Plates

In order to appropriately simulate with the LTspice software all the thermal processes taking place inside the thermoelectric module, all the physical parts must be transferable. So, the two equal dimension aluminum plates, (Length 56mm, Width 56mm, and Height 12.7mm), purposely grooved to hold the hot and cold side thermocouples during the laboratory experiment need be accounted for in the computer model. The parameters of interest in the electrical analogy are the thermal resistance and the thermal capacity of the above mentioned plates.

3.2.4.1.1 Thermal Resistance, R_{AL}

$$R_{AL} = \frac{1}{\kappa \cdot (A/l)} = 2.29 \cdot 10^{-2} [K/W] \tag{10}$$

Where $\kappa = 177 W/m$ is the thermal conductivity, A is the surface area, and l is the length of the plate.

3.2.4.1.2 Thermal Capacity, C_{AL}

$$C_{AL} = \rho \cdot Cp \cdot V$$

$$= \frac{2770 kg \cdot 875 J \cdot (0.056)^2 \cdot (0.0127 m^3)}{m^3 \cdot kg \cdot K}$$

$$= 96.53 J \tag{11}$$

Where, ρ is the density, C_p is the specific heat capacity, and V is the volume of the Al. plate.

3.2.4.2 Thermoelectric Module, TEM

It is essential to first have a sound knowledge of the exact mass the TEM, its molar mass, M and its molar heat capacity for us to be able to reproduce the heat capacity of the module in LTspice. Hence, the mass was simply determined by a sensitive electronic balance and compared to the one given on the datasheet. The heat capacity, C_p, of a material can be determined as follows:

$$Cp = \frac{C_{mol}}{M} \ [\frac{J}{kg} \cdot K] \tag{12}$$

Where, C_{mol} is the molar heat capacity in $J/mol \cdot K$, and M represents the molar mass in g/mol.

The molar heat capacity of Bi_2Te_3 was found in [67] to be 126.19 $J/mol \cdot K$ at normal temperature, i.e. 298.15 K. In a like manner and for simplicity in the approach, the molar mass, M of the aforementioned material, was accessed at [68] website. It was found there to be 800.760 g/mol. Additionally, the mass of the semiconductor devices can be obtained through a mere subtraction knowing the entire mass ($m_T = 4.8.10^{-2} kg$) of the TEM and that of the ceramic plates

as can be seen from Eq. (14) below. Hence, the following values can be easily computed, Eq. (13)—(15).

3.2.4.3 Mass of the ceramic plates, m_{cer}

$$m_{cer} = \rho \cdot V \ [kg] = \frac{3570 kg}{m^3} \cdot (0.056m)^2 \cdot (0.002m)$$

$$= 2.239 \cdot 10^{-2} kg \tag{13}$$

3.2.4.4 Molar heat capacity of the ceramic plates, C_{cer}

$$C_{cer} = \rho \cdot Cp \cdot V \ [J/K]$$

$$= \frac{3570 kg \cdot 837W \cdot (6.272) \cdot (10^{-6} m^3)}{m^3 \cdot m \cdot K}$$

$$= 18.74 J/K \tag{14}$$

3.2.4.5 The mass of Bi_2Te_3, m_{Bi2Te3}

$$m_{Bi2Te3} = m_T - m_{cer} \ [kg] = (4.8 - 2.239) \cdot 10^{-2} kg$$

$$= 2.561 \cdot 10^{-2} kg \tag{15}$$

3.2.4.6 Molar heat capacity of Bi_2Te_3, C_{Bi2Te3}

$$C_{Bi2Te3} = \frac{C_{mol}}{M} \cdot m_{Bi2Te3} \ [J/K] = \frac{126.16 J \cdot mol}{800.76 g \cdot mol \cdot K} \cdot 25.61 g = \frac{4.036 J}{K} \tag{16}$$

3.2.4.7 The Overall Heat Capacity of the TEM, C_{TEM}

The heat capacity of the thermoelectric module, under preliminary investigation in the laboratory, can be estimated based on the knowledge of the two previous heat capacities already determined in Eqs. (13) and (15) by

$$C_{TEM} = C_{cer} + C_{Bi2Te3} \cong 23 J/K \tag{17}$$

Furthermore, the above calculated heat capacity was split into two equal parts to fit in the LTspice model, as this technique yielded to accurate TEG modeling and the best possible solutions. The idea behind the technique is that, the capacitance value has to be equally

distributed between the cold and the hot side of the TEM, or else the results would not be precise.

In order to model the actual thermal behavior of the TEM, its internal parameter variations are taking in account in the present model based on the work done in [35]. Hence, the internal parasitic inductance and capacitance values for both TEG and TEC are already available to use in the latter reference. Thus, they are used in the present work, because the current setup [63] is not meant to characterize the internal parameters or their variations with temperatures.

Thus, it is a paramount importance to point out that, in this work, priority was given to the most dominant physical phenomena that take place in a TEM. Therefore, among all the potential mechanisms, *Seebeck*, *Peltier*, and *Joule effects* were given the most attention. As part of the knowledge assimilation process, occurring whenever a known theory has to be verified through practice, the TEM was first run as a heat pump, also identified as thermoelectric cooler (*TEC*). A TEC energy flow is solely based on *Joules effect* as given in the following, Eqs. (18) — (21), energy balance equations by

The heat flow at the absorbing (cold) side is given by Eq. (18).

$$Qc - \alpha \cdot T_C \cdot I + \frac{1}{2}I^2 \cdot R_{Int} + \kappa \cdot \Delta T = 0 \tag{18}$$

The heat flow at the emitting (hot) side is given by Eq. (19).

$$Qh - \alpha \cdot T_H \cdot I - \frac{1}{2}I^2 \cdot R_{Int} + \kappa \cdot \Delta T = 0 \tag{19}$$

The overall energy balance equation is represented by Eq. (20).

$$Qh - Qc - P_{Elect} = 0 \tag{20}$$

Hence, the electrical power consumed by the device necessary to remove the heat from one side relative to the other is as written in Eq. (21).

$$P_{Elect} = Qh - Qc = \alpha \cdot \Delta T \cdot I + R_{Int} \cdot I^2 \tag{21}$$

Where, T_H and T_C represent the hot and cold side temperatures respectively; R_{Int} is the internal resistance of the TEM; α, κ, and ΔT as mentioned above are the Seebeck coefficient, the thermal conductivity, and the differential temperature ($\Delta T = T_H - T_C$), respectively.

According to the study performed in [35], the Spice model behavior of the TEC will be unrealistic if the internal parasitic capacitance is neglected, as it was done in [56]. In addition to that, α, κ, and R_{Int} variations with temperatures must be accounted for toward the same objective. This study is meant to accommodate all the aforementioned issues that might affect the realistic Spice implementation of the thermoelectric module [63].

3.3 LTspice Modeling of TEG Energy-Harvesting System

Most of the EE engineers have a limited knowledge when it comes to analyzing the real behavior of transient heat in a semiconductor device since the concept of heat transfer through any medium is entirely exclusive to their curriculum. Thus, modeling a *TEM* system with LTspice would have been confusing, had it not been clearly explained methodically step by step in Sec. 3.2.3. In practice, STEG applications are continuously dynamic. The practical environments change as the local insolation changes during and throughout the days, the seasons, and the years. The electrical load of the system may also vary at each instant, as the energy demand is constantly changing. These dynamic variations tremendously affect the way STEG operates in terms of efficiency, reliability, and life span. These dynamical changes govern even the way the external DC converter performs. Hence, it is important in this study not only to understand those transient behaviors and their impacts on the system, but also to accurately describe them through thermal-to-electrical analogy techniques. How transient heat is being transferred in TEG is analytically cumbersome. Therefore, we propose to analyze numerically the transient heat transfer in TEG by means of the LTspice simulator. One of the standard

methods of heat transfer analysis is to convert the thermal problem statement into an equivalent electrical analogy. The latter is helpful in investigating and understanding any thermal problems. Furthermore, the thermo-electrical analogy facilitates not only visual conception of the heat transfer problem at hand, but also the subsequent analysis.

3.4   DC-DC Converter

It should also be mentioned that the intent of this work is not to design a DC-DC converter, but rather to utilize a prefabricated converter that works best for the proposed STEG energy-harvesting system. All DC-DC converters' primary function is to boost the low DC output voltage, and then stabilize the power output ripples due to intermittencies. Otherwise, the sensitive household appliances would malfunction in such a manner that would be detrimental to their life spans. The subsequent figures, *viz.* Figure 6 through Figure 11, present an in-depth illustration of the concept of impedance matching and that of STEG output power's intermittency.

3.4.1   Brief Description of the Converters

Two types of converters are under investigation. The first kind is the LTC3105, which is a step-up DC-DC converter with power point control and a low dropout (LDO) regulator. It is provided on a demonstration circuit (1587A) as a boost converter for relatively high impedance and very low voltage input power sources. This type of converter has operating input voltages ranging from 250mV to as high as 5V. Figure 3 illustrates the 1587A circuit board, including the LTC3105, the MPPC, the three LDO regulator output voltages, and the rest of its functionalities.
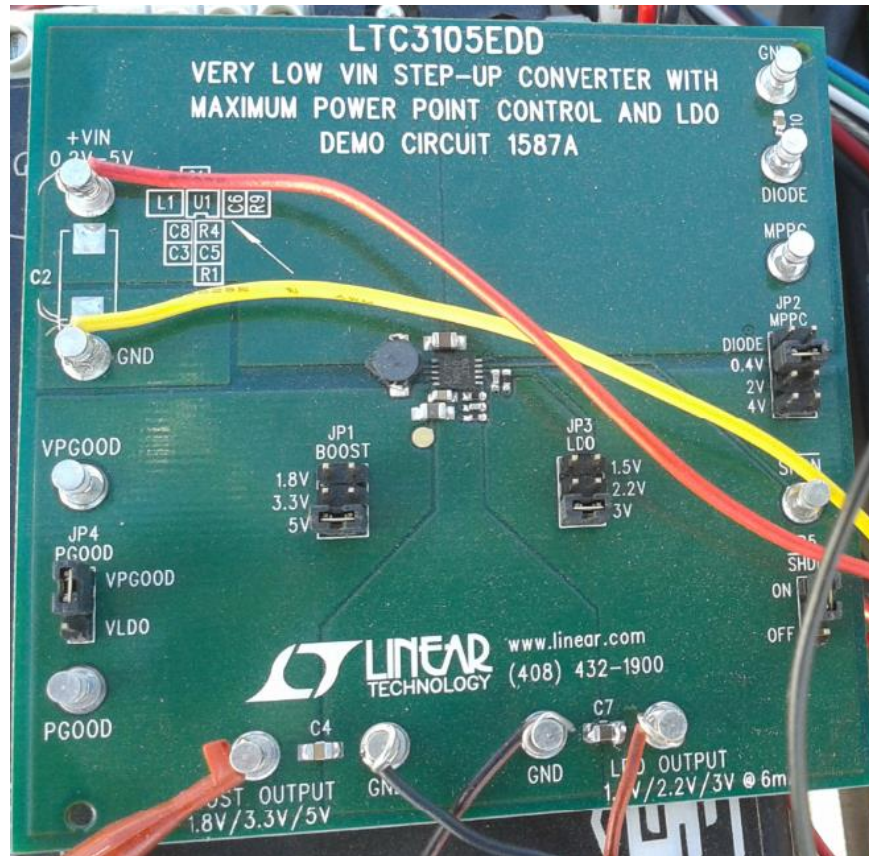
Figure 3 – 1587A circuit board

The second type of DC-DC converter is the LTC3525 micropower synchronous step-up converter with an output disconnects functionality. This converter has an advanced feature valuable for low-power harvesting, unlike the LTC3105. It was perfectly designed with the advanced capability of maximizing the overall energy-harvesting system's efficiency. Hence, it is important to note that this demonstration board comes in two assembly versions: 1) DC879A-A and 2) DC879A-B. The latter board was solely chosen, as it fits the current need by offering a constant 5V output for any input voltage ranging from 1VDC to about 4.5VDC. For clarity, Figure 4 has been inserted to depict the DC879A-B board in question, showing the LTC3525 chip in the center and the rest of the embedded functionalities.
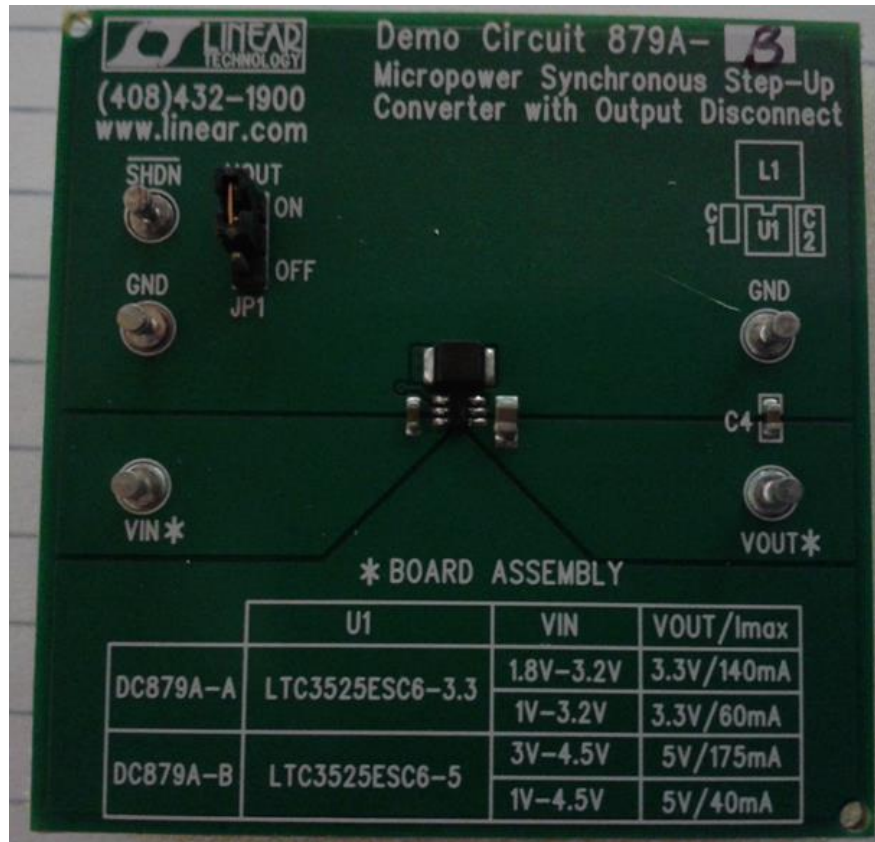
Figure 4 – DC879A-B demo board

3.4.2 Impedance Mismatch

The relatively low-level voltage usually generated by STEGs is not appropriate for direct usage as power source for most electronic devices. Therefore, as stated above, for many of the practical intents and purposes, it is necessary to utilize DC-DC converters to boost the output voltage to the desired level. An additional functionality of a DC-DC converter is its ability to regulate the fluctuating TEG output under intermittent temperature conditions. Thus, the

converter is solely the intermediate stage between the TE generator and the electrical load, as simply depicted in Figure 5.
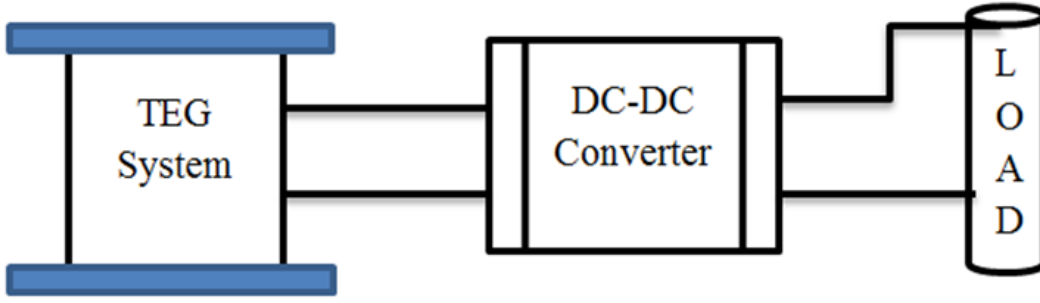
Figure 5 – Basic thermoelectric generation system block diagram

The impedance mismatch between the internal resistor, R_{Int}, of the TEG, and the input resistance of the converter, R_{CONV}, is the main problem a DC-DC converter experiences. The power supplied by the TEG system to the DC-DC converter can be estimated by

$$P_{IN} = V_{OC}^2 \cdot \frac{R_{CONV}}{(R_{Int}+R_{CONV})^2} \tag{22}$$

Where, V_{OC} denotes the TEG's open-circuit voltage, and P_{IN}, the DC-DC converter's input power.

The variation of the DC-DC converter's input power as a function of the converter's input impedance was studied by [69]. Figure 6 portrays that dependence.
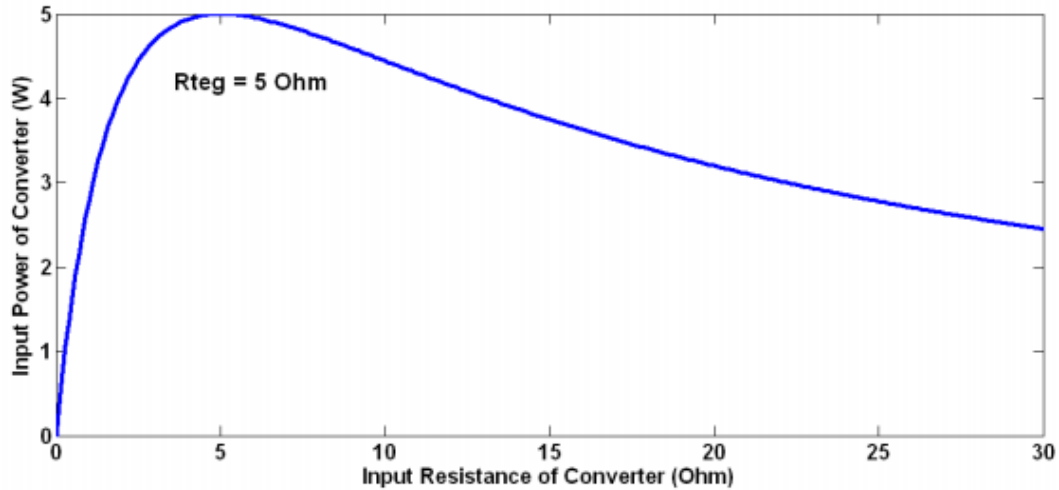
Figure 6 – TEG power supplied as a function of R_{CONV}. [69]

As can be observed from the above graph, maximum power is transferable only when the two resistors match each other, which is highly unlikely to be achievable in real-environment solar applications.

3.4.3 Effects of Solar Variability

First, variability in solar energy affects the way solar renewable energy-harvesting devices, such as PV systems and TEGs, operate on a daily, seasonal, and yearly bases. This is true in the sense that the amount of solar radiation arriving on Earth is influenced by all kinds of weather events, such as cloud coverage, storms, and even the Earth's rotation on its own axis and its revolution around the sun. During cloudy weather conditions, the PV power output changes suddenly by responding instantaneously to fluctuations in sunlight as reported in [70]. In a similar fashion, it has been empirically demonstrated by this study that STEGs also respond instantly to variations in the solar radiation. Although the unit is meant to supply light loads in a typical remote household in developing regions, its operation may create challenges for system

41

owners without a proper DC-DC converter. Hence, it is essential to point out that adverse weather events, such as cloud coverage depend on: 1) the size and shape of the STEG system in question; and 2) the clouds' transparency, speed, and direction of movement. A specific emphasis will be put on STEG output variability in the analysis section of this study.

3.4.3.1 Direct Normal Irradiance

Direct normal irradiance (DNI) is basically the amount of solar electromagnetic radiation received per area unit by a measurement device or any surface that is constantly held normal to the solar rays, which are assumed to come in a straight line from the sun. The solar energy-harvesting system designed to achieve the goals of this work was mounted on a solar tracker. In other words, the local DNI was selected to be the only energy input in order to maximize the amount of insolation annually received by the STEG system. Hence, Figure 7 depicts the Las Vegas DNI for the months of April and May 2015 recorded during the course of this experiment. It can be seen that the DNI varies throughout the days, weeks, and months. This is a strong sign that the energy harvested by the STEG system will continuously vary.
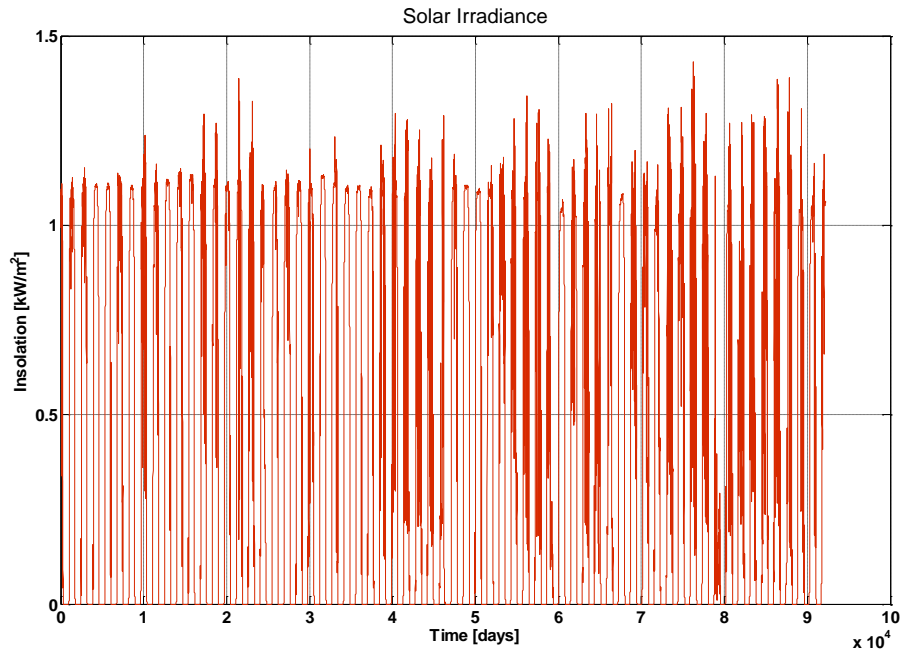
Figure 7 – Solar DNI recorded in Las Vegas, April and May 2015

This renewable solar energy-harvesting system takes full advantage of the free and abundant solar energy by conducting an open air test, whereby the only heat source is solar electromagnetic waves. As a direct consequence, variability of incoming solar energy due to weather events is not only a great issue to the converters, but is also affecting the way TEG systems perform in the real-world environment.

3.4.3.2 Real-Environment Performance of the LTC3105

Figure 8 portrays the real-world performance of converter with two different outputs prior to the connection of any external load. For both the 5VDC and 3VDC, the effects of variability are remarkable; it will certainly create severe damage to the sensitive electronic appliances and gadgets.
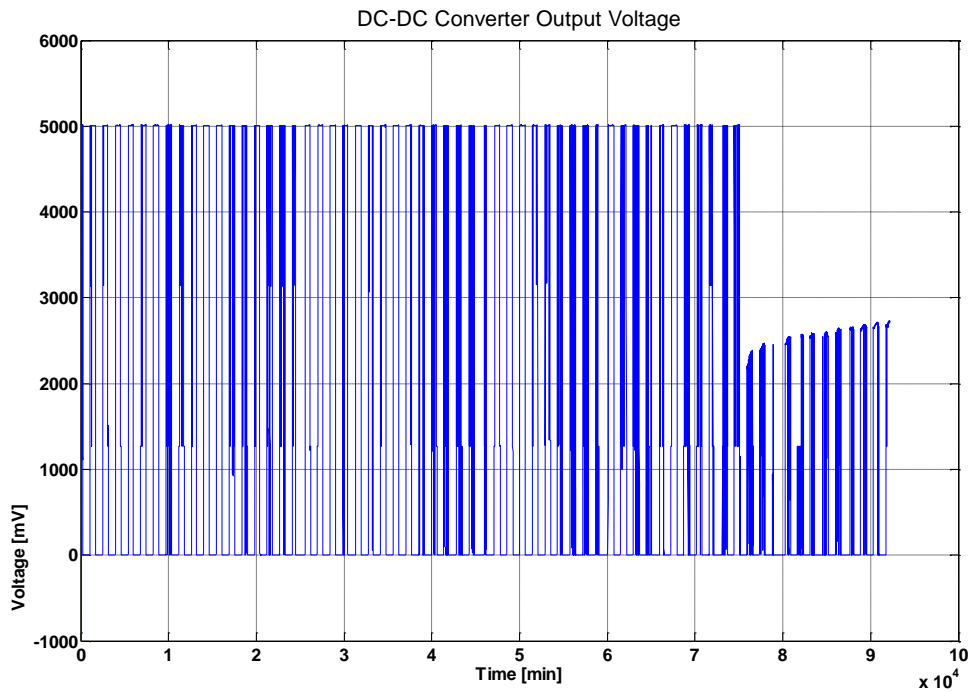
Figure 8 – Real-environment performance of LTC3105

3.4.3.3 Voltage Expanded View (5V select)

It is much easier to decipher the concept of a DC-DC converter's output variability through an expanded view of specific days. Figure 9 clearly shows the actual performance of the LTC3105 during the course of its real-environment operation for a week. The output is highly intermittent and dependent on insolation. Hence, during cloudy weather days, the TEG power output changes by responding instantaneously to the fluctuations of sunlight. Therefore, output power issues, related to variability of incoming sunlight, remain a great technical challenge for the DC-DC converter. The converter's output, by essence, is supposedly free from any variation, but counter-intuitively demonstrates the opposite, as can be seen in Figure 9. Furthermore, it has also been demonstrated, as can be understood from Figure 9 and Figure 10, in addition to the

converter, a reliable energy storage system is strongly needed because the converter is only designed to handle a constant input which is obviously not the case in real-environment solar applications. Therefore, these momentary power outages, also known as power flickers, which last for fraction of seconds to few seconds, are annoying because they can briefly shut down, if not totally damage, the appliances and electronic devices in households or businesses.
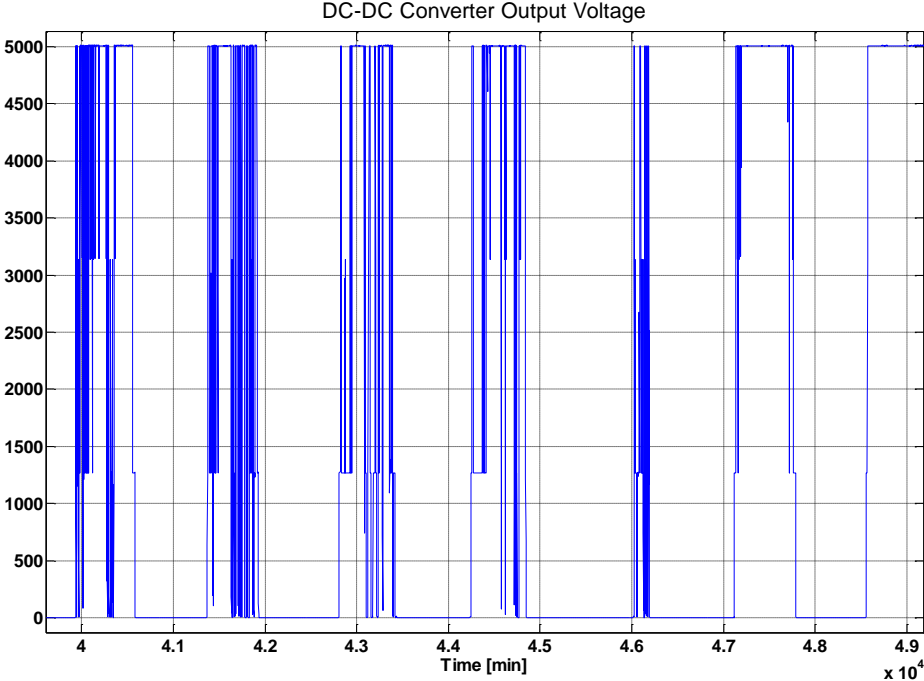
Figure 9 – Weekly performance of the LTC3105

3.4.3.4 Comparative Performance (5V select)

Figure 10 compares two distinct days. The first day, the converter performed as intended by outputting a constant voltage throughout the day. The second day, it did not fulfill its main duties of boosting and stabilizing the output voltage. Also, these two days clearly highlighted

45

distinctly the output patterns of a clear summer day versus a cloudy one. Therefore, solar variability is particularly challenging to the DC-DC converter although the output responded with some delays to the intrinsic inertia of the entire thermal STEG system. It is worth mentioning that this study, once again, demonstrates both the future challenges of a real STEG system and the real-time performance of any DC-DC converter in terms of solar applications for remote residential usage. Hence, the design of the next generation DC-DC converters should incorporate a new *solar feature* especially when they are to be utilized in real-world solar experiments. The new feature must have the capability of responding instantly to the unpredicted and stochastic variations of solar radiation.
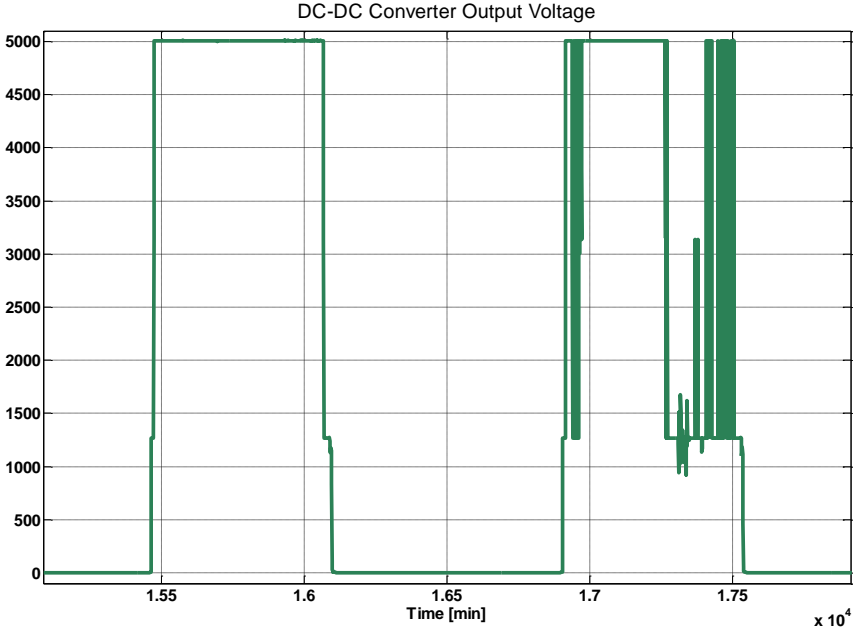
Figure 10 – Real performance of LTC3105—Clear summer day versus Cloudy day

3.4.3.5 Voltage Expanded View (3V select)

How the voltage progressed after the insertion of the energy storage unit shed additional light on the significant issues with the converter in terms of real solar environment applications. The energy storage system (ESS) tested was a 3.2V K2 technology. The battery was placed at the very end of the STEG energy-harvesting system in order to store energy for a later usage. As can be seen from Figure 11, the converter surprisingly entered in a somewhat new mode of operation similar to load following. It is worthy of note pointing out that the new state of operation was noticed soon after the K2 battery was completely discharged to 1.5VDC and 0ADC by means of the Maccor 4200 series. More details about the test procedures are provided in Sec. 3.5. The output of the LTC3105 was not constant as specified by the datasheet. Although the output voltage increased as the battery was recharged by the STEG system during the testing period, the effects of solar variability were still observable. This phenomenon casts doubt on the real behavior of any DC-DC converter applied to an open-air solar thermoelectric generation system.
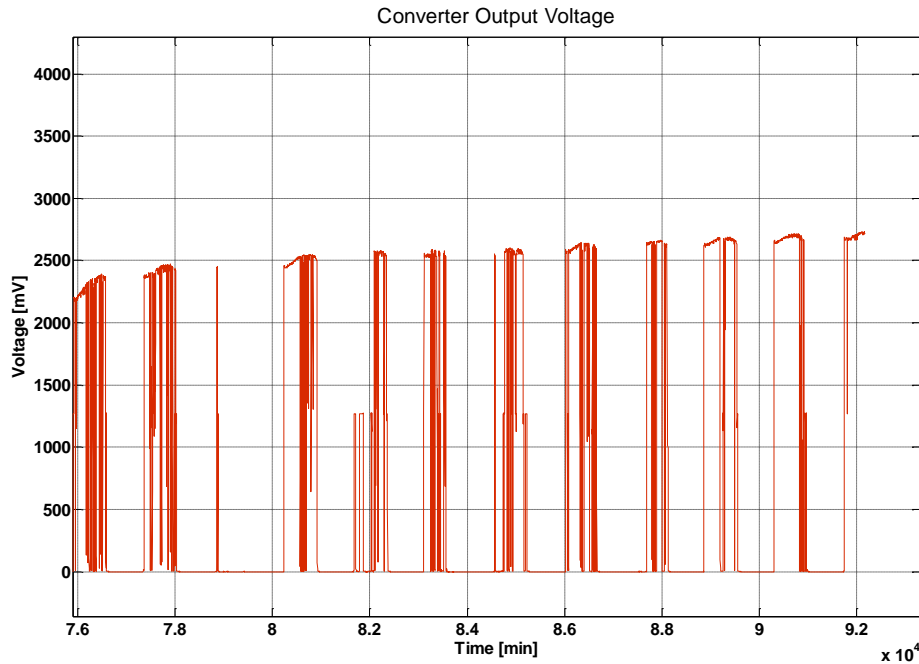
Figure 11 – LTC3105 output voltage

3.4.3.6 Real-world Performance of the LTC3525 Converter

The LTC3525 was compared to the LTC3015 for STEG real-environment performance analysis. Unfortunately, this comparative analysis is far from being conclusive since it did not yield to any significant result. This failure is directly attributable to the fact that the input voltage to the TEGs was not up to the level specified by the manufacturer datasheet. Hence, no further assessment is required beyond this point regarding the LTC3525.

3.5   Battery Tester

Modern battery testers are fully programmable and automated multiple stations for charging or discharging secondary cell (rechargeable battery) systems. They even have the ability to sense the external temperature of the battery or the electrolyte's temperature by means of numerous built-in thermocouple ports. It is important to note that the temperature studies

48

simulate the real-environmental conditions experienced by the system. Performance in different climates, types of crank start in case of EVs, and dependence of EV's acceleration or deceleration versus temperature studies to determine anode/cathode performance during cycling are some of the conditions. Since sensing the temperature of the device under test will prevent irreparable damage, this can enhance the lifespan of the energy storage system. However, energy storage system testing is intended, most of the time, to answer some of the following questions about individual cells and batteries: 1) Is the energy storage device fully charged or discharged?; 2) Does the ESS meet the STC specifications?; 3) What is the device's degree of deterioration in performance?; and 4) What is its life time?

There are basically three methods of ESS testing, i.e. constant current with voltage monitored by a predefined algorithm; constant voltage, but stop charging when current drops to certain predefined value; and the combination of both methods, which is definitely the best way thus far because it guarantees a better lifetime for batteries. Most of the modern smart chargers, such as the Maccor 4200 series, have the capability to combine the aforementioned two methods of battery testing. Still, it should be pointed out that higher voltages augment capacity, but when charging/discharging beyond specifications, the ESS cells deteriorate and deliver a reduced service lifespan.

3.5.1   Special Battery Test Stand: The Maccor 4200 Series

The Maccor 4200 is multifunction and fully automated ESS testing equipment. Many types of products, ranging from batteries and super-capacitors to fuel cells are testable with these types of stands. This Maccor model is so versatile that it can virtually perform any type of sophisticated test. It has 16 channels, and each one can supply up to 5ADC current. Also, each channel can deliver a maximum of 15VDC. Depending on the model or customer preferences,

the Maccor test stand may come with a maximum system charge/discharge power of 2400 Watts. Alternately, if the customer wishes to charge/discharge at a much higher current than specified by the manufacturer, the system can be configured for higher voltages and currents by combining two or more channels. Figure 12 is an illustration of the Maccor 4200 energy storage test stand utilized to purposely check the performance of the 3.2V K2 battery. The batteries were kept in a wooden box located under the table for safety reasons, as can be seen from the same figure. The goal, prior to the real solar investigation, was not only to check whether the K2 battery complies with manufacturer's specifications, but also to assess how these results compare to true solar-environment's performance data.

It is crucial to note that the K2 batteries were selected for this solar design solely because of their availability to us, rather than their being the best of the technologies. Nevertheless, the appropriate batteries, regardless of technology, can smoothly fit in to meet the energy demands of any rural household by connecting the batteries electrically in an appropriate series and/or parallel arrangement to deliver the necessary operating voltage and current levels based on the owner's needs and budget.

Figure 12 – Maccor 4200 ESS test stand

3.5.2 Test Procedures

The Maccor 4200 energy-storage tester comes with Windows-based sophisticated software that has six main Graphical User Interfaces, (GUI). Without going too much into details, some of the important GUIs are: Main Screen, Intermediate Screen, Detail Screen, Build Test, and View Data. To to perform the tasks at hand (either charging or discharging), valid test procedures must be clearly written in accordance with the needs. Hence, when writing any test procedure, it is of a good practice to always start with a *rest state* because it places the channel in an open-circuit mode, safer for both personnel and material. Likewise, it is also recommended to insert a *rest* statement, for at least few seconds, at the end of each command before the next one starts. By obeying these simple rules, both soft and hardware transition smoothly, at no risk, between the major states, such as *charge* and *discharge*.

3.5.2.1 Charge Test Procedures

Table 3 illustrates typical test procedures built with the Maccor Windows based software for the purpose of testing the 3.2V battery. Moreover, the results of this test serve as a benchmark to the open-environment and solar-charging scenario. In addition, this test helps, not only to calibrate the real charging results in terms of the time it takes to fully charge and the energy capacity, but also to indicate whether the STEG system under investigation is technically sound and ready for remote applications in developing regions.

Table 3 - 3.2V K2 battery charge procedures

Step	Type	Mode	Value	Limit	Value	End Type	Op	Value	Goto	Report Type	Value	Options
1	Rest					Step Time	=	00:00:10	002	Step Time	00:00:01	4NNN
2	Do1											
3	Advance Cycle											
4	Discharge	Current	0.75c	Voltage	1.6	Current	<=	0.005	005	Voltage	0.1	4NNN
						Voltage	+	0.05	010	Step Time	00:00:10	
						Voltage	<=	0.45	010	Current	0.005	
5	Rest					Step Time	=	00:00:10	006	Step Time	00:00:01	4NNN
6	Charge	Current	0.5c	Voltage	3.5	Current	<=	0.005	007	Voltage	0.1	4NNN
						Voltage	-	0.05	010	Step Time	00:00:10	
						Voltage	>=	3.55	010	Current	0.005	
7	Rest					Step Time	=	00:00:10	008	Step Time	00:00:01	4NNN
8	Loop1					Loop Count	=	100	009			
9	Rest					Step Time	=	00:00:10	010	Step Time	00:00:01	4NNN
10	End											

3.5.2.2 Discharge Test Procedures

After getting the results for the previous test, *viz.* time span, cycle chart, and voltage level, among others, at the end of the 100th loop count the program was automatically terminated. Additionally, it is worth noting that before charging the battery with the designed STEG energy-harvesting system, another test procedure was required. Therefore, Table 4 lists the most relevant codes necessary to instruct the Maccor 4200 to discharge the battery before the real world-solar test begins. As mentioned above, this program starts with a *rest statement* and then terminates whenever the voltage reaches 1.5VDC if any of the three conditions is fulfilled (See *Go to 008* in Table 4), so as to avoid deep discharge. In the worst case scenario, the test terminates on the 150th loop count after 10 seconds of *rest* time.

Table 4 - 3.2V K2 battery discharge procedures

Step	Type	Mode	Value	Limit	Value	End Type	Op	Value	Goto	Report Type	Value	Options
1	Rest					Step Time	=	00:00:10	002	Step Time	00:00:01	4NNN
2	Do1											
3	Advance Cycle											
4	Discharge	Current	0.75c	Voltage	1.5	Current	<=	0.005	005	Voltage	0.1	4NNN
						Voltage	+	0.05	008	Step Time	00:00:10	
						Voltage	<=	0.45	008	Current	0.005	
5	Rest					Step Time	=	00:00:10	006	Step Time	00:00:01	4NNN
6	Loop1					Loop Count	=	150	007			
7	Rest					Step Time	=	00:00:10	008	Step Time	00:00:01	4NNN
8	End											

3.5.3　Some Test Results

Not all the test results are considered in this section. Only some of the most relevant outcomes are reported here for illustrative purposes. The performance of a commercial K2 3.2V battery is under investigation. Consequently, various tests were conducted in the power laboratory, both on charging and discharging, with the Maccor 4200 ESS tester. Hence, only ½ C-rate and 1C-rate were considered as inputs in the programs' pop-up menu. It should also be mentioned that C-rate is simply a measure that governs the current at which a battery charges or discharges. For example, a 1C-rate means that the whole battery's capacity is discharged in just one hour. For this purpose, the above programs were each run two times in accordance to the number of C-rates.

3.5.3.1 Comparative Charging Graphs

The charging and discharging mechanism's default option is a constant-current type for the Maccor 4200 test stand. As can be seen, all the graphs below were plotted based on the constant-current theory. As already stated, the test started with a *rest period* of fractions of seconds. Therefore, Figure 13 portrays the experimental results of the time period when the voltage stayed nearly constant at 3.2V and the current at 0.36A.
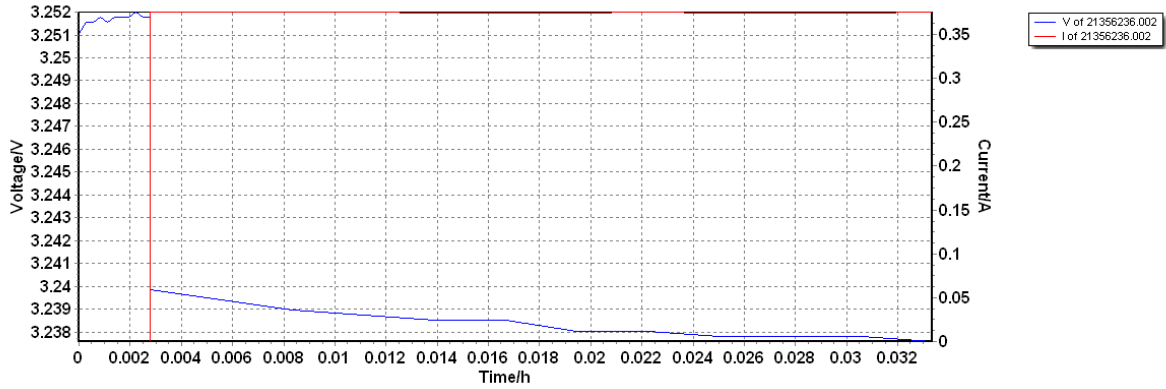
Figure 13 – Short rest time

Figure 14, on the one hand, shows the 1C-rate constant current charging scenario. As can be seen from the abscissa, the experiment took seventy-five hours to complete the cycle of *discharge-then-charge*. Close attention to the graph shows that 78 percent of the time frame was consumed while the system was executing the discharge command. Hence, the next half-cycle began as soon as the voltage and current reached 1.6V and 0A, respectively.
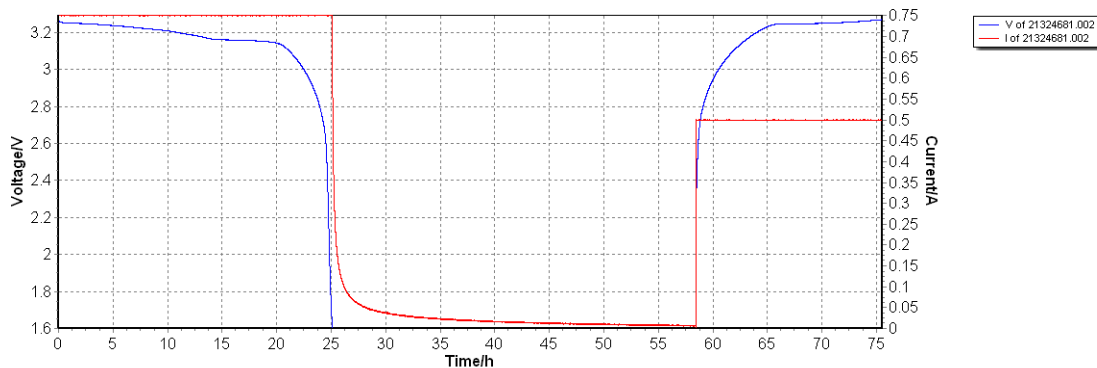
Figure 14 – Constant current charging at 1 C

On the other hand, Figure 15 illustrates the ½ C-rate constant-current charging sequence. This figure is quite different from Figure 14 in many ways. First, this experiment took seven hours less to complete. The direct implication is that injecting a lesser current while charging or discharging a battery has the potential to saving both energy consumed and time spent. The second discovery worth mentioning is that only about 50 percent of the whole time was spent in executing the discharge command. This also reveals a huge discrepancy compared to the 1C-rate's first half-cycle. However, the third finding is that, it took the battery 50 percent more time to be fully charged under ½ C than it took at 1C. So, these events reveal that charging an energy storage system with the Maccor 4200 at ½ C burns enormously more power than the discharging process of the same ESS. Conversely, the opposite is true under 1C-rate. Hence, if we were to only discharge the battery at ½ C-rate, we would have saved twenty-five hours, which represents a real gain of more than a day, compared to the 1C-rate. The difference in electrical power consumed to perform the experiment is tremendous.
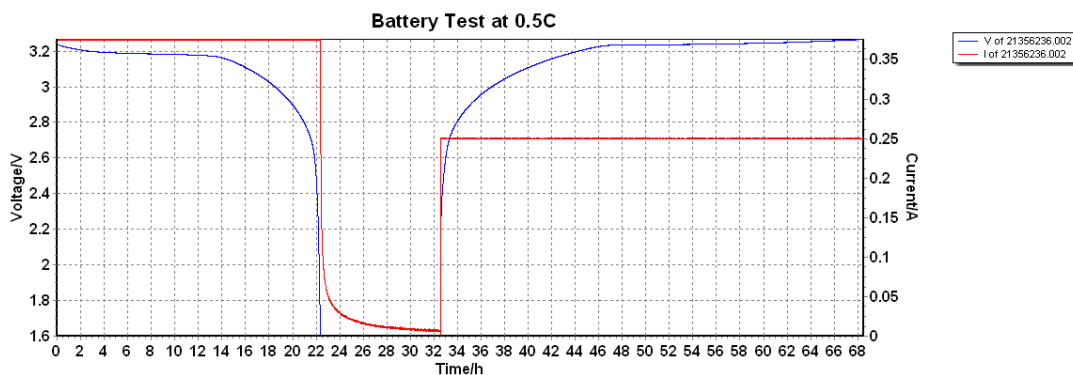
Figure 15 – Constant current charging at 0.5 C

In addition, it can be seen from Figure 16 that different C-rates have, each one, a unique discharge pattern. Interestingly, as can be clearly observed from the graph, it took the Maccor 4200 longer time (or more energy) to discharge the 3.2V K2 battery at 1C than at ½ C-rate. This graph helps to confirm the previous analysis. Thus, these experimental results seem, not only unusual, but also cast a serious doubt on the existing knowledge on battery testing theory. Therefore, a further investigation is required to either re-test a different battery technology or re-write a different programming code, and then re-test the same battery with the same equipment.
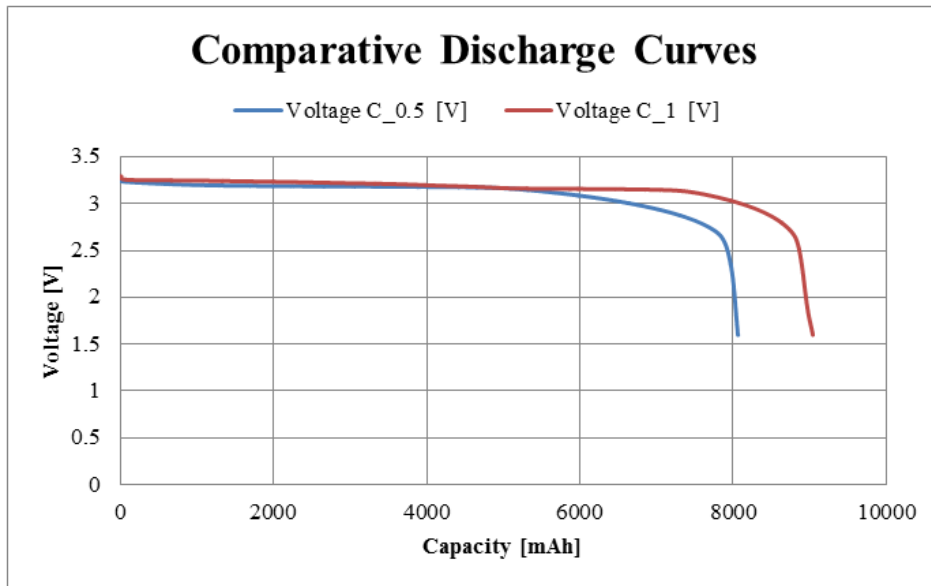
Figure 16 – Discharge at different C-rates

3.5.3.2 Complete Discharge at 1C-rate

As opposed to the K2 battery testing the under various C-rates, Figure 17 simply presents the results of section 3.5.2.2. Additionally, this figure technically highlights the state of charge of the battery prior to the real world charging scenario. As can be noticed from the left side coordinate, the voltage was safely fixed at 1.5V. Likewise, the right coordinate enlightens about the severity of the discharge and the emptiness of the battery in terms of current. It should also be remarked that to achieve the desired goal, more than twenty hours were spent to complete the test. Afterward, the battery was ready to receive new carriers from novel STEG energy-harvesting system.
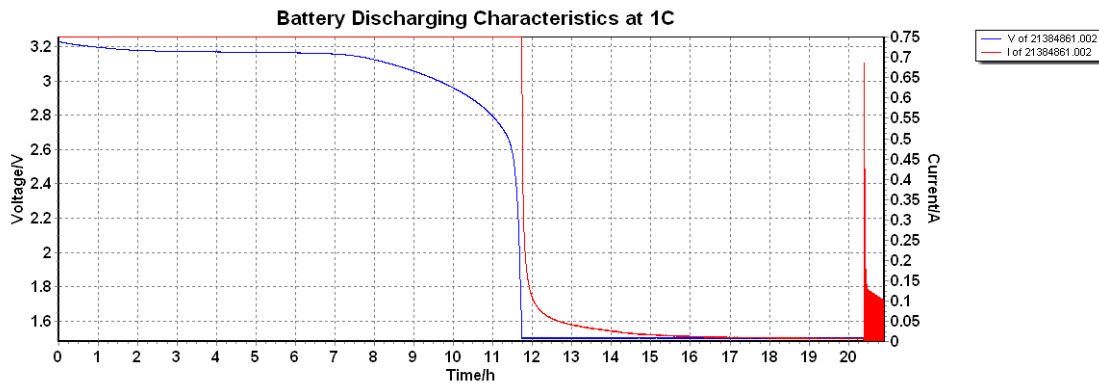
Figure 17 – Constant current discharge at 1C

Finally, the number of cycles necessary for the K2 battery to be completely emptied is shown in Figure 18. This figure helps in showing that none of the conditions set forth in the procedure (*See Sec 3.5.2.2*) were fulfilled prior to the completion of the cycle count.
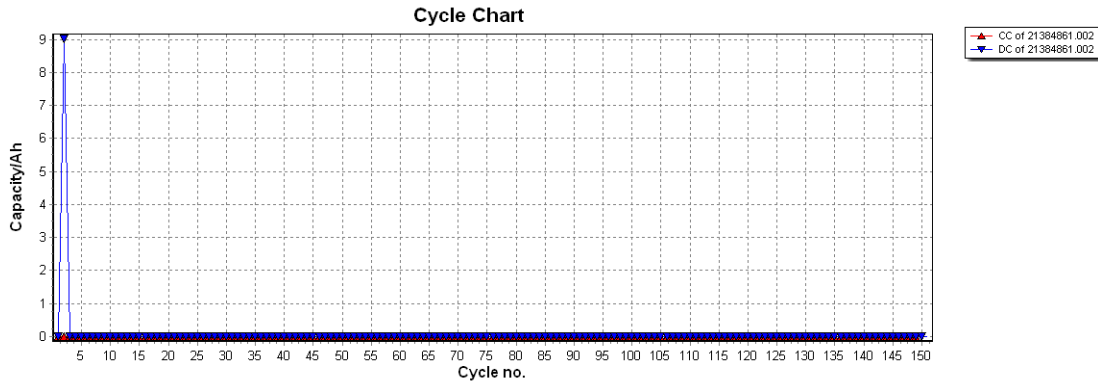
Figure 18 – Discharge cycle chart

3.6 Assessment of Battery Technologies

An energy storage system, such as battery stocks electricity produced by a conventional generator, wind power, solar PV, or solar thermoelectric generator in a different form and then restores it through a reversible electrochemical reaction, when needed, in its original form, by means of an electrochemical oxidation-reduction reaction (redox). In remote residential applications where the electric grid is absent, battery banks, irrespective of the technology, are most frequently used. This section presents an overview on battery basics, including some helpful information on how to maintain and manage them safely.

3.6.1 Types of Batteries

Remote households in developing countries are most of the time with no access to electricity. They often depend on isolated renewable energy systems, such as wind, solar, and thermoelectric generators to meet their daily energy demand. Therefore, in order to optimally utilize these renewable energy systems by providing continuous and reliable power supply, battery buffers play an essential role and are also dependable energy reservoirs.

59

Batteries can be categorized based on size, chemistry, smartness, and functionality as well. Although considerable time and investment are spilled into new battery technologies, there currently exist essentially six types of batteries for commercial usage: 1) Nickel-cadmium; 2) Nickel-metal-hydride; 3) Lead-acid; 4) Lithium-ion; 5) Lithium-ion-polymer; and 6) Reusable Alkaline. Analysis of these types immediately follows, and a short note on smart batteries concludes this section.

3.6.1.1 Nickel-Cadmium

NiCd batteries are a mature energy-storage technology with reasonable energy density invented in 1899. The compound NiCd is utilized to manufacture batteries where long lifespan, high discharge level, and lengthy temperature range is imperative. The active elements of NiCd batteries, in the charge mode, are Nickel Hydroxide (NiOOH) for the anode and Cadmium (Cd) for the cathode. This technology performs better on fast and pulse charge. Additionally, NiCd is one of the rare technologies that performs satisfactorily under challenging working conditions by providing over one thousand (1000) charge/discharge cycles, if it is maintained properly.

The drawback to NiCd technology is that a periodic full discharge is necessary in order to avoid the crystallization of the cell plates that is known as *memory*. The latter effects will severely impact the performance of the NiCd. Hence, it is of a good maintenance practice to periodically exorcize the NiCd to avoid memory. Cadmium is an extremely toxic metal; this toxicity imposes some additional environmental restrictions on the technology's use. It has also the following disadvantages: high self-discharge rate and lower energy density.

3.6.1.2 Nickel-Metal-Hydride

Tremendous time and investment were put in NiMH technology back in the seventies. As a result, this technology was mainly utilized for space applications, such as powering satellites.

Their bulkiness, far from being a limitation, offers them 30 to 40 percent more capacity than the standard NiCd counterpart. Additional advantages are: 1) NiMH batteries are less inclined to *memory effect* than the NiCd technology; 2) they are environmentally friendly though they contain minor pollutants; and 3) they have the potential for larger energy densities.

In contrast to NiCd batteries, NiMH have a shorter lifetime if repetitively deep cycled at higher load currents. After 200 to 300 cycles, their performance starts to significantly deteriorate [71]. Therefore, they are better off under shallow discharge and require frequent full discharge to avoid crystalline formation. Since their advantages outweigh by far their limitations, compared to NiCd, NiMH batteries are more expensive.

3.6.1.3 Lead-acid Batteries

Invented in 1859 by the French physicist Gaston Planté, Lead-acid batteries are the oldest of all types of rechargeable batteries. Lead-acid batteries are the most mature and most economical energy storage technology. These features make them attractive for use in automobiles to provide high startup current [72]. They have proved to be outstanding in power applications where weight is a concern. In addition, they are the most widely used electrochemical energy-storage systems as reported in [73] and [74]. Also, nowadays, lead acid batteries are utilized in conjunction with 1) emergency power systems; 2) stand-alone renewable energy systems, such as PV; or 3) to support wind generators, etc. This energy-storage technology can further be classified as *flooded* and *valve regulated*, also known as sealed [75]. Its main advantages compared to other battery technologies are, as stated in [74], 1) cost-effectiveness; 2) low self-discharge; 3) quick response; and 4) the maturity of the technology. The drawback of this technology is that, the environmental operating conditions tremendously affect its performance to the extent that its lifetime may be significantly reduced [76].

3.6.1.4 Lithium-Ion

Li-Ion batteries, although relatively new energy storage technology, are widely used today since they offer substantial benefits to end-users. Since Lithium is the lightest of all metals, it has not only the highest electrochemical capability, but also the greatest energy-density-to-weight ratio. In addition to that, they are durable, have high specific energy, and can respond quickly to charge/discharge events. Consequently, they have the largest market share of the portable consumer electronic devices, such as cell phones, laptops, and other gadgets. Moreover, Li-Ion's high efficiency and its relatively significant lifespan in addition to its high-capacity utilization at high C-rates render it valuable in the field of emergency power supply applications [77]. Although Li-Ion's chemistry is diverse, it is important to note that the most reliable and most often cited are $LiFePO_4/C$, which stands for Lithium Iron Phosphate (LFP) and $LiMn_2O_4/Li_4Ti_5O_{12}$, which stands for Lithium Titanate Oxide (LTO). The biggest drawback of this technology is the price.

3.6.1.5 Lithium-Ion-Polymer

Li-Ion-P batteries are gaining popularity in both renewable and EV applications because of their high energy and power densities [78]. This technology distinguishes itself from other energy storage systems in the type of electrolyte utilized. A non-conductive plastic-like film both supplants the conventional porous divider and allows the exchange of charged atoms between anode and cathode. Some of their additional benefits include higher safely standard, supple form factor, light weight, just to mention a few.

The drawback with Li-Ion-P batteries is that they are expensive unless mass-produced. In addition to their low energy density, their charge/discharge cycle count is very low, compared to

Li-Ion technology [71]. Also, the use of this dry lithium polymer scheme makes the Li-Ion-P batteries suffer from low conductivity.

3.6.1.6 Reusable Alkaline

Two of the dominant characteristics of Reusable Alkaline (Re-Alk) are narrow cycle life and low load current. However, this technology has a much higher energy density and longer shelf life than other batteries. Re-Alk battery is much cheaper than batteries containing Nickel or Cadmium, but obviously the cost per cycle is much higher. They are also bulkier than Lithium batteries and have a shorter lifetime. Consequently, their higher internal resistance prevents them from lasting longer in applications that require a high startup current.

3.6.1.7 Smart Batteries

Most of today's rechargeable energy-storage systems, such as batteries are of the smart types. Even though the smart batteries appear identical with the other types of batteries, in reality they do possess special built-in circuitry worth further discussion. In fact, smart batteries are manufactured with extra internal microchip which allows them a two-way communication strategy with the charger in order to monitor: 1) the performance of the battery; 2) the output voltage; and 3) the temperature. Thus, the smart batteries instantly provide the smart charger with the charging voltage and current information. They also have the ability to warn the charger about the sate-of-charge (SoC) and when it encounters any problem [79]. Hence, the battery acts as its own charge controller by being the *master* while the real charge controller performs as the *slave*. It is stated in [71] that for an energy-storage system to be labelled smart, it must at least provide a clear indication of the SoC. Some of the main features that make battery smart are 1) the charge controller; 2) the fuel gauge, i.e. the sate-of-charge; and 3) the fault protection [80]. Smart batteries generally run 15 percent longer than regular batteries due to the smart control

over the energy management. Finally, the major areas of application for these smart batteries are 1) defense; 2) biomedicine; and 3) PCs.

3.6.2   The Ideal Technology

The ideal battery energy-storage system would have the following characteristics: 1) infinite energy that will never run down; 2) constant output voltage independent of load current profile and working temperature; 3) internal impedance of zero, which means the battery is not subjected to joule heating; and 4) it has no parasitic elements, such as internal inductance (L) and capacitance (C) which may incur other energy losses.

Based on the above explanations, such a battery technology is purely imaginative. Each of the aforementioned battery types was designed to meet a specific goal, either economic, technical, or both. None of the battery technologies is universal; system owners simply select them based on their needs and means. In addition to these constraints, some battery types may be selected for their small size and longer runtime (the pack will not last for long and wear out rapidly), or large size for a shorter runtime, but with a higher energy rate per second. Besides, another battery pack could be manufactured for a longer lifespan, but would have two major limitations: 1) it will be bulkier and 2) the cost will be higher. In short, a battery pack may offer all the required qualities, but the price might be too high for commercial utilization.

3.6.3   Battery Sizing for a Typical Remote Household

The types of batteries recommended for typical usage in conjunction with solar PV or STEG systems are mainly deep cycle batteries. The deep cycle batteries are explicitly designed to withstand discharge at a very low energy state, say 20%, and to be rapidly recharged in a relatively short amount of time, typically five to six years. Hence, the energy-storage system

(ESS) should be large enough to accumulate adequate amount of energy to drive basic remote household appliances at night and/or on cloudy days.

3.6.3.1 Factors Influencing Battery Sizing

As reported in [81], many factors must be considered in the course of sizing energy-storage systems. Toward that end, only the most important and essential characteristics are addressed in this work. They are: 1) the anticipated household daily kWh of energy consumption and 2) the number of hours or days of autonomy.

Fundamentally, three out of the six aforementioned battery technologies, 1) Lead-acid battery; 2) Lithium ion battery; and 3) Nickel Cadmium battery, are chosen solely to perform the task at hand for their advantages outweigh by far their disadvantages. Additionally, they turned out to be the most promising energy-storage devices and demonstrated themselves to be the most marketable thus far. Besides their cost-effectiveness (low initial cost), they present a greater lifespan though, may require regular service.

Irrespective of the type of battery technology utilized on the solar thermoelectric generation system, the greater battery capacity would more efficiently achieve a net positive aspect. But from an economic standpoint, the larger energy storage system may become relatively too expensive for a remote household in developing regions.

3.6.3.2 Battery Sizing Scenario

Knowledge about existing electricity use and expenditure patterns of remote household in developing regions is essential for proper battery sizing schemes not only to enhance the living standards, but also to alleviate the vicious poverty in rural areas. Without any exception from fundamental Engineering principles, some assumptions have to be set forth as guidelines. In this regard, the average daily household electricity consumption is estimated at about 2kWh [82].

This energy is mainly used for lighting, most of the time in the evenings, although other uses may include 1) watching televisions; 2) listening to the radio; and 3) ventilation for domestic interior comfort.

Therefore, about 2kWh of energy must be stored by the ESS of any rural household in West Africa, South America, and Asia to keep the home lit and comfortable. It is worth pointing out that the average sunlight hours in West Africa, as estimated by the *Programme Regional de Promotion des Energies Domestiques et Alternatives au Sahel* in May 29, 2009, was around 7h per day. As a result, the customer's future battery bank will charge and then supply a continuous amount of energy for a period of 7 hours on a daily basis. An additional assumption is that there is no critical load in those remote areas. So, the daily power requirement, *P*, of the remote residential household is given by

$$P = \frac{E}{t} = \frac{2kWh}{7Hours} = 0.30kW \tag{23}$$

The battery discharge time, t_b, is deliberately set up to be 10 hours, just to be on the safe side, as the nights are longer in winter than in summer.

Hence, the equivalent amount of energy (*E*) required to continuously supply power to the basic appliances during that period of time is determined by

$$E = P \cdot t_b = 3kWh \tag{24}$$

Assume also 12% of combined loss such as charging, discharging, and wiring from the STEG to the load as reported in [83]. Also, a depth of discharge (DOD) of 60% (*assumption*) is factored in since the innovative energy-storage system will only be utilized sporadically during the daytime to charge cell phones and other portable electronic gadgets. Nevertheless, it will be more frequently used during night time from twilight to dawn.

Next, Some small PV panels or STEG are good candidates to run DC lighting in rural residential areas. Consequently, system owners have the ability to safely parallel connect as many 12 volt DC lighting fixtures as needed to the battery bank to meet their lighting needs. These DC fixtures can be directly supplied by the STEG in conjunction with the sized energy-storage system. Therefore, by directly feeding the DC fixtures from the battery bank, the expenses of adding and installing an inverter are automatically reduced. By not having the inverter, energy losses due to inverter conversion activities are minimized as well. That DC lighting fixtures are commonplace, more cost-effective than standard halogen and incandescent lighting fixtures, and much more energy efficient in terms of lumens and lifetime than other technologies for remote applications leads to this simplification. The load on the battery is therefore determined by

$$Battery\ Load\ = \frac{3kWh}{0.88 \cdot 0.6} \approx 5.70 kWh \tag{25}$$

In which, *Battery Load* stands for the actual battery capacity.

Unlike TEGs or photovoltaic modules, which are less affected by ambient temperature variations, a battery's lifetime and capacity are drastically reduced by temperature. Since the annual low temperature in the Sahel is 10°C, which is equivalent to 50 $^{\circ}$F [84], the latter was considered the battery bank's ambient average low temperature, as well. The derate battery bank's factor (*multiplier*) accounting for that is approximately 1.19 [85]. Therefore, the *Battery Load*, including the effects of local temperature, can be estimated by

$$Battery\ Load = Battery\ Load_{Previous} \cdot Multiplier$$

$$= 5.70 kWh \cdot 1.19 = \ 6.78 kWh \tag{26}$$

To have an alternative perspective of the above calculated capacity, a division by the assumed battery nominal voltage, 12V, is necessary to find the actual battery bank. The unit of the subsequent equation is in Ah.

$$Battery\ Load\ = 6.78kWh \cdot \frac{1000}{12V} = 565Ah \tag{27}$$

In order to avoid deep discharge, the control algorithm, or, in some cases, the smart battery bank itself, should prevent the batteries from delivering more than 80% of their nominal capacity. The factor accounting for this strategy is 1.25 [86] as can be seen in Eq. (10). In other words, if 20% of their capacity remains, either the smart charge controller or the smart battery automatically shuts off the energy supply. This technique will not only preserve the lifespan of the batteries, but will also save on frequent maintenance.

$$Actual\ Load = 565Ah \cdot 1.25 = 706.25Ah \tag{28}$$

Consequently, the real battery size required to constantly supply 10 hours of basic energy to any remote residential household in hot and arid developing regions is 706.25Ah.

As a final step, the theoretical equivalent energy capacity, E_{GROSS}, of the battery bank deemed ready to enhance not only the remote house's interior comfort, but also at the same time boosting the living standards of these rural inhabitants, can be determined by Eq. (29).

$$E_{GROSS} = Ah \cdot V = 706.25Ah \cdot 12V \cong 8.50kWh \tag{29}$$

It is worth pointing out that one of the objectives of this study was to investigate ways to increase the number of remote residential households with access to renewable electricity. With that respect, 706.25Ah energy storage systems, independent of the technology, were needed to store approximately 8.50kWh for 10 hours of energy autonomy per day. Hence, the appropriate batteries, regardless of the technology, can smoothly fit in if connected either in series and/or in parallel based on homeowner needs and budget.

3.6.4   Battery Maintenance

This section just provides a small side note on routine battery maintenance, as this topic is out of the scope of the current work. It is as important to maintain a battery as it is to buy it. Proper maintenance prolongs the life expectancy of an energy-storage system and will help assure that it is capable of meeting design requirements. A well-documented battery maintenance guide is a valuable tool in preparing financially and technically for the replacement of the battery in a timely and professional manner [87]. The battery should not only be clean, but also well ventilated in a cool environment, i.e. far away from direct sunlight. For further information about how to maximize the performance and life expectancy of batteries refer to the IEEE 1188-2005 recommended practice for maintenance, testing and replacement of valve-regulated lead-acid (VRLA) batteries. Nevertheless, some good practices are summarized as follows: 1) Performing frequent visual inspection to assess the general condition of the battery bank; 2) Taking corrective action if needed before the next planned maintenance; 3) Reading the cell's voltage because cells of higher temperature will indicate lower cell voltage; 4) Taking frequent temperature readings of each cell and recording them for future comparison, etc.

3.6.5   Real-Environment Battery Charging With STEG System

When a remote load is being fed by solar energy, the diurnal availability of the supply is as important as the nocturnal presence. Unfortunately, the sun only shines on a particular location on Earth some hours and disappears during the night because of the inherent working of the solar system. Hence, the need for energy storage systems, such as batteries arises due to this nocturnal absence of solar energy. Therefore, batteries have long been regarded as a special way to accumulate solar energy during the day to be utilized at night. In short, battery energy-storage systems are mainly needed in combination with solar PV or TEG for two important reasons: 1) to

smooth out any intermittency in the supply and 2) to store the surplus energy for later usage, especially at night.

Figure 19, as opposed to the Maccor 4200 series, shows in the real-world how the K2 3.2V battery is charged by the designed STEG system after being completely emptied of current by the Maccor tester to below 1.5VDC. Additionally, it is important to note that more of the battery's real-performance analysis is treated in great detail in Sec. 4.2.11.
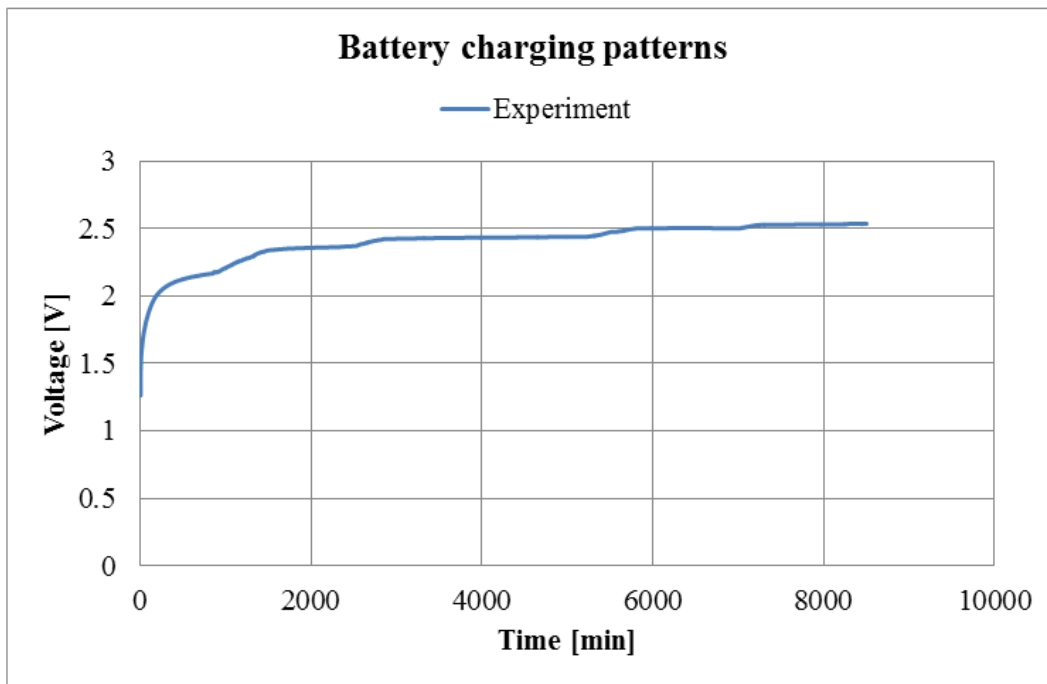
Figure 19 – 3.2V Battery charging from STEG

3.7 Architecture of the STEG Energy-Harvesting System

This STEG system was designed to investigate real solar electromagnetic energy harvesting, i.e., direct conversion of solar heat to DC power for remote residential applications in

developing regions. The system consists of five TEGs connected electrically in series, but thermally in parallel. Figure 20 shows the electrical block diagram of the entire system. The same schematic shows the five series-connected thermoelectric modules attached to the power module. The module is comprised of one DC-DC converter, one charge controller, a battery bank, and a load. The latter is symbolically represented by a DC fan for illustration purposes. It is worth mentioning that both converter and controller are linear technology based products.
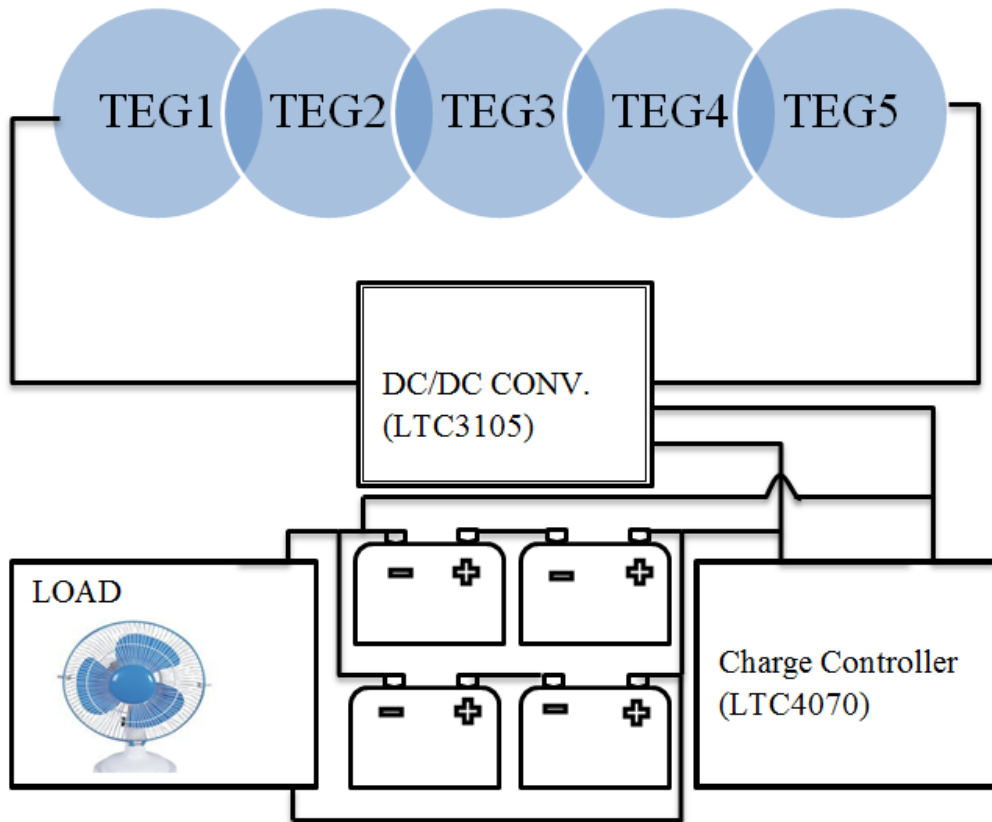
Figure 20 – Electrical block diagram of the STEG system

3.8   STEG Energy-Harvesting System Flow Chart

This part of the study is explicitly dedicated to the outdoor solar harvesting system. The basic steps of the analysis, i.e. the fundamental energy balance equations (Eq. 20), were already covered in Sec. 3.2.4.7. The energy flow chart is presented in Figure 21. The STEGs receive four suns through the collectors that are assumed to be perfect reflectors. The heat exchanger considered in this work is a finned type made of pure aluminum. The overall results in terms of useful power output could have been much better if either a vapor-cooled heat sink or a water-cooled heat sink were utilized, although complications in the modeling and analysis could have increased manyfolds.
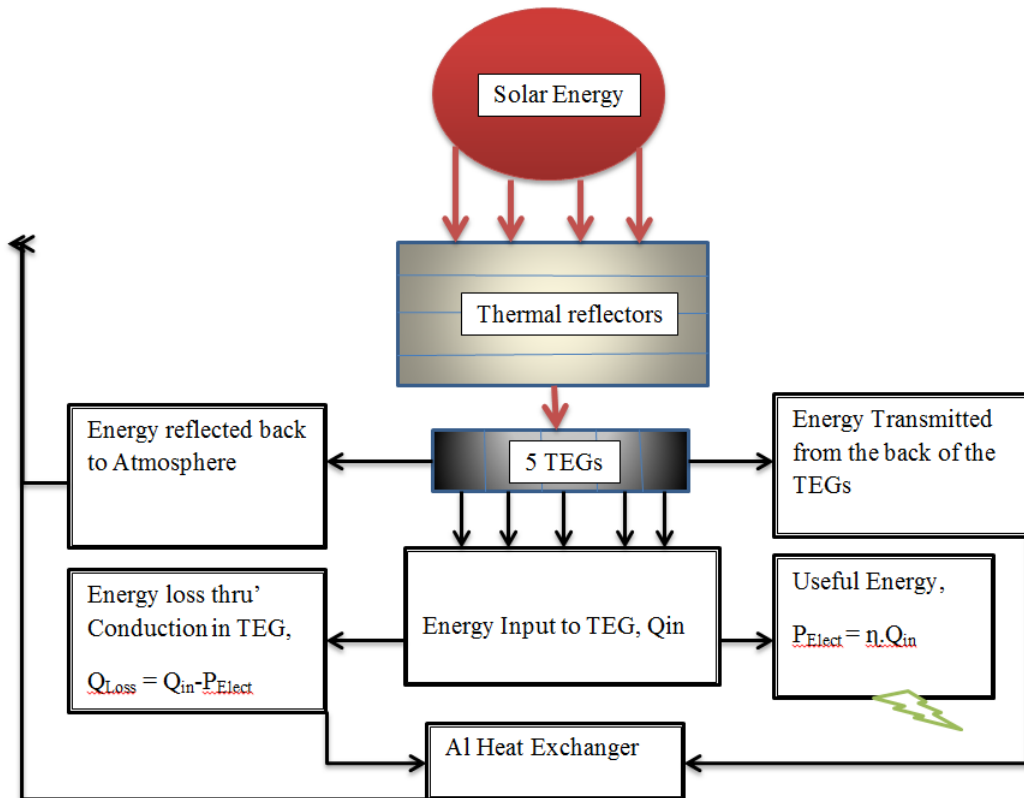
Figure 21 – Energy flow chart of the STEG system

3.9   Battery Economic Analysis

The proper evaluation of prospects for commercial batteries for renewable applications requires sound feedback on current market trends as well as future projections. Generally quoted in the forms of $/kWh or $/kW, the cost of energy-storage devices are often related to the satisfaction of a particular application, although some systems will have a higher cost/kWh of energy, but obviously a lower cost/kW of power than others, or vice versa. It is shown in [83] that the interdependency of the application and its economic feasibility has a lot to do with the aforementioned assertion. In addition to that, the market structure, which is sometimes uncertain and fluctuating, also plays an important role in the economics of certain types of storage technology. According to a recent survey on rechargeable energy storage systems, battery costs have fallen dramatically [88]. This same paper reported that the cost of Li-ion battery packs declined significantly by 14 percent from 2007 to 2014, i.e., from beyond $1,000/kWh to as low as $410/kWh. As a consequence, this significant decrease in price has led to a twofold increase in battery sales per year. Despite the fact that some market-leading battery competitors cost/kWh range from $225/kWh to $300/kWh, the United States Advanced Battery Consortium's (USABC) goal is to cut the cost to $150/kWh in order for the market to grow. Thus, for that to be accomplished, a major breakthrough has to occur in the field of battery technology as a whole. In fact, the US DOE had set for the year 2014 the battery prices for PHEV to be sold at $200 to $300/kWh, which seemingly failed to happen. Obviously, the current prices, ranging from $250-$670, and sometimes as high as $1 000/kWh, are still good estimates.

3.9.1 General Cost Estimation

The battery-energy capacity required to bringing joy, happiness, and security to the hearts of the inhabitants of remote residential households was estimated to be 8.5kWh. So, by considering the $410/kWh [88] of storage for simplicity, confirmed by the survey published in *Nature Climate Change*, the battery bank, irrespective of the technology, could be purchased as

$$Battery_{Cost} = \$410/kWh \cdot 8.5kWh \approx \$3,485 \qquad (30)$$

As can be observed, the price of the battery pack necessary to procure approximately 2kW of power each hour for ten hours is exorbitant and unaffordable by any typical rural inhabitant.

3.9.2 Comparative Cost Analysis

This section focuses on the comparison of two major battery chemistries: Lithium Ion (*Li-Ion*) and Lead acid. The analysis is based 8.50kWh of energy storage previously calculated for remote standalone solar TEG energy-harvesting system. The application needs can simply be summarized in Table 5.

Table 5 - Energy-storage system specifications

	Battery Specifications	Values
1	Estimated Energy Storage	8.50 kWh
2	Running Time	10 hours
3	Discharge Power	0.85 kW
4	Cycling Frequency	1 charge-discharge/charge/day
5	Average ambient Temp.	25°C
6	Life Expectancy	1900 Cycles (5.2 years)

The transportation and installation fees per kWh of energy-storage systems, in this case Li-Ion and Lead-acid, in hot and arid regions were estimated by Albright et al. [89]. Hence, Table 6 lists these two major secondary financial parameters. Additionally, an important parameter to consider in this comparative assessment is that Li-Ion is 2.5 to 3.5 times energy-denser than Lead-acid [89] and [90]. Also, the discharge rate is 85 percent for Li-Ion compared to 50 percent for Lead-acid battery. These factors will dramatically not only influence the overall cost-benefit estimates, but also affect the way customers perceive the commodities.

Table 6 - Comparative delivery and installation fees

	Lead acid (Hot climate, 25 to 35°C)	Li-Ion
Installation	$20/kWh	$3.6/kWh
Transportation	$28/kWh	$5/kWh

Therefore, based on the estimates of 8.50kWh of desired energy storage, the installed capacity of Lead-acid battery pack is 17kWh since this technology is only good for 500cycles at 50% DOD. Moreover, the Lead-acid solution-base must be replaced once for temperate climates and three times for hot and arid climates due to its inherently lower energy density [89]. However, based on the same aforementioned estimates, Li-Ion solution-based batteries are not only a one-time investment, but also represent 60 percent more than Lead-acid batteries' energy capacity. So, in terms of kWh, the Li-Ion battery's installed capacity is 9.775 for 1900 cycles at 85% DOD.

Finally, to better understand this introductory energy business model, we need to further estimate the cost per cycle. The measurement unit of the cost per cycle is $/kWh/Cycle. Thus,

the following computations clearly simplify the procedures. The total cost of Lead-acid battery is calculated by

$$Total\ Cost_{Lead-acid} = \left(\frac{\$}{kWh} + Trans + Instal\right) \cdot Num\ of\ Replacement$$

$$= \left(\left(\frac{\$125}{kWh} + \frac{\$20}{kWh} + \frac{\$28}{kWh}\right) \cdot 17kWh\right) \cdot 4 = \$11,764 \tag{31}$$

Where, *Trans*, *Instal*, and *Num of Replacement* stand for Transportation cost, Installation cost, and the Number of time a new ESS is needed, including the first install.

The cost per kWh per cycle is estimated by dividing the above product by the net energy throughput of the selected storage system in question, the total number of cycles per year, and the duration of the project, as in Eq. (32).

$$\frac{Cost}{kWh \cdot Cycle} =$$

$$\frac{TotalCost_{Lead-acid}}{Useful\ capacity \cdot Total\ number\ of\ Cycles \cdot Number\ of\ years\ of\ use}$$

$$= \frac{\$11,764}{8.5 \cdot 365 \cdot 5.2} = \frac{\$0.72}{kWh \cdot Cycle} \tag{32}$$

The total cost and cost per kWh per cycle of the Li-Ion battery can also be assessed in a similar manner. The results are summarized by Eq. 33 and 34, in that order.

$$Total\ Cost_{Li-Ion} = \left(\left(\frac{\$410}{kWh} + \frac{3.6}{kWh} + \frac{5}{kWh}\right) \cdot 9.775\right) = \$4,092 \tag{33}$$

Correspondingly, the cost per kWh per cycle of the Li-Ion technology for the entire period of 5.2 years is given by

$$\frac{Cost}{kWh \cdot Cycle} = \frac{\$4,092}{8.5 \cdot 365 \cdot 5.2} = \frac{\$0.25}{kWh \cdot Cycle} \tag{34}$$

In sum, the lifetime cost throughput of Lead-acid battery and Li-ion battery are found to be $0.72 per kWh per cycle and $0.25 per kWh per cycle, respectively. These results revealed

that lithium-ion is much more cost effective in hot and arid climates than lead-acid batteries. So, despite its higher initial upfront cost, Li-Ion has the lower $/kWh of energy charged and/or discharged. This fact is attributable to many factors, such as the higher intrinsic energy density, lower delivery and installation costs, and Li-Ion batteries' stability over Lead-acid technologies at temperatures lower than or sensibly equal to 50°C.

3.10   Conclusion

This work designed, built, and tested a solar thermoelectric generator system. Thermal-to-electrical analogy schemes were adopted to simulate the designed energy-harvesting model by means of the LTspice simulator software. Besides the most commonly used thermal-to-electrical analogies presented in this section, the seven most fundamental steps of parameters' extraction were also elucidated succinctly as a core and genuine part of this work.

In addition, as part of the performance analysis of the commercial solar TEGs, the real effects of solar energy on DC-DC converters was not only investigated, but also demonstrated for remote applicability purposes under both indoor and outdoor conditions and hot and arid weather conditions. Likewise, the performance of the Maccor 4200 battery tester was verified under various C-rates and then compared to the real solar-environment battery-charging events.

Finally, in order to successfully store the harvested energy in durable and efficient manners, the major rechargeable battery technologies were thoroughly evaluated and compared in terms of intrinsic qualities and overall cost-effectiveness.

Chapter 4: Experimental Verification and Results

In order to acquaint ourselves with the theory and the physics behind TEM technology, the research was first divided and then conducted into two separate but interrelated phases. The primary research was conducted in one of the ECE laboratories whereby a thorough understanding was sought, developed, and acquired at the end of the experiment. In addition to that, the secondary and most challenging complete solar energy-harvesting system was set up on the roof of the TBE-B building in order to both apply the fundamental knowledge attained and to put into practice our understanding of power and renewable systems in general.

Finally, how closely the experimental and simulated results match one another may be subjected to some minor errors. Under a certain threshold point, however, the error rate is considered insignificant or acceptable and consequently, the proposed model is validated. Due to the complex device geometries and the different material properties of the parts associated with the system, the thermal-to-electrical analogy is difficult. Any inaccuracy can be explained by either one or both of the following: 1) the internal parasitic components' variation, and/or 2) the non-homogeneity of the physical blocks that were assumed to be of pure metals during the thermal-to-electrical parameters computations.

4.1   The Indoor Test Stand Description

For the purpose of this study, one thermoelectric manufacturer's TEM was selected, i.e. *Custom Thermoelectric* [66]. The particular device's model number is 2411G-7L31-15CX1. Basic specifications for this TEM were supplied by the manufacturer and the other parameters used in the model were extracted in a concurrent work [91]. That the aforementioned internal parameters, although given as a constant factor, were revealed in [58] to vary over time with

temperatures is worth pointing out. Hence, in order to achieve accurate results, these variations were accounted for in the model presented.

4.1.1 Indoor Experimental Setup

The module was originally configured to operate as a TEG, but for this specific investigation and to accommodate the current needs, it was first run as a Thermoelectric Cooler (TEC), which is the same as a heat pump. To achieve that, the polarities of the TEG were reversed in order to constrain it to function as a TEC. The purpose was to create a temperature differential on each side of the device by applying a stepped 5 VDC, as depicted in Figure 24.

The experimental setup is illustrated by Figure 22. The experiment included the following items: 1) one TEM; 2) two K-type thermocouples; 3) two aluminum (Al) plates having dimensions of 56*mm* by 56*mm* by 12.7*mm*; 4) one data-logger; 5) one Variable DC power supply; 6) an insulation chamber in order to minimize the effects of the ambient temperature; 7) a laptop; 8) a two-way switch (SW); 9) two resistors; and 10) wires. The TEM was sandwiched between the Al plates.
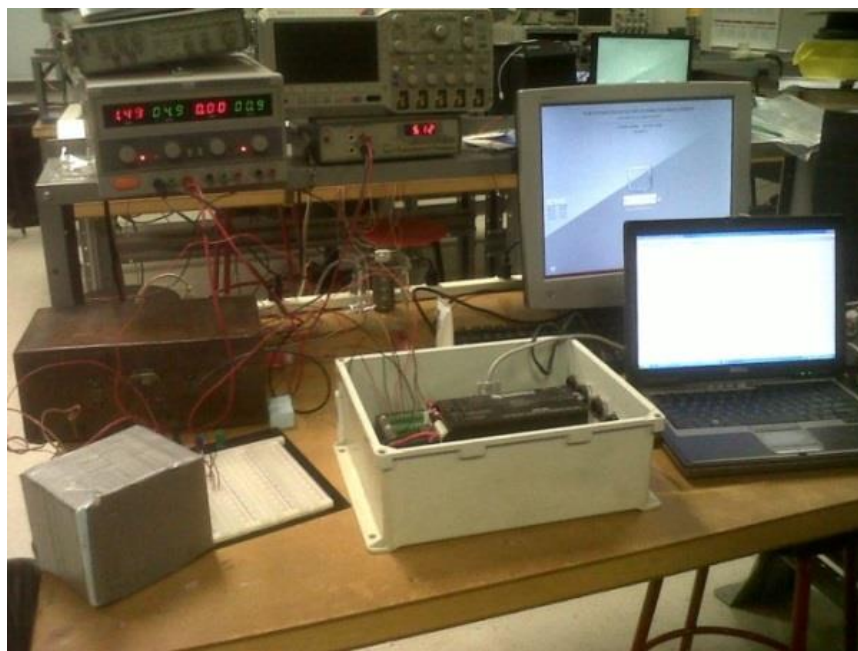
Figure 22 – Indoor experimental setup

Between the two aluminum plates and the two sides of the TEM, heat transfer grease was meticulously applied. The thermocouples for temperature measurement were located one on each side of the module. These sensors were first engraved into the Al plates via a U-notch groove made by an automatic milling machine. Through the laptop computer connected to the logger as depicted in Figure 22, the data were collected and further arranged in a tabular format through the loggerNet software. The 1.7Ω resistor, as seen in the schematic depicted in Figure 23, served to determine the multiplier ($1/R$) needed to record the current through Ohm's Law. The second variable resistor was used as a load. It should be noted at this point that maximum power is transferred only when the internal resistor and the load match each other. Finally, a programming code was written and transferred onto the data-logger through the computer. The code is used to facilitate communications between the data-logger and the devices.
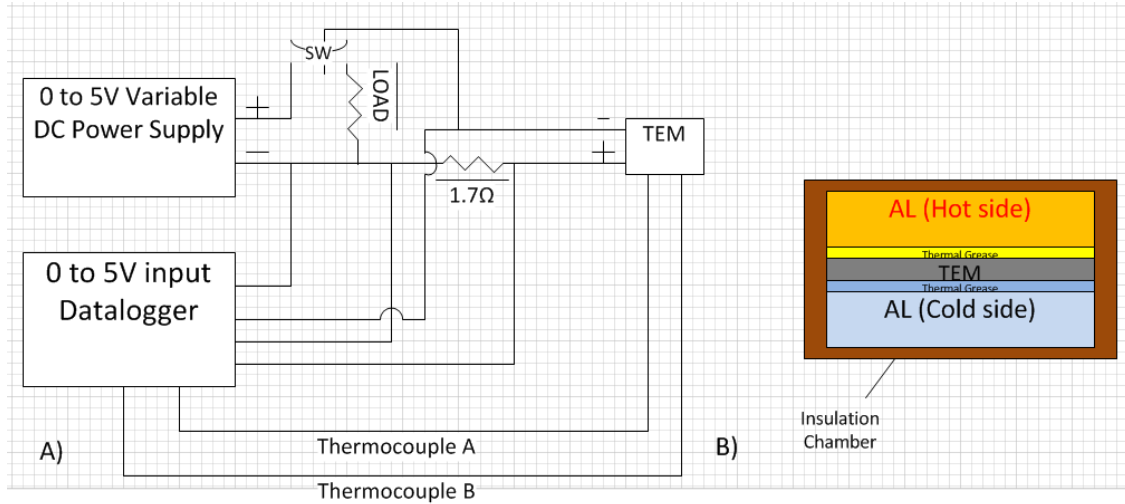
Figure 23 – Block diagram of the setup: a) electrical and b) thermal diagrams

4.1.1.1 Applied Stepped DC Voltage

As mentioned earlier, Figure 24 portrays the applied stepped 5 VDC needed to ran the TEG as a heat pump to achieve the desired experimental goals. These primary but fundamental goals were meant to create a meaningful differential temperature across the TEM device not only as a solid foundation for the current work, but simultaneously as a way to apprehend the Peltier effect in a real test environment. Another significant purpose of this indoor experiment was to first characterize the device, as to whether or not it performs as postulated by manufacturer's datasheet, and to get researchers accustomed to this technology before analysis. As can also be seen from Figure 24, after reaching the maximum allowable voltage that the data-logger could handle, i.e. 5V, the supply was kept constant for a while, so as to reach thermal steady state conditions, and then cut off afterward.
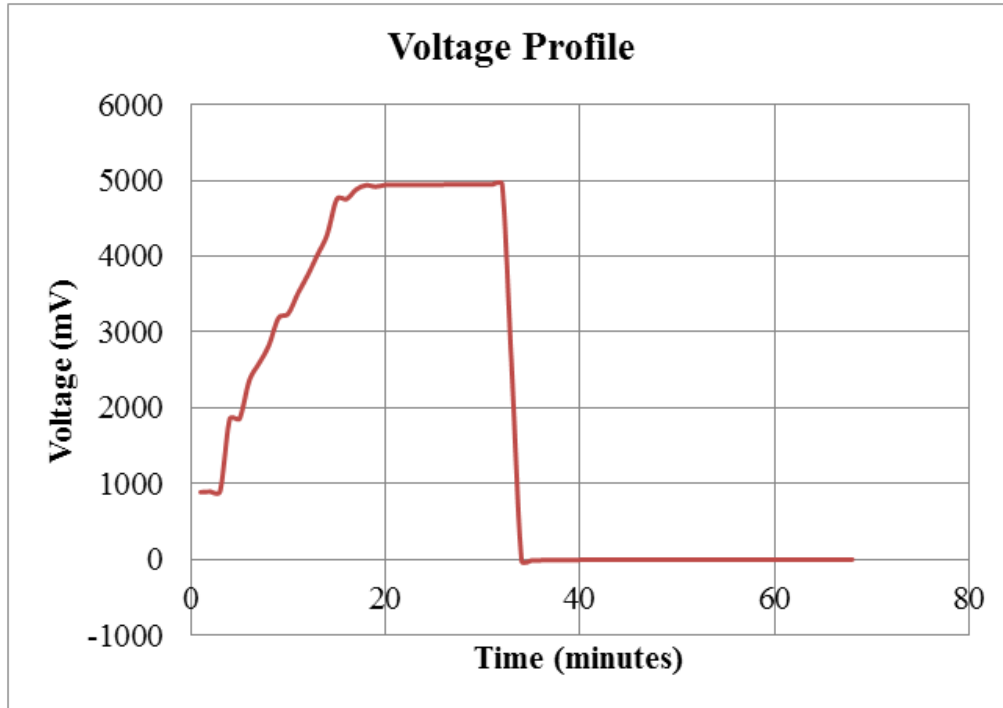
Figure 24 – Applied stepped 5VDC

4.1.1.2 Profile of Drawn Current

Figure 25 illustrates the experimental current drawn by the system. As can be seen, there is a linear relationship between the current drawn and the applied voltage, thus confirming Ohm's Law. The maximum current drained by the system at steady state is approximately 75 percent of an Ampere. Therefore, these two variables help to determine the exact amount of power consumed over the short period of time (32 min) during which the test was conducted.
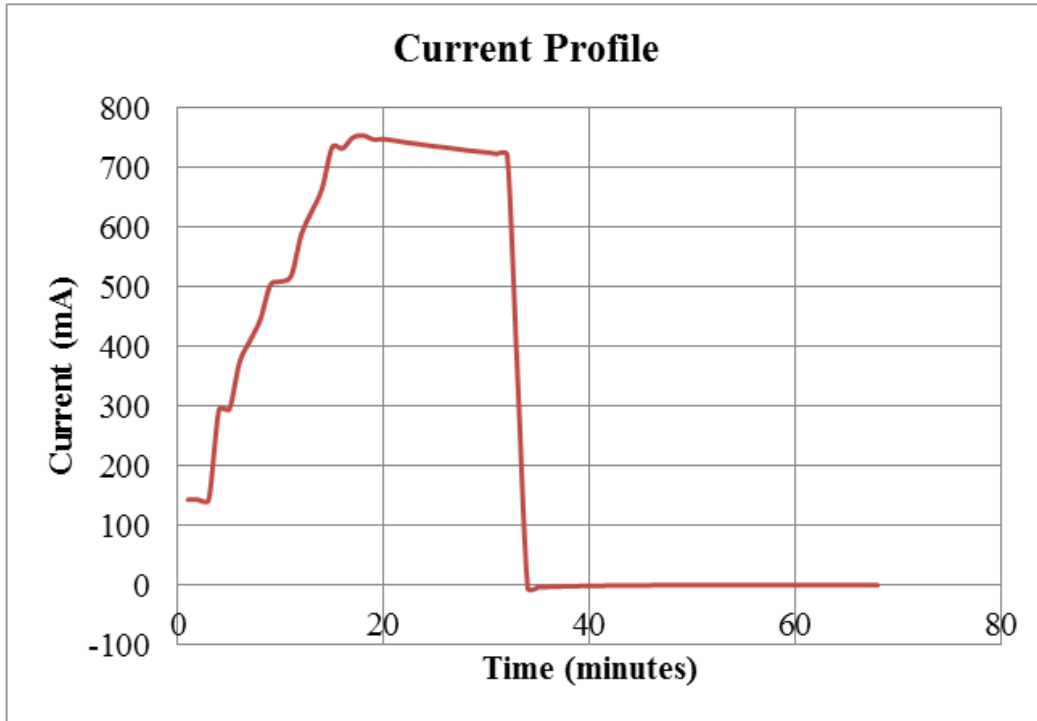
Figure 25 – Current profile

4.1.1.3 Power Consumed

As power is the rate of doing work, it can be clearly seen from Figure 26 that the TEG system has consumed, under reverse polarity techniques, a significant amount of energy per unit time in order to perform as a heat pump in accordance with the Peltier theorem. Hence, from basic circuit theory, since power is the product of voltage times current, the shape of the power burned to do the intended work followed the identical combined pattern of the two previous profiles.
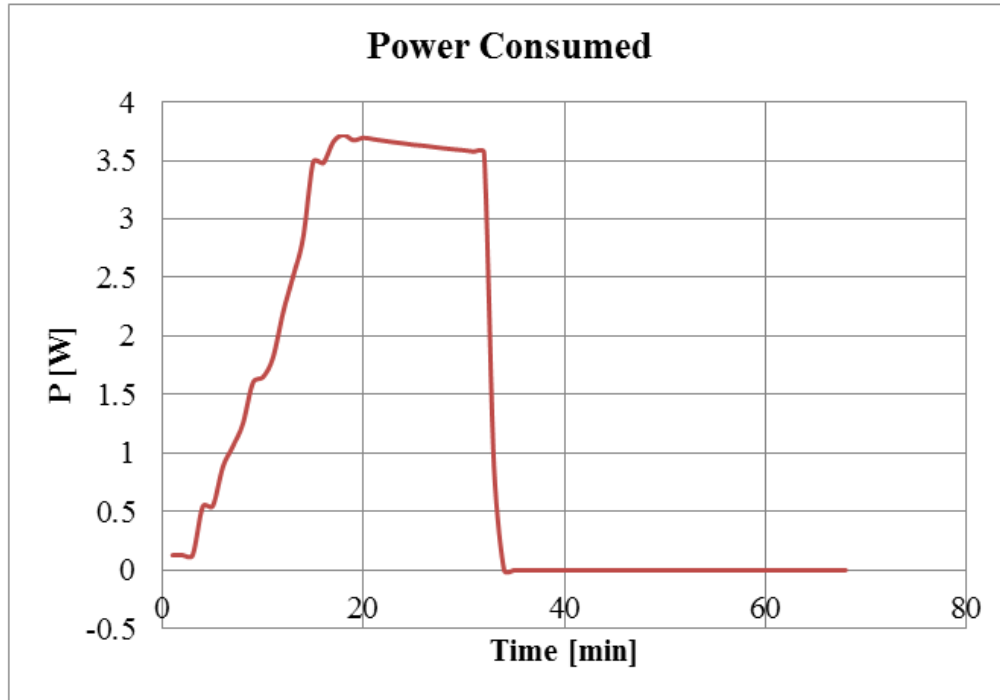
Figure 26 – Power consumed

4.1.2 Model Implementation

It is worth noting that a couple of assumptions were made in order to facilitate the simulations presented in this work. A lookup table of real experimental data was fed into the circuit to improve simulation speed. Due to the complexity in the geometry of the insulation chamber used and the corresponding longer time constant, the thermal capacitance value associated with the chamber was neglected. Again, the resistance of the thermal grease was assumed to be $0.45 K.W$ based on previous studies [57] and [35].

The specific placement of the 23 *J/K* internal heat capacitance of the TEM was a concern [91]. The heat capacitance could either be placed on one node or distributed equally between the hot and cold sides. After a few trial simulations, it was clear that the latter yielded better results.

The proposed model based on a current-dependent source is presented in Figure 27. It is an improved version of the circuit presented in [35]. The latter model had the drawback of not utilizing the thermal resistances of the Al plate heat exchangers located on the two sides of the thermoelectric module.

It is of a paramount importance that some parameters be explained at this stage of the study. The model was implemented using the LTspice software [92] and the work done in [35]. The parameter "Seb" in the model stands the Seebeck coefficient. Likewise, "R_{Grease}" and "C_{Al}" represent the thermal resistance and thermal capacitance of the thermal grease and the Al plates, respectively. The thermal resistances of the hot and cold side Al plates are represented by "R_8" and "R_9". Similarly, "R_{Insul}" with a value of 5.9 *K/W* is the thermal resistance of the insulation chamber, whereas the internal electrical resistance of the TEM, "R_{Int}", is 2.4Ω. Also, "R_{Ther}" refers to the thermal resistance of the TEM (*here 0.6365 K/W*), as was determined from the datasheet. The heat capacities of both the ceramic plates and the semiconductor material (Bi_2Te_3) were summed and then equally split into two 12.5 *J/K* capacitances [91]. Each capacitance was then placed different side of the module for thermal equilibrium purposes. They were represented by C_4 and C_5, as shown in Figure 27. The values of the parasitic components, capacitance C1 and inductance L1, were borrowed from previous work reported in [35] because they cannot be determined with the available equipment.

.params R_Int = 2.4 R_Ther = 0.6365 Seb = 0.0534 Tamb = 27 C_Al = 96.53 R_Insul = 5.9 R_Grease = 0.45 Off = 0 Val = 2 Freq = 100k

.tran 0 500s 0

.save V(Te) V(Ta)
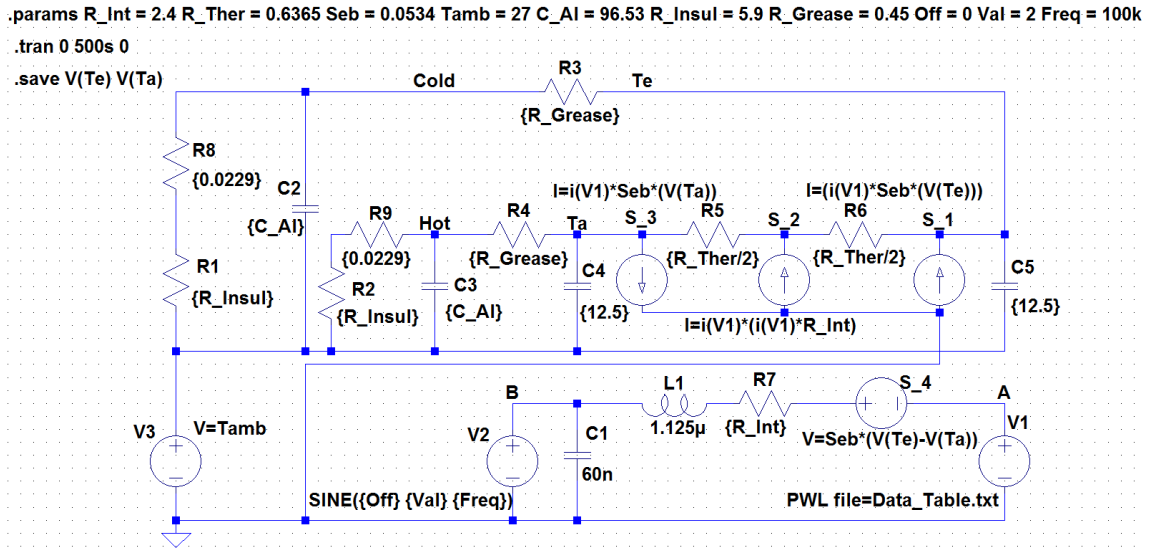
Figure 27 – LTspice model of a TEM with the internal parasitic LC values

4.1.3   Results and Analysis

This section presents the outcomes of the study, on one hand, and a comparative analysis between the experimental results and theory developed thus far, on the other hand. It is worthy to note that this improved model was run as a TEC under the reverse polarity feature rather that a TEG. Thus, the results of the earlier models (TEG) were expressed in terms of voltage whereas the outcomes of the current model are in degrees. Therefore, a direct comparison between the two models is solely excluded in this analysis for simplicity purposes.

The experimental measurements were taken in the period of approximately half an hour, say 1920 seconds. The necessary voltage values used to simulate the real behavior of the heat pump were organized in a table and stored for the simulation in a text file, labeled as *Data_Table.txt* in the LTspice simulation schematic seen in Figure 27. It is worth mentioning that the length of the simulation was 500 seconds since longer simulations can take a considerable time to run.

A significant temperature difference was developed across the two sides of the thermoelectric module as can be seen in Figure 28. The maximum differential value attained within that short period of time was $13.43^{o}C$, as illustrated by the green curve. Indeed, as expected, the TE device performed as a heat removal device, that is, it worked as a perfect TE cooler.

So, during the course of this study, it was clearly observed that the hot and cold sides were continuously departing from one another with the former absorbing heat and the latter releasing it to the surroundings, as can be seen from Figure 28. This fact holds for not only the period whereby the applied voltage was increasing in a step by step fashion, but also for the whole period that it stayed constant at 5 VDC, as stated earlier.
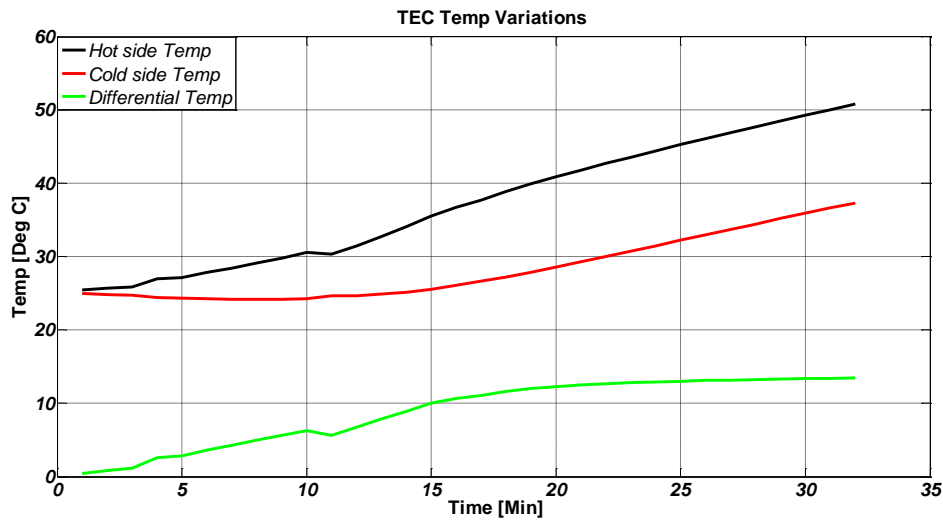
Figure 28 – Experimental temp profile on both sides

In contrast, as can be observed from the coordinate-axis of Figure 29, simulation results express temperatures as voltages. Also, as already stated above, the simulation time was shorter than the actual time. In a like manner, the hot and cold sides were continuously departing from one another as thermal energy is being increasingly supplied to the bottom and removed from the top.
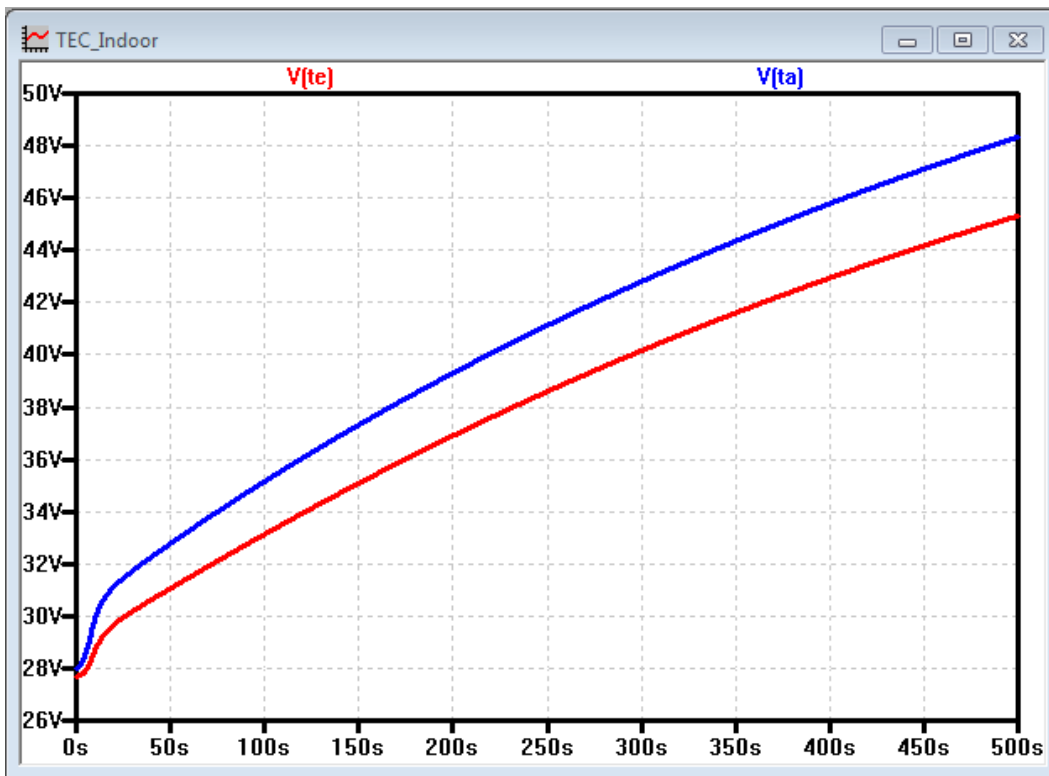
Figure 29 – Simulated temp profiles: 1) V(ta) represents the hot side and 2) V(te) stands for cold side

Finally, Figure 30 compares the experimental results against the simulated results. The overall percent error between the experiment and the Spice simulation was 5.47% on the hot side as compared to 2.52% on the cold side. The error rate can be explained by either one or both of

the following: 1) the internal parasitic components' variation and 2) the non-homogeneity of the physical blocks that were assumed to be pure metals during the thermal and/or electrical parameters computations [61] and [91].
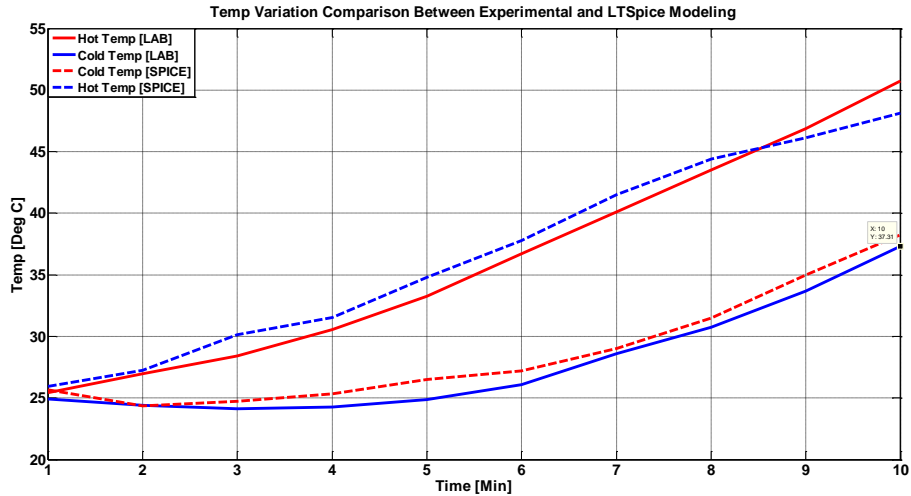
Figure 30 – Temperature profiles: 1) simulated (dashed) and 2) experimental curves (solid)

4.1.4 Summary of the Indoor Experiment

An experimental setup was designed and built to characterize and study the performance of a commercial thermoelectric module (*TEM*). An LTspice TEM modeling scheme was developed through thermal-to-electrical equivalence strategies. The module, though manufactured to be operated as a thermoelectric generator (*TEG*), was run in this preliminary work as a thermoelectric cooler (*TEC*) under the technique of the reverse polarity features. The experiment was conducted for a short period of time (32 minutes) with a variable input DC supply voltage starting at 0.8VDC. The DC source was incremented by 0.5 V every minute until the maximum limit of 5 V DC was reached. At the end of the experiment the data were arranged

in a lookup table and then fed into the LTspice model through the piecewise linear (PWL) built-in command. Despite the test being conducted for a short period of time, a significant differential temperature (ΔT) of 13.43°C was achievable. Finally, the experimental and simulated results were presented, compared, and concisely contrasted.

4.2   Solar Thermoelectric Generator (STEG)

New alternatives and inventive renewable energy techniques which encompass both generation and power management solutions are fundamental for meeting remote residential energy supply and demand today, especially if the grid is quasi-nonexistent. Solar thermoelectric generators mounted on a dual-axis sun tracker can be a cost-effective alternative to photovoltaics for remote residential household power generation. A complete solar thermoelectric energy-harvesting system is presented in this work for energy delivery to remote residential areas in developing regions. To this end, the entire system was built, modeled, and then validated with the LTspice simulator software via the thermal-to-electrical analogy schemes. Valuable data in conjunction with a novel LTspice circuit were obtained, showing the achievability of analyzing transient heat transfer with the Spice simulator; however, a few practical problems remain to be solved. Nonetheless, despite the unusual operation of the thermoelectric modules with solar radiation, the simulation and measurements agreed, thus validating the new modeling strategy.

In addition, any discrepancy in the outcome could be attributable to some minor undetectable errors of imperfect interconnections and/or incompatibilities at a microscopic level. The overall efficiency and system performance sought turned out to be counter-intuitively below research expectations. How heat is lost in the system due to the material defects certainly played a key role as different manufacturers may have different quality standards. This latter point is schematically addressed in Sec. 3.8 in an energy flow chart.

4.2.1   Pre-Design Considerations

The design of a solar thermoelectric generation system from scratch has never been free from challenges in terms of transient heat transfer analysis and the amount of heat to be converted into electrical power. One of the key challenges worth mentioning in solar thermoelectric power conversion is how to achieve a significant differential temperature across the TEG devices only using the local direct normal insolation (DNI). The STEG system would likely utilize the infrared (IR) portion, which is about 42% of the solar spectrum, to achieve the ΔT needed to supply power to remote households. Hence, the temperature drop across the devices would have been, under certain specific conditions, in the range of 1—5$^{\text{o}}$C [52], if exclusively based on the conventional heat conduction, whereby

$$\Delta T = \frac{qL}{\kappa} \tag{35}$$

Where, q is the heat flux traversing the TEG, L is its length, κ is the thermal conductivity, and ΔT is T_H (*hot side temperature*) minus T_C (*cold side temperature*).

Obviously, the above temperature drop would have been too small for efficient power generation. In order to differ from the conventional wisdom in terms of TEG, which stipulated that thermoelectric modules (TEM) were only good and suitable for waste heat recovery, the aim of this study, as already mentioned above, is twofold: 1) to demonstrate that TEGs remain an attractive renewable technology that can convert solely solar irradiance into electrical energy for energy delivery to remote residential areas; and 2) to show that STEG's transient heat transfer analysis through thermal-to-electrical analogy by means of the LTspice simulator in comparison to the traditional analytical methods can not only be achieved, but can also greatly simplify the task at hand by improving the system's overall understanding.

4.2.2 The Main Components of the System

As reported in [2] and [93], the complexity of any engineering system comes not from the multitude number of parts, but rather from the inner complexity of each single unit. Having that concept in mind, in designing an STEG, there are many more complexities that must be meticulously considered. In essence, each single unit must be assessed thoroughly and separately, and then evaluated in conjunction with the rest of the system as a whole. Hence, the major components are: 1) the sun, as the only source of energy; 2) a dual-axis solar tracker; 3) 5 TEG modules; 4) a Pyrheliometer, for recording the local DNI; 5) a Solar flux sensor, for estimating the four sun coming off the collectors; 6) two aluminum heat exchangers, details are in Sec. 4.2.5; 7) two K-type thermocouples; 8) one data-logger; 9) a DC-DC converter; 10) one 3.2 volts battery, for storing energy; 11) a charge controller; 12) wind speed/direction sensors; 13) a relative humidity sensor; 14) and thermal insulation foam, just to mention the major units.

4.2.3 Descriptive Functionality of the Fundamental Components

This work designed, built, and tested a solar thermoelectric generation system. Figure 31 and Figure 32, together illustrate the actual STEG setup and the equivalent schematic overview of the system, respectively. The former depicts the complete proposed energy-harvesting system under investigation. Five commercial TEGs, 2411G-7L31-15CX1, made by *Custom Thermoelectric* with a size of 56 by 56 millimeters were tested for energy delivery to remote residential areas in developing regions. The five TEGs were all connected electrically in series and thermally in parallel. Above the cold side of the TEGs was a customized aluminum HEX, which not only removes the heat, but also provides an adequate differential temperature across the TEGs. Along the focal point of the tracker was a solar flux sensor. It was intended to measure the magnitude of the four suns, obviously different from the DNI recorded by the Pyrheliometer.

The secondary HEX was utilized to cool the flux sensor. The rest of the components mounted on a separate iron structure built for the purpose are the relative humidity sensor and wind speed and direction sensors, as can be seen on the right hand side of Figure 32. The output of the TEGs, the two thermocouples, and the Pyranometer in conjunction with all the sensors, were all connected to a data-logger. A laptop was utilized in order to collect the experimental data once a week. Knowledge of the *DNI*, relative humidity, the wind speed and its direction, tell us how the local weather affects the instant, average, and total power generated by the energy-harvesting system. Finally, the battery energy-storage system is meant to store the harvested energy for a later usage.

Figure 31 – Complete STEG energy-harvesting system

4.2.4 System Schematic and Short Research Overview

The schematic overview of the investigated solar TEG energy-harvesting system is presented in Figure 32. This schematic helps not only to better understand the design as whole, but also to better distinguish the physical separations between the thermal and the electrical aspects. Possible methods to enhance the system's efficiency, understand its functionality, and optimize its performance, i.e. the heat transfer capabilities between the top and the bottom surfaces, were investigated as well. The thermal-to-electrical analogy scheme was adopted to simulate the designed energy-harvesting model by means of the LTspice simulator software.
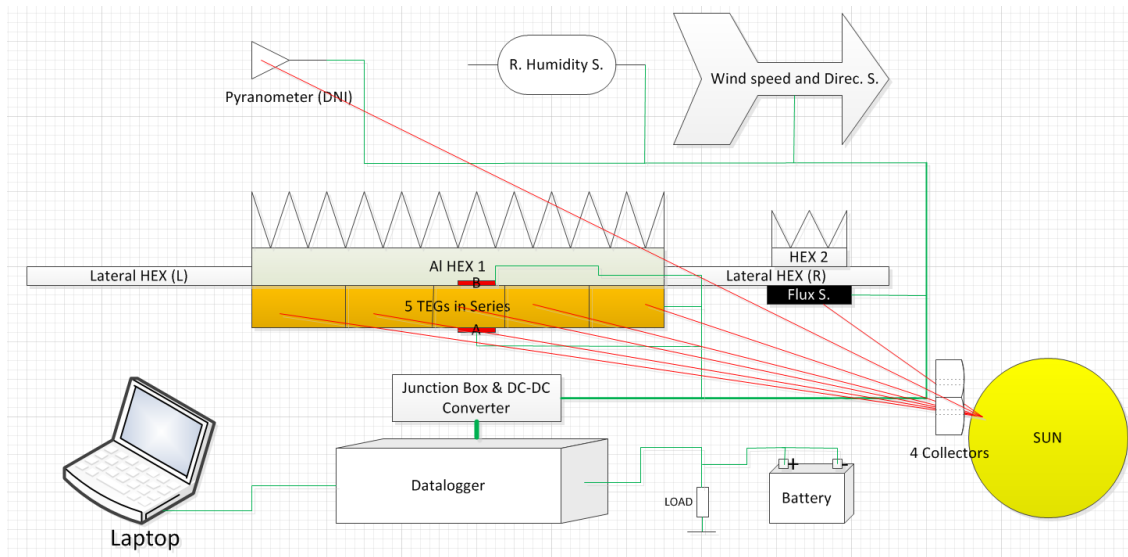
Figure 32 – STEG schematic overview—A and B denote thermocouples

Furthermore, this study achieved the following objectives: First, to investigate the performance of commercial solar TEGs under arid weather conditions comparable to the Southwest US or the Sahel in Africa. Five TEG devices made of bismuth telluride (Bi_2Te_3) were

mounted on a dual-axis solar tracker. The heat-absorbing side of the TEGs was exposed to four reflectors covered with a highly reflective thin film material. These reflectors, attached to the tracker, were positioned in such a way that the sun was concentrated four times on the devices. In addition, on top of the emitting side of the TEGs sat on aluminum (Al) heat exchanger (HEX), which created the requisite differential temperature between the two sides. In order to prevent the four suns from shining directly on the HEX, polyurethane insulation foam was glued around the set of TEGs as can be seen in Figure 33. Also, two lateral aluminum flat plates of equal dimensions were utilized to lengthen the aluminum heat exchanger in order to fasten it to the main iron structure. The secondary purpose of these Al plates, just as important as the first, was to enable them to actively participate in the overall heat-removal process away from the colder side of the TEGs. In other words, they increased the functionality of the main HEX. For illustration purposes, Figure 34 shows a side view of the above mentioned aluminum heat sinks. Additionally, the base of the HEX was grooved to form a meandering channel with an oval shape to accommodate a K-type thermocouple (A), which was placed on the back of one of the TEGs to measure T_C. Also, a second K-type thermocouple (B) was placed on the polyurethane foam, between the two sets of TEGs, via the same technique, to record T_H, as can be seen in Figure 33.
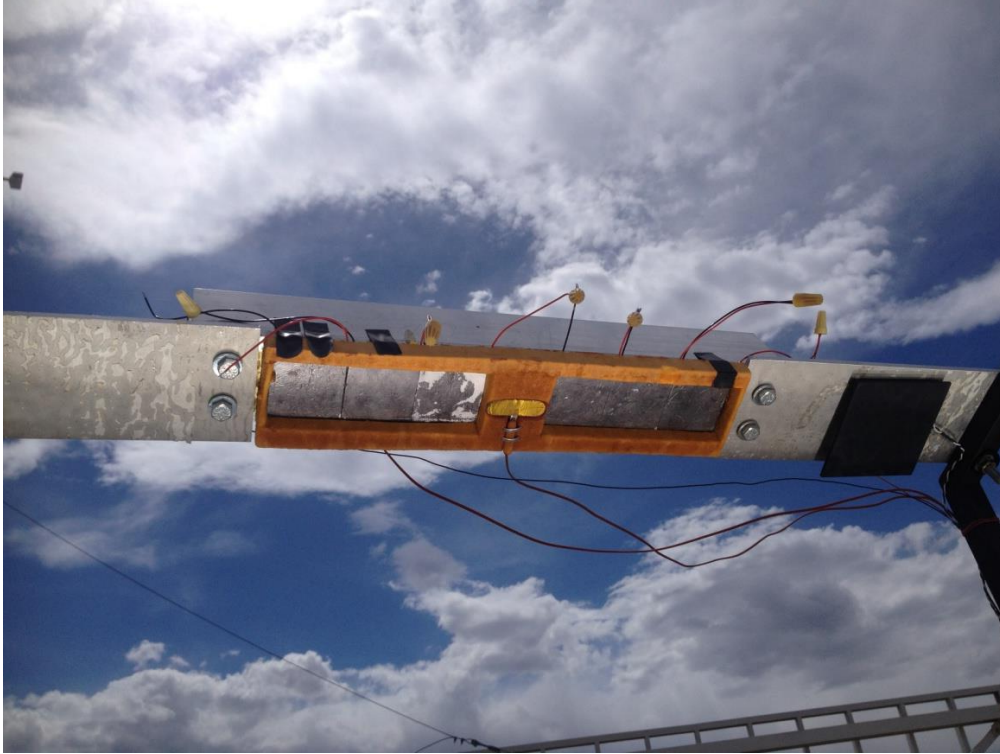
Figure 33 – Front view of the STEG system

The second part of the research aimed not only to compute the electrical parameters from both device geometries and properties, but also, and most importantly, to accomplish the electrical analogy of the whole system with the Spice simulator. The basic idea of the present model was derived from previous works done by [55], [61], [62], and [97]. So far, this study is the only one to attempt to model a real-world environment STEG energy-harvesting system utilizing LTspice software as a simulation tool. The temperature dependence of the internal resistance was taken into account in the model via the arbitrary behavioral voltage source technique. Also, a lookup table of real experimental data (*the local DNI, meaning the hot side Temp.*) was fed into the circuit to: 1) simulate the real system's behavior; and 2) to improve simulation speed. Moreover, all the heat capacitance values calculated in Sec. 3.2.4 were scaled

down in the Spice model in order to significantly reduce the running time created by the magnitude of the electrical-equivalent circuit. The LTspice built-in piecewise linear (PWL) command was purposely utilized in order to facilitate the achievement of the anticipated goals set forward.

Figure 34 – Side view of the STEG system

4.2.5 Preliminary Assumptions

Due to the complexity in the geometry, the unique nature of the STEG system and the longer projected simulation time, some assumptions were essential. Therefore, the thermal capacitance of the dynamic volume of air between the four collectors and the five TEGs was calculated based on the assumption that the air was confined in addition to the sound knowledge

of the specific heat capacity of dry Air at 80°C. In a like manner, the thermal resistance of that same unquantifiable amount of air was also determined based on the aforementioned assumption combined with its known thermal conductivity, $\kappa = 0.0299\ W/m.K$ for simplicity in the approach. The thermal resistance of the heat transfer grease, as mentioned above, was assumed to be $0.45K.W$ [57].

Ultimately, all the thermal components, such as L, C, and R determined in Sec. 3.2.4 or assumed for technical limitation purposes were strategically connected either in series and/or in parallel to construct the electronic model of the entire physical STEG system in LTspice. As a decisive step, the STEG is ready to be modeled in Spice provided the relevant codes have been properly written.

Finally, due to the stochastic nature of solar energy most of the time, there is a potential need for energy storage, as stated previously. The harvested energy is stored in a rechargeable 3.2-volt K2 battery, connected to the load via a charge controller for a later usage (*See Figure 32 for more details*).

4.2.6   Infinite Source of Energy

At this point, it is worth highlighting some of the technically relevant facts about this giant fire ball, the sun, since it is the only heat input to the system. So, solar energy, or solar radiation, is basically energy in the form of heat, particles, and shock waves from the sun, which result from nuclear fusion and eruptions on the sun's surface that travel all over space, as shown in Figure 35. These nuclear explosions are self-sustaining and are one of the greatest natural phenomena in the entire universe. This phenomenon results from two hydrogen atoms being compressed together into one helium atom by the enormous pressure and temperature of the sun. During the transformation, some of the mass of the two hydrogen atoms disappears and is

converted into a huge quantity of energy that appears as sunlight. As an example, the heat and light that we experience every day are evidently solar energy.

Figure 35 – Solar eruptions at the surface of the sun [95]

Remarkably, there exists a clear limitation on how the sunlight arrives on Earth every day due to the Earth's revolution around the sun. For thousands of years, humans believed that the Earth was in the center of the solar system rather than the sun being at the center of the solar system. Hence, the limitation of the solar system is that the sun shines only during the day and may be intermittent even then due to cloud coverage. Moreover, due to the Earth's rotation on its axis, only part of the Earth is illuminated at once. Therefore, we need to find other means of providing power when the sun is covered is technically essential and economically viable when using solar energy with back up energy storage for our daily energy needs. Although solar

energy suffers from some drawbacks, it is important to note that its advantages far outweigh the shortcomings related to variability.

4.2.6.1 Some Advantages of Solar Energy

It is imperative that some of the advantages of solar energy be outlined before getting into the solar thermoelectric generator modeling proper, which represents the main focus of this study. Therefore, some of the advantages of solar energy are: 1) it is infinitely renewable at a human scale; 2) when harvested, it produces zero greenhouse gases (GHG); 3) it utilization can help cut down utility bills at an individual level and at societal level; 4) it can help save scanty forests at global levels; 5) its large-scale integration into the grid can help utilities avoid and prevent power outages and blackouts by controlling the quality of the voltage, frequency, and power factor angle; 6) it can help utilities generate inexpensively the extra energy needed during peak hours instead of firing expensive and dormant peaker plants; 7) it can help arid and remote regions attain energy independence without necessarily being interconnected to the grid, etc. Nonetheless, many of the environmental issues the planet Earth currently faces result from our dependence on nonrenewable resources.

4.2.6.2 Direct Consequences of Nonrenewable Energy Sources

The global temperature increase was provoked and aggravated by the ways humans, mostly in the industrialized world, utilize nonrenewable fossil fuels. This fact certainly leads to the continuing global weather and climate changes. This will consequently constitute serious public health threats facing all nations, and most severely, the poor and arid regions around the world equipped with the least protective means. It is specifically reported in [37] that the most vulnerable people affected are children, the elderly, and communities living in extreme poverty. Therefore, to ensure healthy air, clean water, and stable climates for future generations,

responsible decisions about energy sources must be made *ipso facto*. The vicious dependence on fossil fuels that currently dominates US power generation can be affordably reduced through the use of sound and existing technologies. The major existing energy conversion technologies, as already mentioned above, pollute at an alarming rate, and the heat-trapping gases will certainly cause irreversible harm to communities around the world [96]. Consequently, some of the damage caused by the massive usage of fossil fuels are, as reported by [97]: 1) sea-level rise causing flooding and erosion in coastal communities; 2) air and water pollution; 3) acid rain; 4) extreme weather conditions, including more intense droughts and hurricanes; 5) reduced productivity of some agricultural regions; 6) loss of many treasured landscapes; and 7) loss of various animal and botanic species, just to mention a few.

For all the aforementioned reasons, there is a vital and crucial need to promote renewable sources, such as solar, wind, geothermal, thermoelectric generator (TEG), etc. Although the concept could be ambitious regarding the current US energy policies, a remodeling of the global energy system is desirable in order to provide sustainable and green energy for the present and the future generations. The desire is to satisfy not only the present energy needs attained in the developed nations, but also, and most importantly, to meet the quickly growing energy demands of developing countries through green technologies. This will further mitigate the negative effects of climate change [98]. Furthermore, at the core of the global synergies stand the new and renewable sources of energy that could kick start the model of green economies, eradicate poverty, and, ultimately, trigger sustainable development throughout the world. Hence, the cost of renewable energy technologies and off-grid systems must be significantly reduced by a worldwide, coordinated energy strategy and established national energy policies, such as selective incentives or technological breakthrough. Achieving these goals will enable wide-

spread standalone systems, either photovoltaics or TEG systems, to be utilized by the poorest fragments of populations living in rural and arid areas.

4.2.6.3 Effect of Excessive Heat on TEG Devices

In a similar way that temperature beyond certain limit affects the efficiency of PV systems by means of the temperature coefficient, it also does affect the performance of TEG in the sense that they are both made out of pn-junction semiconductor devices.

The maximum ambient heat a TEG can withstand depends on many factors, such as the: 1) heat exchanger; 2) types of cooling system (whether fan, air, liquid, or temperature cooled; 3) desired reliability); 4) amount of heat being dissipated to the ambient; 5) temperature rating of the TEM; and 6) quality of the insulation material. How excessive heat can affect STEGs may, however, be viewed under two different perspectives. On the one hand, if the heat is so intense and the setting of thermal insulation and heat exchanger are not good enough, the STEG system would perform poorly since the differential temperature, which is fundamental for the Seebeck theory, may not be significant. On the other hand, the carrier density of doped semiconductor devices is strongly dependent on temperature. Also, as temperature increases more and more, the extrinsic region, originally flat, will flip into an intrinsic region; thus the number of thermally generated carriers exceeds the number of donors or acceptors depending on the type of doping [99]. Therefore, if that eventuality occurs, the overall efficiency of the STEG would significantly drop since it would no longer behave as a semiconductor, but rather as a mere piece of conducting material. In essence, the performance of any TEG system is exclusively dependent on the quality and type of heat sink utilized, but also on how well the insolation foam was manufactured.

4.2.7 Parameter Extraction

A total of five TEGs were used in the proposed energy-harvesting system. The heat capacity and the internal thermal resistance of each module were estimated in the previous work to be 23J/K and 0.64K/W, respectively [91]. The former value was further split into two equal parts to fit in the LTspice model, as that yielded to accurate STEG modeling and the best possible solutions.

The modules were specified by the manufacturer to be bismuth telluride (Bi_2Te_3) and that the ceramic substrates were made of alumina (Al_2O_3). By virtue of that, some of the properties that turned out to be useful in the succeeding computations were densities, specific heat capacities, and the thermal conductivities of the Al HEXs, the substrate, and the Bi_2Te_3, as mentioned in [91]. Hence, the most relevant thermoelectric properties are listed in **Error! Reference source not found.** of Sec. 3.2.4.

Two heat exchangers were used in this design: 1) the main heat sink was placed on the cold side of the TEGs in order to keep them as cool as possible; and 2) the secondary heat sink was utilized to remove the heat from the bifacial solar flux sensor. To re-iterate, the role of each one of these heat exchangers is independent from one another and they are of the extruded type, made of pure aluminum material. Besides, in computing the thermal resistance and capacitance of the following parts, the geometries and properties were also taken into account.

4.2.7.1 Aluminum Heat Exchanger, Al HEX

The dimensions of the primary heat exchanger were carefully documented, and then listed in Table 7. In addition to that, the lateral aluminum plates were also measured and documented in the same table. These plates also contributed to the removal of some of the heat from the TEGs, since they were not only fastened directly beneath the main heat exchanger, but

were also adjacent to the insulation foam. The overall Spice simulation of the thermal process would not be accurate without properly taking into consideration the aforementioned plates.

4.2.7.1.1 Purpose of the Aluminum Heat Sink

Among all the components that made up the design, the main finned heat sink is a parameter of sufficient importance to merit further consideration. One of the reasons for stating the above postulate is that for the TEG to moderately generate electrical power, the differential temperature between the hot and cold sides has to be within some threshold values. In other words, the two sides have to be maintained apart as far as possible in terms of temperature. Hence, that can only be achieved through a cooling mechanism. For this specific application, owing to the simplicity in the procedures and design (*this research focuses on remote and residential application of TEGs*), a dry and natural cooling system was chosen. It is worthy of note to emphasize that in natural convection, heat transfer relies exclusively on the free buoyant flow of air surrounding the heat sink. Therefore, an efficient aluminum (Al) heat sink was conveniently chosen to do the task at hand at the expense of some reduction in the overall efficiency.

Heat sinks are devices that augment heat dissipation from a hot media, such as a heat generation component, to a cooler ambient which is usually air [100]. Far from the electrical grid, energy utilization has to be solely minimized to basic daily energy needs by all means and its conservation be thus maximized as much as possible. This theory of energy efficient utilization started at the early stage of the novel energy-harvesting project by cutting down any active cooling device, such as a water pump, oil pump, and any temperature controlled device in the design. For the aforementioned reason, air is simply selected to be the cooling fluid. The main purpose of the heat sink can be mainly break down into two functions: 1) to not only lower

the solid-air interface barrier to heat flow, but also to increase the contact area that is in direct contact with the air; and 2) to maintain the device differential temperature within the allowable TEM manufacturer's specifications for satisfactory electrical power to be generated. Furthermore, choosing the right heat sink is paramount as the aim was to achieve a significant differential temperature across the TEGs by dissipating away more heat. Therefore, high purity extruded aluminum material has at all times been a good heat exchanger for electronic components.

Table 7 - Dimensions of the physical components

Nº	Components	Length(*cm*)	Height (*cm*)	Width (*cm*)	Thickness (*cm*)
1	Heat exchanger 1	50.165	7.112	7.62	0.985
2	Lateral Al plate (*R*)	30.48	0.635	10.16	
3	Lateral Al plate (*L*)	30.48	0.635	10.16	
4	*PUR* Insulation foam	40.132 (*l*)	1.905 (*h*)	31.115 (*W*)	
5	Insulation foam (*hole 1*)	16.764 (l_1)	1.905	5.715 (W_1)	
6	Insulation foam (*hole 2*)	16.764 (l_2)	1.905	5.715 (W_2)	
7	TEG	5.6	0.445	5.6	

To better understand the physical nature of all the components listed in Table 7 above, see Figure 33 in Sec. 4.2.4. Apart from the dimensions, it is necessary to point out that the two heat exchangers are of the same kind, in all aspects, i.e. physical shape and chemical composition (pure Aluminum); the only exception is their size.

4.2.7.1.2 Thermal resistance, R_{HEX}

Besides the dimensions listed in Table 7, it is worthy of note to point out that the heat exchanger is of pure Aluminum. As a result, the total number of fins is eight (8) and the distant

between them is in the neighborhood of 0.635 cm. So, the area, A_{HEX}, of the heat exchanger can be calculated simply by Eq. (36).

$$A_{HEX} = l \cdot W = 0.50165 \cdot 0.0762 = 0.0383 \ m^2 \tag{36}$$

Where, l is the length of the Al heat exchanger in meters (m) and W is its width, also in meters. With the perfectly documented knowledge of all the physical dimensions of the Al HEX's contact area, the associated thermal resistance can be found by Eq. (37).

$$R_{HEX} = \frac{1}{\kappa \cdot (A/l)} = 0.074 \ [K/W] \tag{37}$$

Where, $\kappa = 177 W/m$ is the thermal conductivity, A is the surface area, and l is the length of the Al heat exchanger.

4.2.7.1.3   Thermal Capacity, C_{HEX}

In a similar fashion, the volume of the plate-fin HEX needs to be computed although it is much more cumbersome and involved compared to ordinary aluminum plates. So, the aluminum heat sink has eight (8) fins, whereby the first seven (7) fins are of the same dimensions, but the eighth one, i.e. Fin_B, has a different size as displayed in Table 8,

Table 8 - Fins' dimensions

Designation	Quantity	Length (l)	Height (h)	Thickness (t_a)	Thickness (t_b)
Fin_A	7	501.65	62.20	3.60	2.40
Fin_B	1	501.65	62.20	2.70	2.10

in which, all the units were measured in millimeters (mm).

For simplicity purposes, we assumed the thicknesses at the bottom and the top of the two categories of fins to be the same size and then utilized their average (t_{avg}) in the calculations.

Therefore, determining their volume is reduced to calculating the volume of a rectangular parallelepiped, as can be seen in Eq. (38).

$$V_{Fin\_A} = l \cdot h \cdot t_{avg} = 0.00009361 \ m^3 \tag{38}$$

Where, l, h, and t_{avg} are the length, the height, and the average thickness, respectively.

The volume of the seven fins, V_{Total}, of equal size can be calculated as follows, Eq. (39).

$$V_{Total} = 7 \cdot V_{Fin\_A} = 0.00066 \ m^3 \tag{39}$$

Following a similar judgment, the volume of the unique Fin_B, can be determined after averaging its bottom and top thicknesses as in Eq. (40).

$$V_{Fin\_B} = l \cdot h \cdot t_{avg} = 0.00007489 \ m^3 \tag{40}$$

The volume of the two categories of fins can be summed up to the overall volume, V_{Fins}, by

$$V_{Fins} = V_{Total} + V_{FinB} = 0.000735 m^3 \tag{41}$$

The Al HEX's compact base volume computation, where all the fins originated, is now made straightforward, knowing the length, the width, and the height, as can be seen by Eq. (42).

$$V_{Base} = l \cdot w \cdot h = 0.00037652 \ m^3 \tag{42}$$

Finally, the volume of the entire HEX, V_{HEX}, as written in Eq. (43), can be assessed by summing up the individual volumes calculated above.

$$V_{HEX} = V_{Base} + V_{Fins} = 0.00111152 \ m^3 \tag{43}$$

Hence, the heat capacity proper, C_{HEX}, to accurately model the heat exchanger's effect on the STEG system, via the Spice simulator, can be computed by Eq. (44).

$$C_{HEX} = \rho \cdot Cp \cdot V_{HEX}$$

$$= \frac{2770 \ kg \cdot 875 \ J \cdot \ 0.00111152 \ m^3}{m^3 \cdot kg \cdot K}$$

$$= 2694 J/K \tag{44}$$

Where, ρ is the density, C_p is the specific heat capacity, and V_{HEX} is the volume of the Al HEX.

4.2.7.2 Lateral Aluminum Plates

Two aluminum plates of equal dimensions were utilized as part of the components to build this solar energy-harvesting system. Their primary purpose was to lengthen the aluminum heat exchanger (HEX) in order to be able to fasten it to the main iron structure. The secondary purpose of the Al plates, which is as important as the first one, is that they actively participate in removing the heat away from the colder side of the TEGs by acting as an extension to the main heat sink mentioned earlier.

4.2.7.2.1   Thermal resistance, R_{LAl}

As already mentioned, the physical dimensions are all summarized in Table 7. Consequently, the thermal resistances of the twin Al plates can be evaluated simply by Eq. (45).

$$R_{LAl} = \frac{1}{\kappa \cdot (A/l)} = 0.056 \ K/W \tag{45}$$

Where, $\kappa = 177 W/m$ is the thermal conductivity, A the surface area of the plate, and l its length. It is therefore worth noting that the actual thermal resistance of the twin aluminum plates, R_{LAl_Total}, is twice as much as R_{LAl} shown in Eq. (46).

$$R_{LAl\_Total} = 2 \cdot R_{LAl} = 0.112 \ K/W \tag{46}$$

4.2.7.2.2   Thermal capacity, C_{LAl}

Having measured with ultimate care, the length (l), width (w), and height (h) of the two lateral Al plates as listed in Table 7, it is now of paramount importance to compute the total volume, V_{LAl_Total}, using Eq. (47), since it is needed in the subsequent equation.

$$V_{LAl_{Total}} = V_{LAl_R} + V_{LAl_L} = 2 \cdot l \cdot w \cdot h$$

$$= \ 2 \cdot 0.3048 \cdot 0.1016 \cdot 0.00635 = 0.0004 \ \text{m}^3 \tag{47}$$

Where, V_{LAl_R} and V_{LAl_L} denote the volumes of the right and left lateral Al plates, respectively.

So, the heat capacity of the two lateral Al HEXs, C_{LAl}, needed to accurately model the whole new concept of the energy-harvesting system with the Spice software is determined by Eq. (48). It would then be converted into an equivalent electrical value by means of the thermal-to-electrical analogy theory and then fit in the circuit to simulate its real-world impact on the performance of the STEG system.

$$C_{LAl} = \rho \cdot Cp \cdot V_{LAl_{Total}}$$

$$= \frac{2770 \ kg \cdot 875 \ J \cdot 0.0004 \ m^3}{m^3 \cdot kg \cdot K} \approx 970 J/K \tag{48}$$

Where, ρ is the density of the lateral Al plates and C_p is their specific heat capacity.

4.2.7.3 Thermal Insulation Foam

To study the effects of insulation materials in this design, a rigid polyurethane foam (*PUR*) was specially selected to best fit the needs. It is important to mention here that the rigid *PUR* is quite different from the common insulation foams, as it is a closed-cell plastic. Also, *PUR* has an immensely great resistance to thermal energy propagation because it is one of the most efficient, high performance insulation materials. This enables a very effective way of preventing the solar radiation to directly shine on the heat exchanger mounted on the cold side of the TEGs. In this regard, the PUR allows the entire system to attain a much higher efficiency by not only enhancing the temperature differential across the two sides as the free solar energy is being harvested, but also by making the STEG system physically robust.

Thermal insulation, in most cases, is needed either to keep a device cool or warm, depending on the application. The thermal conductivity and the heat capacity of the insulation foam were first tested in a laboratory up to temperatures greater than 100°C as can be seen from the water boiling in Figure 36. Thus, an electrical heater, as displayed in the same figure, was used as the heat source during this indoor test. In addition to that, a piece of aluminum was

utilized for comparison purposes, as they were both core parts of the preliminary indoor experiment.

Figure 36 – Insulation foam being tested

Also, how thermal energy propagates through a material, such as aluminum or insulation foam is, generally well known. Heat transfers naturally through a polyurethane foam by conduction in a form of atomic vibration (phonon) as well as radiation to some extent. Further, the particular phonons of interest in this study are the shorter-wavelength ones of higher frequency because they give rise to heat. The purpose of the insulation foam in this experiment was to prevent the solar radiation concentrated four times from reaching the aluminum heat

exchanger. That would not only decrease the differential temperature, but would also offset the accuracy in the measurements.

4.2.7.3.1 Thermal Resistance, R_{Insul}

One of the most important properties of any insulation material is inarguably its insulation performance. The benchmark for such insulation performance is a high thermal resistance or a low thermal conductivity. Furthermore, it is worthy of note to emphasize that the thermal resistance of any PUR is dependent on certain parameters. These parameters includes the cell gas used, density, temperature, behavior in the presence of water and moisture, and the time of measurement [101]. The most commonly utilized properties of this rigid PUR are enumerated in Table 9.

Table 9 - Rigid PUR properties [101]

Material	Thermal conductivity, κ	Density, ρ	Specific heat capacity, C_p
Rigid polyurethane foam, PUR	0.025 $W/(m.K)$	30 kg/m^3	1500 $J/(kg.K)$

As can be seen from Figure 37, computing the area and volume of the insulation foam can be somewhat difficult because of the nature of its shape. The area of the insulation foam, A_{Insul}, can be obtained by Eq. (49).

$$A_{Insul} = l \cdot W - (l_1 \cdot W_1 + l_2 \cdot W_2) = l \cdot W - 2 \cdot (l_1 \cdot W_1)$$

$$= 0.40132 \cdot 0.31115 - 2 \cdot (0.16764 \cdot 0.05715) = 0.106 \; m^2 \tag{49}$$

Where, l is the length of the insulation foam, W is its width, l_1 is the inside length of the hole on the foam's surface located at the right, W_1 is the inside width of the hole on the foam's surface

located at the right, l_2 is the inside length of the hole on the foam's surface located at the left, and W_2 is the inside width of the hole on the foam's surface located at the left.

The above equation is further reduced because, based on the measured values tabulated in Table 7, the two rectangular holes cut into the surface of the foam were of equal dimensions. Hence, the mathematical expression for that is shown in Eq. (50) since l_1 is the same as l_2 and W_1 is identical to W_2.

$$l_1 \cdot W_1 + l_2 \cdot W_2 = 2 \cdot (l_1 \cdot W_1) \tag{50}$$

Now that the area is known, the thermal resistance of the *PUR*, R_{Insul}, can be simply computed by means of Eq. (51).

$$R_{Insul} = \frac{1}{\kappa \cdot (A/l)} = \frac{1}{0.025 \cdot (0.106/0.29)} \cong 109 \ K/W \tag{51}$$

Where, $\kappa = 0.025$ *W/m.K* is the thermal conductivity, A is the surface area, and l is the approximate length of the insulation foam.

4.2.7.3.2　　Thermal Capacitance, C_{Insul}

If we had not accommodated for the thermal insulation foam to fit in the design, the four suns would directly shine on the aluminum heat exchanger. The major consequence would then be purely a bad engineering design. The foam played a crucial role as it was the thermal barrier that kept the hot (front) side and the cold (back) side of the TEGs at different temperatures. Placing the foam around and in the middle of the two groups of TEGs, as portrayed by Figure 37, helped not only to achieve a significant differential temperature, but also allowed the implementation of the Seebeck theory in a real-world experiment.

Figure 37 – Insulation foam facing the solar collectors

Information on the volume of the insulation foam, V_{Insul}, can be easily obtained from the previous knowledge of its area. Therefore, the volume is computed as in Eq. (52).

$$V_{Insul} = A_{Insul} \cdot h = 0.106 \cdot 0.01905 = 0.00202 \, m^3 \qquad (52)$$

Where, h is the height of the insulation foam.

Finally, the heat capacity of the insulation foam can be numerically estimated in Eq. (53) by

$$C_{Insul} = \rho \cdot Cp \cdot V_{Insul}$$

$$= \frac{30kg \cdot 1500J \cdot 0.00202 \, m^3}{m^3 \cdot kg \cdot K} = 91 \, J/K \qquad (53)$$

Where, ρ is the density and C_p is the specific heat capacity of the insulation foam.

4.2.7.4 Air Properties at NTP

At Normal Temperature and Pressure (NTP) air has specific properties that are experimentally predetermined. Therefore, under the NTP that is customarily used as the standard

testing conditions (STC) when it comes to most of the engineering open air tests, the air temperature is 20°C, and the atmospheric pressure is 1atm, equivalent to: 01.325 kN/m^2, 101.325 kPa, or 760 torr. As a result, Table 10 gives the most relevant properties of air needed to compute the thermal resistance and capacitance.

Table 10 - Air properties [102]

Temp. (^{o}C)	ρ (kg/m^3)	C_p [kJ/(kg.K)]	κ [W/(m.K)]
0	1.293	1.005	0.0243
60	1.067	1.009	0.0285
80	1.0	1.009	0.0299
100	0.946	1.009	0.0314

Where, Temp is the temperature in degrees Celsius, ρ is the density, C_p is the specific heat capacity, and κ is the thermal conductivity.

4.2.7.4.1 Thermal Resistance of Air

How the natural and invisible quantity of matter known as *Air* influences the flow of thermal energy in the form of heat, termed R_{Air}, can be simply computed by means of the Eq. (54) below.

$$R_{Air} = \frac{1}{\kappa \cdot (A/l)} = \frac{1}{0.0229 \cdot 0.762} = 57.30 \ K/W \tag{54}$$

Where, κ = 0.0299 *W/m.K*, the thermal conductivity is assumed to an average temperature value of 80°C, *A* is the contact surface area, and l is the length of the five (5) TEGs. It is worth noting that the computation is solely based on some simplifications as previously mentioned since the volume of air in our case is experimentally hard to determine.

4.2.7.4.2 Thermal Capacitance of Air

For simplicity purposes in our steps, we assumed the air to be contained in a fixed volume, i.e. stationary between the solar collectors and the TEGs, though in reality it was dynamic and dependent on the weather. Also, the shape of the imaginary immobile container (*Air volume*) was assumed to be a pyramid, as it is the closest possible shape. Hence, the volume of air can be determined as in Eq. (55).

$$V_{Air} = \frac{l \cdot W \cdot h}{3} = \frac{0.94 \cdot 0.762 \cdot 0.61}{3} = 0.147 \, m^3 \tag{55}$$

It follows that the thermal capacitance of that volume of air can be easily calculated as in Eq. (56), provided the density and the specific heat capacity of air are all known.

$$C_{Air} = \rho \cdot Cp \cdot V_{Air}$$

$$= \frac{1.0 \, kg \cdot 1.009 \, kJ \cdot 0.147 m^3}{m^3 \cdot kg \cdot K} \cong 148 J/K \tag{56}$$

4.2.8 Thermal Resistance Circuit of the STEM System

In order to successfully design a technically sound solar thermoelectric energy-harvesting system, the modules have to be selected based on the highest $V_{MAX} \cdot I_{MAX}$ product in accordance to a certain TEG size. Also, the HEX must be properly sized to fit the TEGs. When placing a TEG between two surfaces at different temperatures, a differential temperature would be automatically developed across it due to its intrinsic semiconducting nature. As reported in[103], TEGs have a fairly low thermal resistance ranging from typically 1°C/W to 10°C/W between its ceramic plates. It is also important to point out that larger TEG devices have astonishingly smaller thermal resistance because of larger contact area. Therefore, utilizing an aluminum heat exchanger with the smallest possible thermal resistance not only boosts the output power, but also has the potential to maximize the differential temperature (ΔT) across the TEG because of its higher thermal conductivity. The STEG system in conjunction with the thermal resistance of the

HEX dictates what percentage of ΔT stays across the TEG, as can be seen from the simple thermal resistance model portrayed in Figure 38.
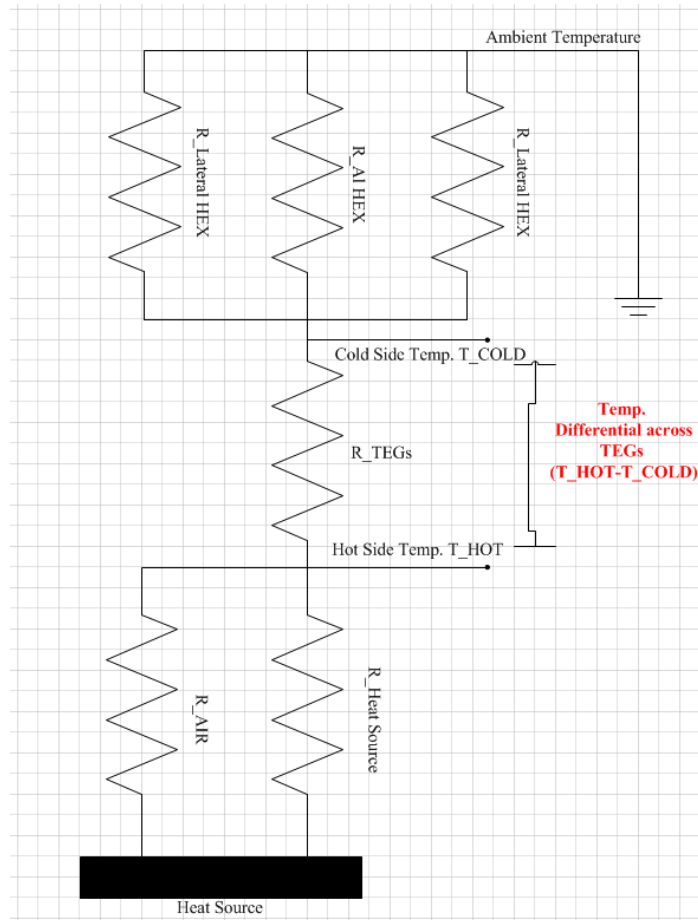

Figure 38 – Thermal resistance model of the STEG system

As already calculated in Sec. 4.2.7, Table 11 summarizes the thermal resistances of the major components that mutually interacted during the solar energy-harvesting process.

Table 11 - Thermal resistance of the main components

S/N	Designations	Thermal resistance [K/W]
1	TEG	0.64
2	Polyurethane insulation foam	109
3	Aluminum HEX	0.074
4	Lateral Aluminum plates	0.112
5	Air	57.30
6	Solar collectors	Neglected

Before getting into the calculation of the resulting temperature differential (ΔT) proper, the equivalent thermal resistances of the top and bottom sides must be evaluated. The equivalent resistance of the top part of the thermal model, R_{TOP} is given by

$$\frac{1}{R_{TOP}} = \frac{1}{R_{Lateral\ Left}} + \frac{1}{R_{Lateral\ Right}} + \frac{1}{R_{AL\ Heat\ Sink}}$$

$$= \frac{1}{0.056} + \frac{1}{0.056} + \frac{1}{0.074} = 49.22 \tag{57}$$

Therefore, the value of R_{TOP} is 0.02 K/W.

In a similar fashion, the value of the bottom equivalent thermal resistance can be estimated to be sensibly equal to that of air since the solar collectors were assumed to be perfect reflectors.

$$R_{BOTTOM} = R_{Air} \tag{58}$$

Therefore, the temperature differential developed across the TEG units can be simply determined by Eq. (59). It is worth mentioning that the ΔT, in this case, does not yield to a single value, but rather to a multitude set of values which are stochastic in nature, depending on some other factors, such as local insolation. These factors may include: 1) seasons of the year; 2) ambient temperature; and 3) cloud coverage, as can be seen in Figure 39 below.

$$\Delta T = (T_{Source} - T_{Ambient}) \cdot \frac{R_{TEGs}}{R_{Air} + R_{TEGs} + R_{TOP}} \ [^oC] \tag{59}$$
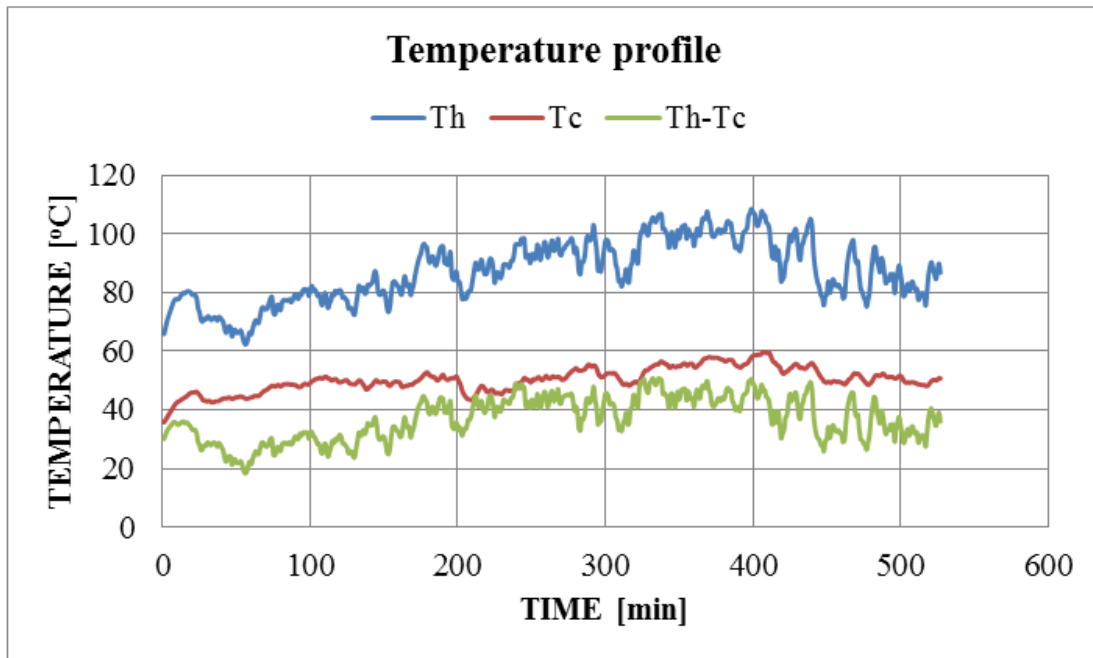
Figure 39 – Temperature differential across the TEGs

4.2.9   The Inner Setup of LTspice Software

This passage emphasizes the description of the algorithms used in LTspice. Hence, this quick side note is meant to give short detail about the uniqueness and powerful insights on the inner mechanisms of LTspice software. In relation to that, a lookup table is utilized to transpose the real-world solar energy behavior on the model. The table is merely a list of pairs of numbers, where the second column refers to the recorded hot side temperature from the experiment, which is indirectly the local DNI. If the control algorithm is beyond the range of the look-up table, the spice simulator linearly extrapolates the output voltage and/or temperature on the cold side as a

118

constant voltage and/or constant temperature, respectively, of the last data point of the look-up table.

4.2.10   STEG Spice Model Implementation

As can be seen from both Figure 40 and Figure 42, the complementary circuits of the Spice model for the whole STEG system are composed of an electrical portion and a thermal circuit, in that order. The most important benefit of utilizing the LTspice simulator to model a complex transient heat transfer process is the convenience in viewing and interpreting the interactions between the four major effects: *Seebeck*, *Joule*, *Peltier*, and *Thomson*.

With a sound knowledge of the energy equilibrium on both emitting and absorbing sides of the TEGs, the electrical power harvested can be simply quantified as seen in Sec. 3.2.4.6, Eq. (18). There are mainly two alternative methods to model the energy balance and electrical power equations, as reported throughout the literature, *viz.* current dependent and voltage dependent sources. The former method was chosen for rapid convergence purposes. In contrast to some previous work, this study did incorporate the Seebeck coefficient, the thermal conductivity, and the internal thermal resistance variations with temperatures in the LTspice model through the arbitrary behavioral voltage sources (ABVS). Also, all the thermal resistances and capacities of the various physical parts of the STEG's system determined in Sec. 4.2.7 above were expressed in their electrical equivalence before reconstructing the energy-harvesting system in Spice. Figure 40 and Figure 42 also show that all the parts obtained via the thermal-to-electrical analogies were either connected in series, and/or in parallel, to achieve the proposed STEG model. In addition to that, some of these components were equally split so that their effect would be perceived on either side of the STEG model.

4.2.11.1 Electrical Portion of the STEG System

The electrical circuit analogy of thermal systems is valuable to electrical engineers and other related branches of physics because circuits offer a good representation for the study of complex energy systems as well as electrical equipment. Thus, Figure 40 depicts the electrical portion of the proposed STEG system, where the positive terminal at the end of the fifth TEG denotes the output voltage of the energy-harvesting system. The communication between the thermal and electrical circuits was made possible by the voltage sources V_2, V_4, V_5, V_7, and V_9 through the current-voltage dependent schemes. It is extremely important to point out that the internal parasitic components (L_n and C_n) were experimentally determined in [35], where the values are $0.54\mu H$ and $41nF$, respectively. In this electrical model, the (L_n, C_n) pairs are respectively from TEG_1 through TEG5: (L_1, C_{21}), (L_2, C_{20}), (L_4, C_{23}), (L_6, C_{25}), and (L_5, C_{24}).
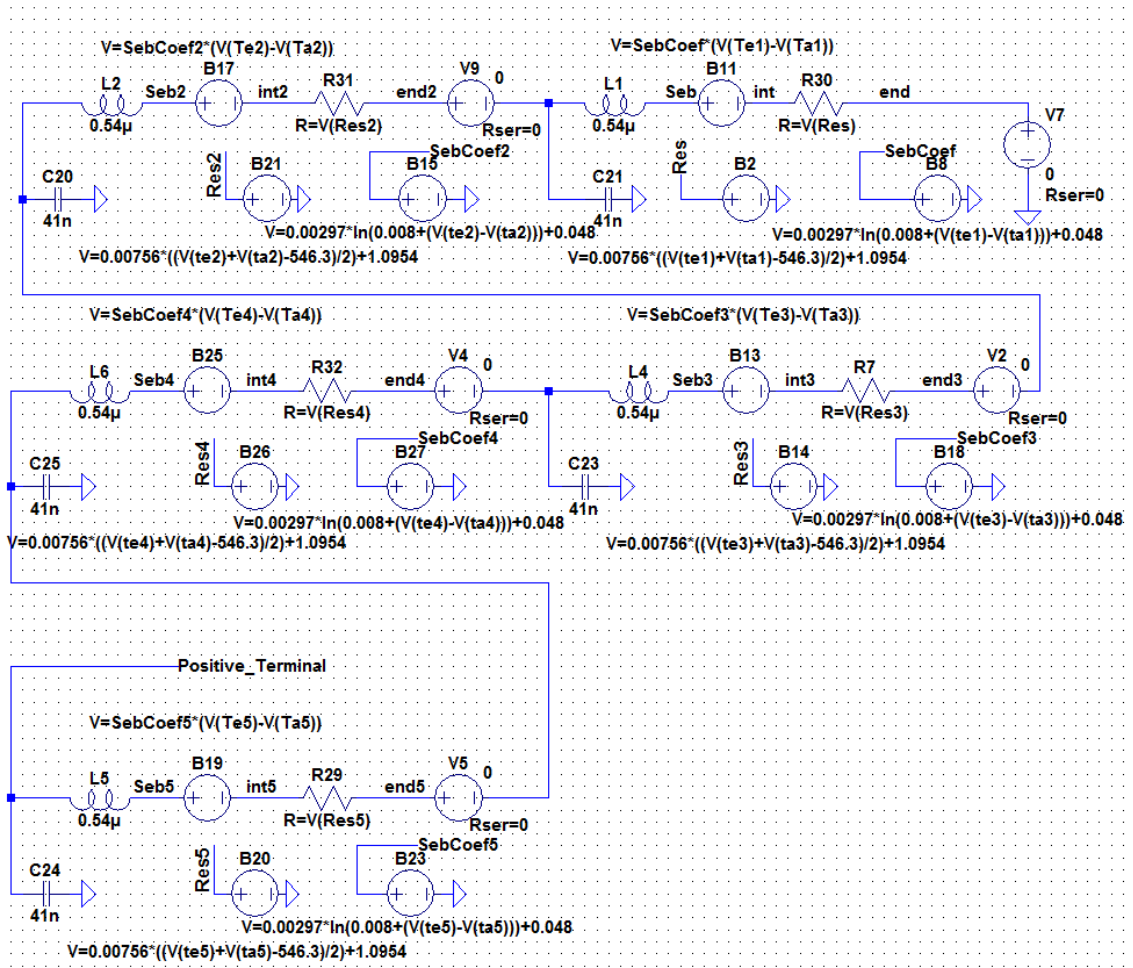
Figure 40 – Electrical portion of the STEG system

4.2.11.2   Spice Representation of the Thermoelectric Generators

Figure 41 depicts the Spice thermal analogy of the five TEGs under investigation. As can be noticed, they are placed electrically in series, but thermally in parallel. As mentioned earlier, an aluminum heat sink sits on top of the emitting side of the thermoelectric module string for cooling intents and purposes. Therefore, the whole energy-harvesting system generates output voltage based on the developed temperature differential across the two sides of the thermoelectric generators. It is important to mention that the same figure shows the

implementation of the electrical resistance, thermal conductance, and the Seebeck coefficient of each individual TEG device through the arbitrary behavioral voltage source (ABVS) technique. The values of the above parameters, extracted from both datasheet and device geometry and property, are uniquely applied in ABVS command and are solely dependent on temperatures. This can be shown through the emitting and absorbing side temperatures, i.e., T_e_n and T_a_n, respectively, in which n is equal to 1, 2, 3, 4, and 5 or the number of TEGs.
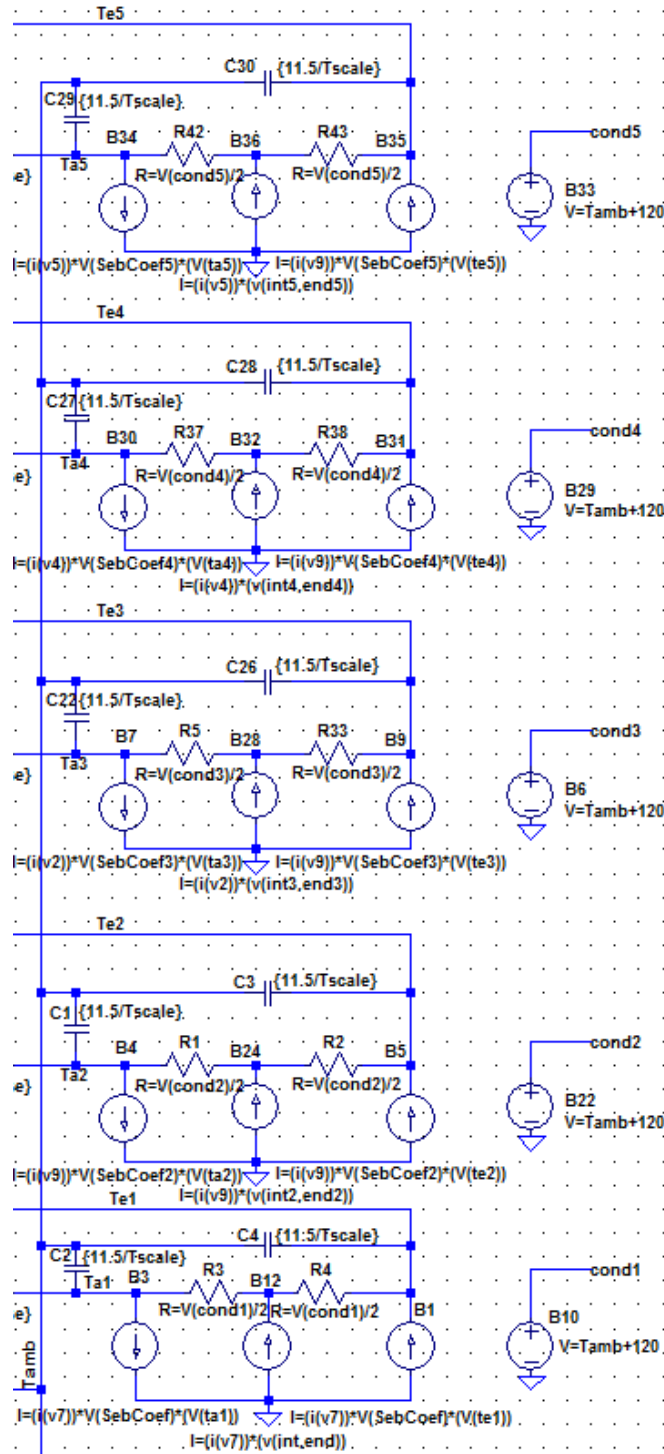
Figure 41 – Spice representation of the series TEGs

123

4.2.10.3   Thermal Portion of the STEG System

The proposed thermal model of our STEG system for Solar Energy Harvesting is based on the initial works [12] and [54]. Figure 42 portrays the LTspice model of the thermal part of the proposed STEG energy-harvesting system, including the 5 TEGs connected electrically in series and thermally in parallel. In line with the above reasoning, the following pairs of capacitances—C_1&C_3, C_2&C_4, C_{22}&C_{26}, C_{27}&C_{28}, and C_{29}&C_{30}—enabled to capture the real-world performance of the STEG in LTspice. R_{Insul} and C_{Insul} represent the thermal resistance and thermal capacity of the polyurethane foam, respectively. In a similar manner, the pairs (R_{23}&C_{14}) and (R_{24}&C_{15}) stand for the thermal resistance and thermal capacity of the two lateral aluminum plates.
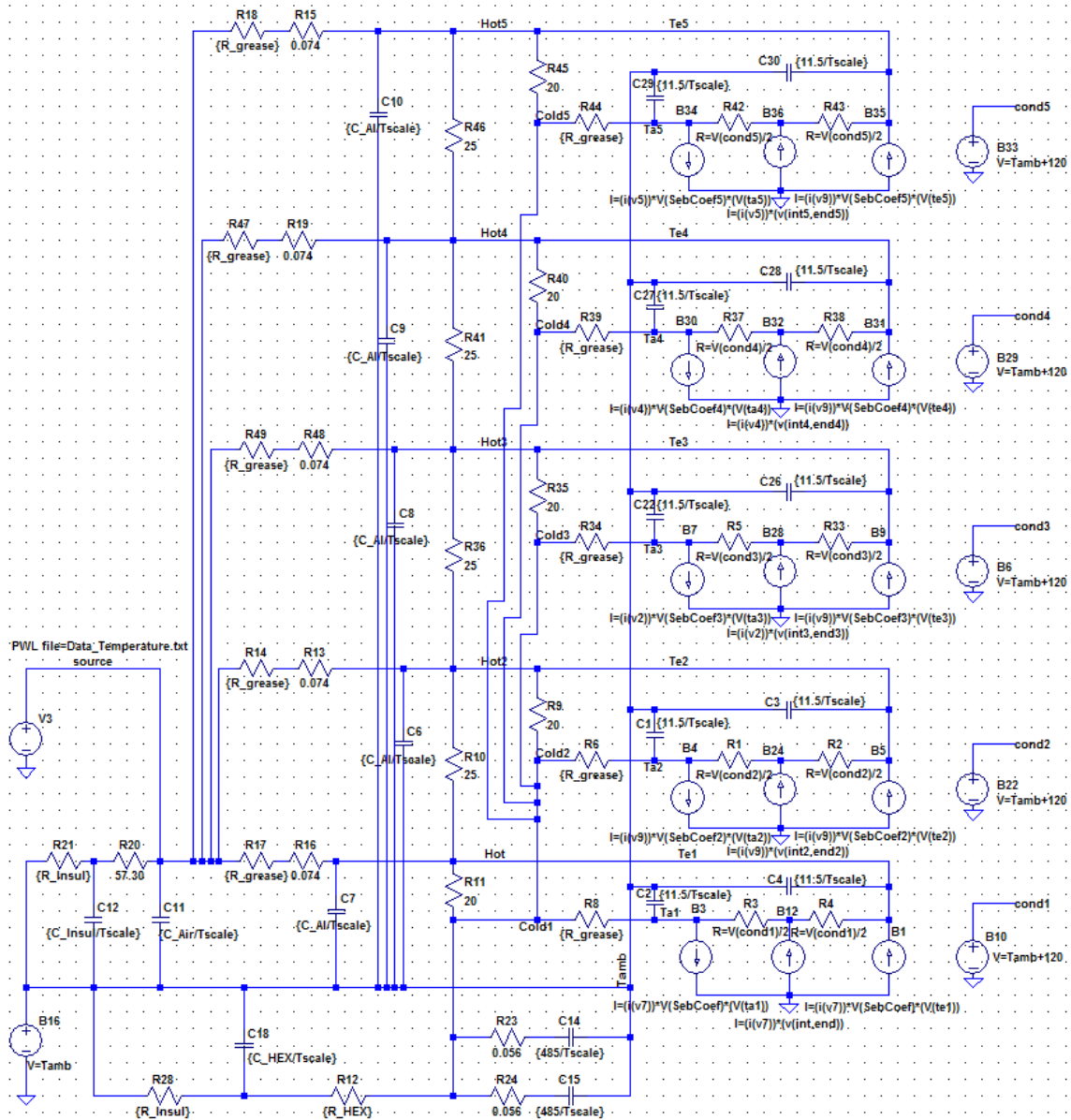
Figure 42 – Thermal portion of the STEG system

Furthermore, the values of the thermal resistances and capacities, computed from both device properties and geometries in order to achieve an accurate electrical analogy of the entire real-world thermal process, are succinctly listed and explained in Table 12. The first part of the table deals with the thermal resistance, followed by the thermal capacitances in the second half.

125

Also, it further sub-divides them into components, designations, and then equation or actual value, depending on the deterministic or stochastic nature of the element.

Table 12 - Thermal parts' descriptions

| Numbers	Components	Descriptions	Equation/Value
		Thermal Resistances [*K/W*]	
1	R_m	Internal resistance of the TEG	$$R_m = \frac{(\rho_n + \rho_p) \cdot \mathrm{N}}{G}$$
2	R_{Insul}, R21 and R28	Resistance of the insulation foam split into two equal parts for convenience	5.9
3	R6, R8, R14, R18, R17, R34, R39, R44, R47, R49 or R_grease	Thermal resistance of the thermal grease	0.20
4	R9, R11, R35, R40, R45	Thermal resistances between the cold and hot side due to any transient or stationary air gap	20
5	R10, R36, R41, R46	Thermal resistances between the TEGs	25
6	R20	Thermal resistance of the ambient Air	57.30
7	R23, R24	Thermal resistance of the lateral HEX, Right and Left, respectively	0.056
8	R12 or R_HEX	Thermal resistance of the HEX to the ambient	0.074
9	R13, R15, R16, R19, R48	Thermal resistance of the aluminum HEX	0.074
		Thermal Capacities [*J/K*]	
1	C18 or C_{HEX}	Capacitance of the Aluminum HEX	2694
2	C11	Thermal capacitance of the ambient Air	148
3	C12	Thermal capacitance of the insulation foam	91
4	C14, C15	Thermal capacitance of the lateral HEX, Right and Left, respectively	485
5	C6, C7, C8, C9, C10	Thermal capacitances of the solar reflectors virtually sitting on the TEGs	25
6	C1, C2, C3, C4, C22, C26, C27, C28, C29, C30	Thermal capacitances of the TEGs split equally into two per device	11.5

4.2.11 Results and Analysis

A good starting point in this analysis is to first address the local insolation and then how the tracker in conjunction with the four mounted solar collectors contributed to input the necessary hot side temperature. The purpose of the collectors is to multiply the incoming solar radiation on the hot side of the TEG by a factor of four. Consequently, the solar energy landing on the absorbing side of the TEGs was four times (4X) bigger than it would have been with a single reflector. Figure 43 portrays a portion of the local DNI, responsible for the above mentioned fact, experimentally recorded with a Pyrheliometer mounted on a dual axis sun tracker. Each single unit represents the solar irradiance recorded during the course of a day. As can be seen clearly, each day shows a unique insolation pattern with the effect of variability, relative to the local weather conditions. Hence, these effects of variability illustrated in Figure 44 through Figure 46, tremendously impacts, in a proportional manner, the outcome of the experiment, *viz. ΔT* and the subsequent energy generated by the system.
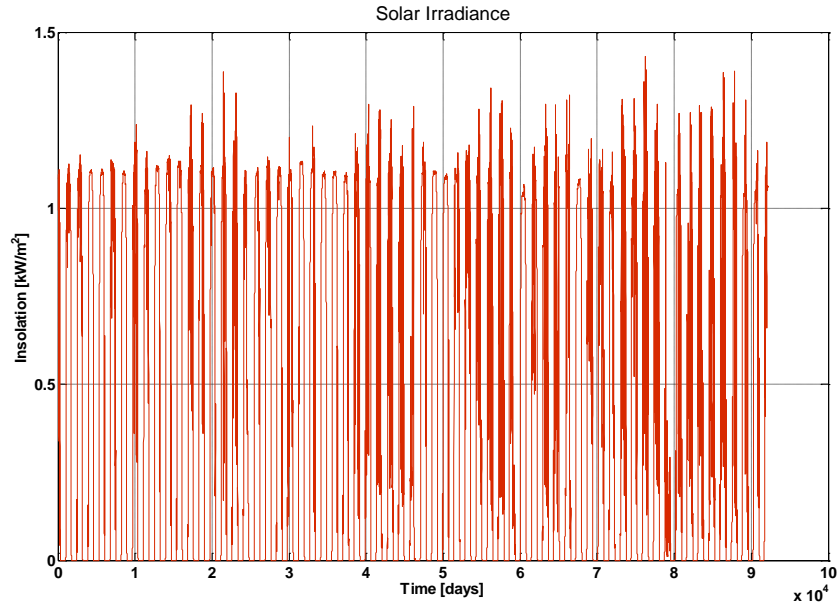
Figure 43 – Local direct beam radiation

4.2.11.1   Hot Side Temperature

Figure 44 presents the absorbing-side temperature determined experimentally over days. This hot side temperature was organized in a lookup table and then fed into the LTspice TEG model as the sole thermal energy source to the system. As can be clearly observed, this temperature varies throughout the days, the weeks, the months, and the seasons of the year. The highest peak, obviously, occurred during day time and was as high as 125 °C, whereas the minima typically occurred after sunset. The hot side temperature, as already stated, is the only thermal energy input to the STEG energy-harvesting system. Therefore, the emitting side temperature is dependent solely on it.
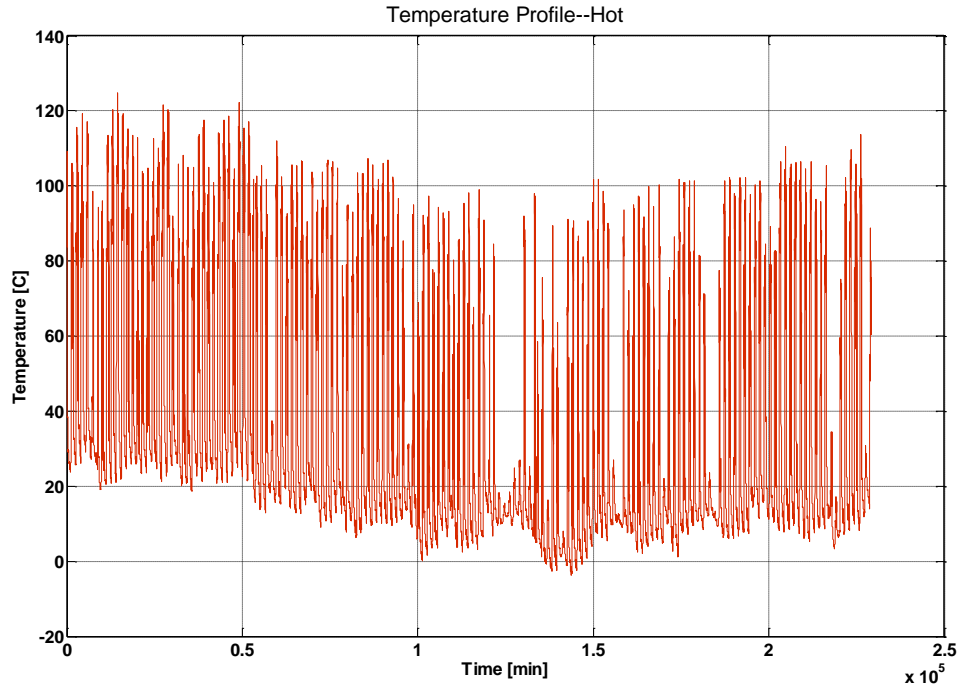
Figure 44 – Temperature variations, Hot side

4.2.11.2 Cold Side Temperature

Figure 45 presents the experimental cold-side temperature results of the commercial TEGs manufactured by *Custom Thermoelectric*. It ought to be mentioned that this temperature is analogous to the one just stated above. In a similar fashion, this emitting-side temperature varies throughout the days of the year and also possesses some peaks and troughs. The peaks generally occur in daytime during summer months; the highest recorded peak value is 72 °C. Conversely, the lowest temperatures occur after sunset, as can be seen from the same graph. Hence, the distance of the instant emitting-side temperature from its instant absorbing-side counterpart would determine the magnitude of the useful temperature (ΔT) necessary to validating the Seebeck theory. The Seebeck effect is thoroughly explained in chapter 1.
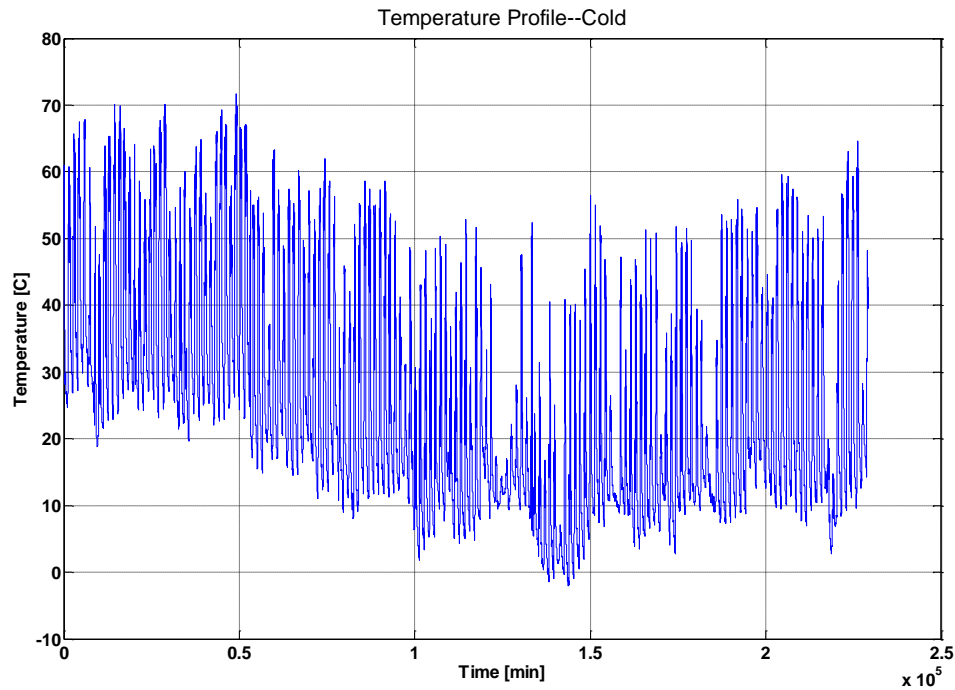
Figure 45 – Temperature variations, Cold side

4.2.11.3 Useful Temperature

Figure 46 shows the experimental temperature differential (ΔT) developed across the TEGs based on the aforementioned two significant variables, i.e. T_H and T_C. It is worth mentioning that without any ΔT, there would be zero potential difference across the semiconductor devices. This fact would negate Seebeck's entire theory. Therefore, it is not only necessary to keep the two sides of the TEGs as far apart as possible, but also to have a good heat sink with the least thermal resistance possible. Figure 46 also shows on average a temperature differential of about 40 °C and above throughout the period, with some maxima in the neighborhood of 60 °C.

Consequently, in order to validate the experiment, a novel electrical-analogy scheme of this STEG system was developed by means of the LTspice simulator. The subsequent section critically analyzes some of the experimental and simulated findings of this work. In addition to that, Sec. 4.2.11.7 and 4.2.11.8 provide more details on these three variables, namely absorbing side, emitting side, and the useful temperatures.
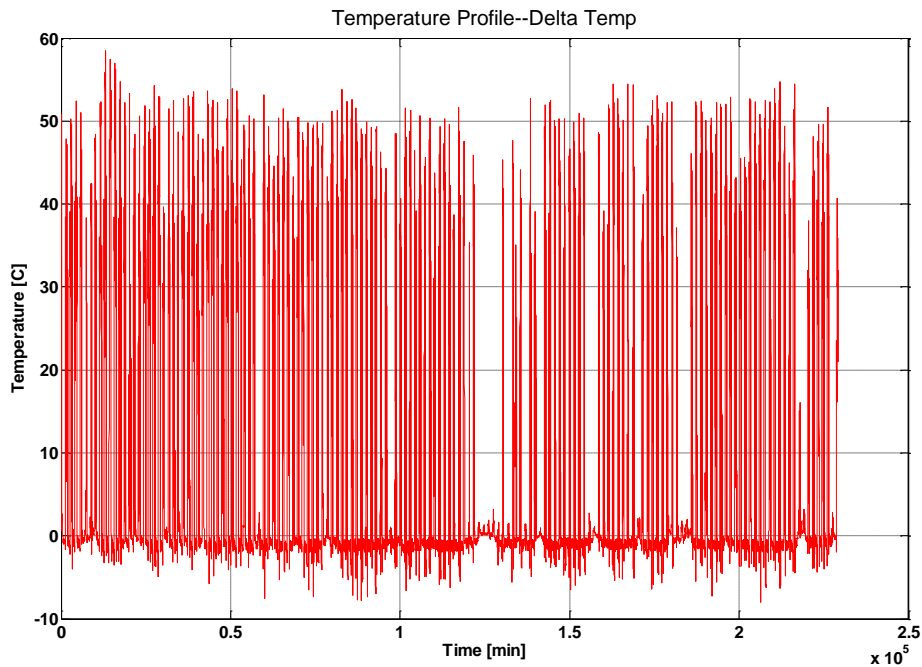
Figure 46 – Temperature differential, T_H-T_C

4.2.11.4   Thermal Efficiency of the System

Figure 47 depicts the thermal energy efficiency of the entire STEG system. This efficiency is consequently estimated based on the daily solar energy received by the absorbing side of the system in conjunction with the resultant useful thermal energy (ΔT). On one hand, the

efficiency is highly variable, with positive values as long as the sun shines. Hence, the average daily efficiency is about 25 percent. On the other hand, the overall average thermal efficiency over the course of 24 hours is estimated to be 14.3 percent. It is worth mentioning that the 25 percent efficiency is more realistic than the latter value due to, again, the nocturnal absence of the sun.

Conversely, the electrical efficiency of these kinds of TEG under investigation was estimated by the manufacturer to be 6 percent under STC. Hence, in these standard and optimal conditions, the hot-side temperature was fixed at 300 °C while the cold-side temperature was 30 °C, thus yielding a temperature differential of 270 °C across the device. In contrast to that, this work aimed at studying the impacts of real environmental situations on the STEG system influenced by many factors, such 1) wind speed and direction; 2) relative humidity; 3) DNI; 4) frequent cloud coverage; and so on.
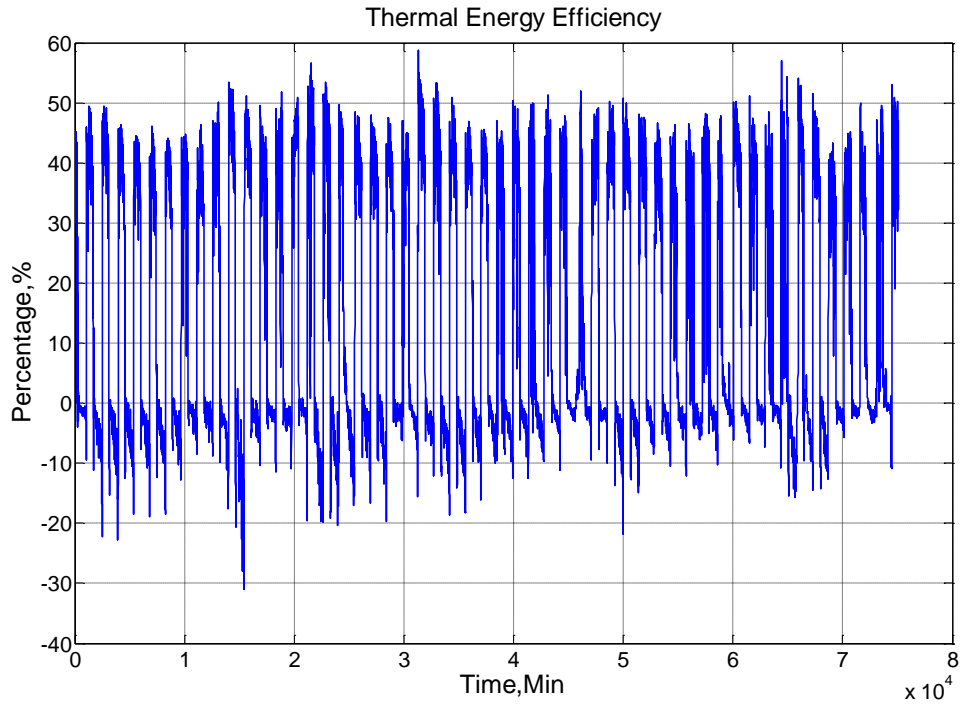
Figure 47 – Thermal efficiency variations

Therefore, far from the STC performance claims made by the manufacturer, the overall real-world solar thermoelectric generator (STEG) test results show an achievable efficiency of 1.30 percent, and are conveniently summarized in Table 13. The real-environment results, as can be seen from the table, vary from zero to a final value, irrespective of the variables because of two major factors: 1) sudden weather events, and/or 2) the nocturnal absence of the sun.

Table 13 - Comparative results—STC vs real-world test

Designations	STC	Real-Environment STEG
Hot Side Temp	300°C	0 to 125°C
Cold Side Temp	30°C	0 to 70°C
Temp Differential	270°C	0 to 58°C
Efficiency	6 %	0 to 1.30 %

4.2.11.5   Comparative Temperature Analysis

Figure 48 shows the typical temperature profiles both recorded and simulated, for the two sides of the STEG system. These temperatures were plotted separately for clarity purposes. Otherwise, it would be hard to decipher if they were to be plotted all together in the same graph. Accordingly, Figure 48 a) and c) on one hand, refer to the experimental and simulated temperatures across the energy-harvesting system respectively, where T_H is the same as $V(Te_5)$ and T_C is represented by $V(Ta_5)$. On the other hand, Figure 48 b) and d) illustrate the useful differential temperatures needed to produce a meaningful output voltage through the Seebeck effect. As can be seen from these two curves (ΔTs), the error rate between simulation and experiment varied from 0°C to about 10°C, and more than 80% of the error rate was attributable to the cold side of the STEG system. This acceptable discrepancy between the real-world solar experiment and the LTspice model can be explained by either or both of the following: 1) the internal parasitic components' variation, and 2) the non-homogeneity of the aluminum blocks that were assumed to be pure metal heat exchangers during the computation of the thermal parameters. Another way of viewing this error is that the LTspice model is roughly 25% less accurate than the actual experiment. The latter lesson would serve as a valid benchmark that would enable the rectification of any future similar solar STEG design and Spice modeling.

Additionally, two main findings can be identified: 1) The ΔT, as significant as 55 °C was in both cases found to be proportional to the local DNI, which was the only input to the system. 2) Because of the laws of proportionality stated above, the variability in the incoming sunlight was likewise noticeable on the two sides' temperature of the STEG as seen in Figure 48 a) and c).
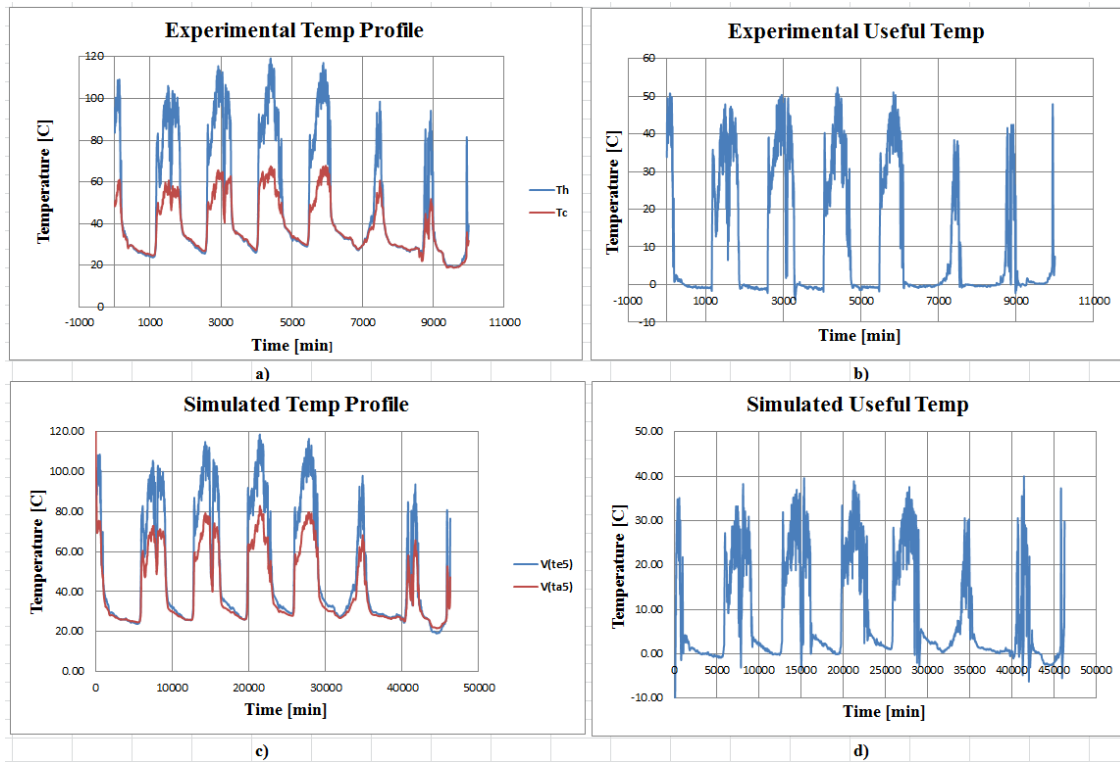
Figure 48 – Temperature variations across the STEG system: a) Experimental temperature profiles, b) Experimental ΔT, c) Simulated temperature profiles, d) Simulated LTspice ΔT

4.2.11.6 Comparative Voltage Analysis (LTspice)

This solar TEG energy-harvesting system was designed and built to serve typical remote residential areas in developing regions. The local direct solar radiation, which was the only input to both experimental and simulated systems, was recorded by means of a Pyranometer. In other terms, the projected energy harvested for the benefit of the remote inhabitants took into consideration not only the actual solar data at the site, but also the typical weather conditions, such as relative humidity, rainfall, and wind speed and direction.

In a like manner, issues of variability remain a critical factor even on the final output of the entire STEG system. As depicted in Figure 49, the continuous voltage supplied, based on the above *ΔTs* developed across the devices, varies between 0V (cases of complete cloud coverage or after sunset) to 8.57V (clear summer sky) throughout the sample of days simulated. Hence, it is worth noting that since there are more sensitive electronic gadgets in rural households today, due to breakthroughs in cellular communication and the medical field, a DC-DC converter is solely recommended for a better lifespan of those appliances.
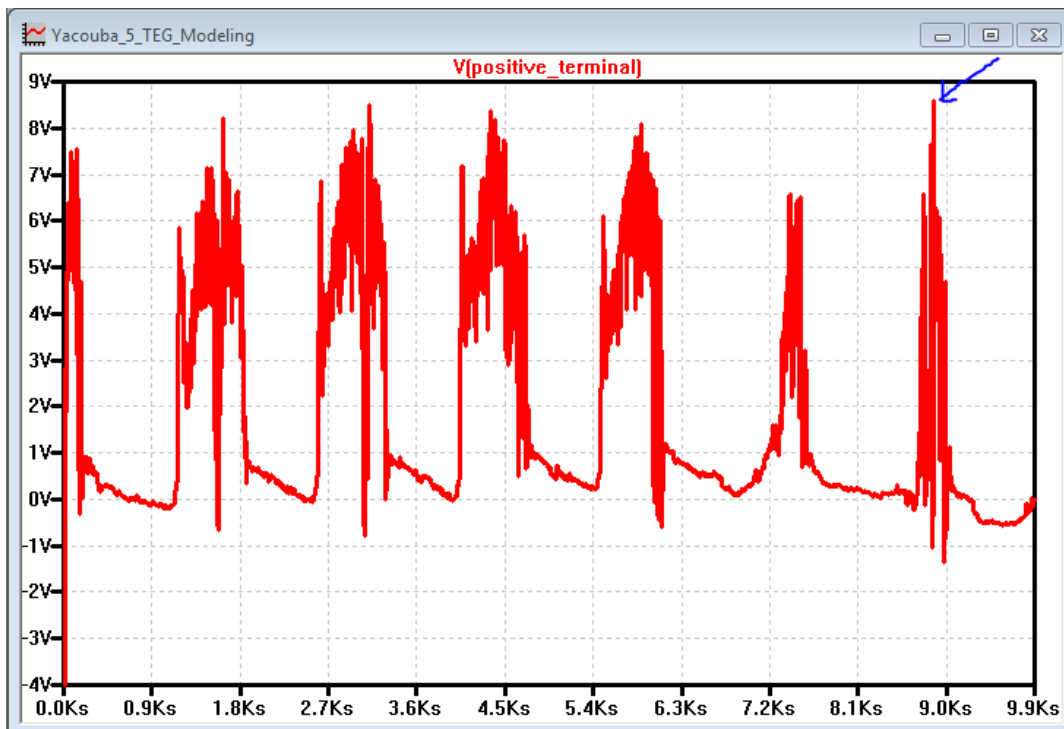
Figure 49 - Voltage waveform over seven (7) days

4.2.11.6.1   Voltage on a Cloudy Day

As real local DNI data from our experiment were imported into the Spice model via the built-in piecewise linear (PWL) command, any intermittency in the insolation would automatically be reflected in the outcome of the model. As an example, Figure 50 portrays the Spice model's output voltage of the system on a typical cloudy day. It is clear that variability remains a big challenge even on STEG energy-harvesting systems. It is important to note that the unit does not always output the exact amount of power that is expected because of random and severe weather events. Therefore, this proves, once again, that variability due to cloud coverage affects real-world STEG systems, the same way it affects PV systems. During cloudy weather conditions, the STEG's output changes suddenly by responding instantaneously to fluctuations in sunlight. An indirect consequence of this finding is that, if a large STEG farm is tied to the grid, the system could have large and frequent ramp events that may create challenges for grid operators. Also, cloud coverage and STEG output variability are intimately related and could be dependent on the system size, shape, speed, and other unknown natural factors. The average and RMS values of the voltage generated by the system on this typical cloudy day are 927.05mV and 2.2065V, respectively (see Figure 50).
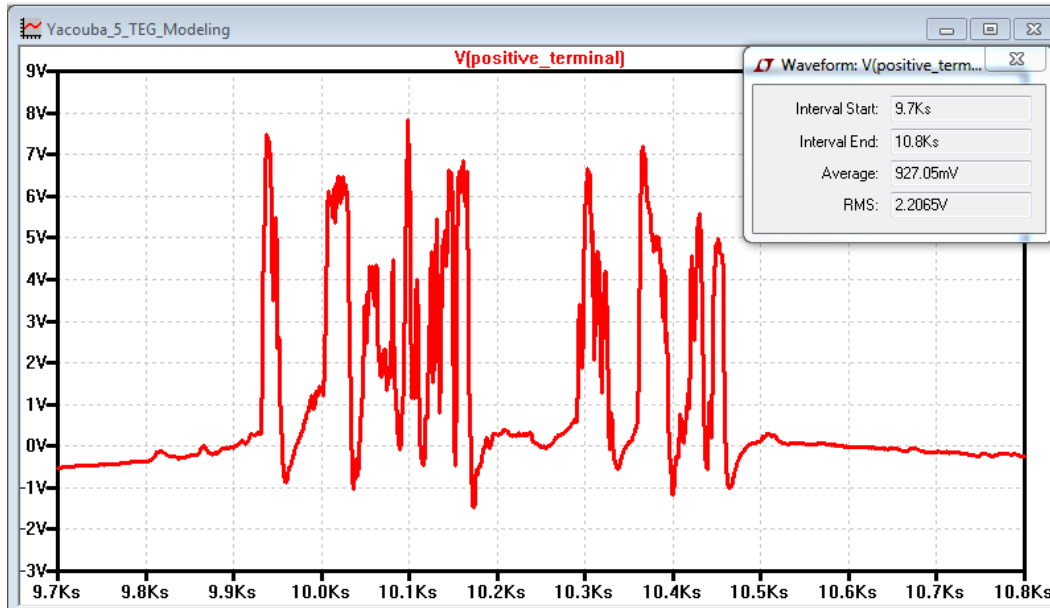
Figure 50 – Voltage comparison—Typical cloudy day

4.2.11.6.2 Voltage on a Clear Day

Similarly, the energy harvested on a typical and fairly normal day is illustrated by Figure 51. As compared to Figure 50, this voltage profile is more like that of a PV system mounted on a dual-axis tracker. It looks coherent and smoother although this curve also replicates, at a somewhat smaller scale, the effects of the inherent variability of solar energy. Thus, it is worth pointing out that the latter changes constantly throughout the days and seasons of the year. Likewise, the average and RMS values of the voltage generated by the system on this clear day are 4.632V and 5.0727V, respectively. As can be seen, the difference between the results of these two days (Figure 50 and Figure 51) is tremendous as the voltage of the clear day is 44 percent better.
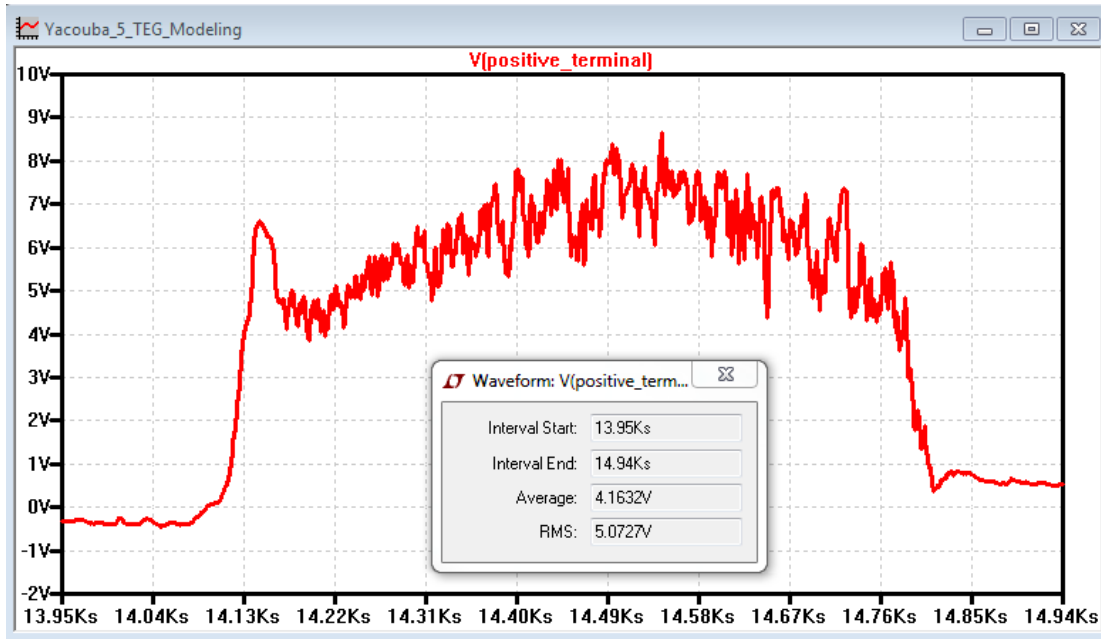
Figure 51 – Voltage comparison—Normal sunny day

4.2.11.7 Typical Cloudy Day before the Converter (Real-world)

Figure 52 presents the results of the STEG energy-harvesting system before the DC-DC converter was added not only to boost the output voltage, but also to stabilize it in a reliable manner. In Figure 52, four important variables are plotted, each in its own quadrant by means of *Matlab* software subplots command: 1) the DNI recorded on the cloudy day; 2) the resulting absorbing side temperature; 3) the emitting side temperature; and 4) the output voltage. Hence, it is important to notice two phenomena that occurred concurrently. First, only the cold-side parameter of the TEG did not replicate the intermittency pertaining to the DNI. This fact clearly implies the existence of a huge thermal inertia between the absorbing and the emitting sides of the system. Second, the voltage on that particular day was not reliable because it was highly intermittent, nor was it high enough to turn on electronic appliances or charge batteries. So, the

139

direct consequence is that without any additional electronic conditioning circuitry, STEG systems would not be suitable in meeting remote residential energy demands.
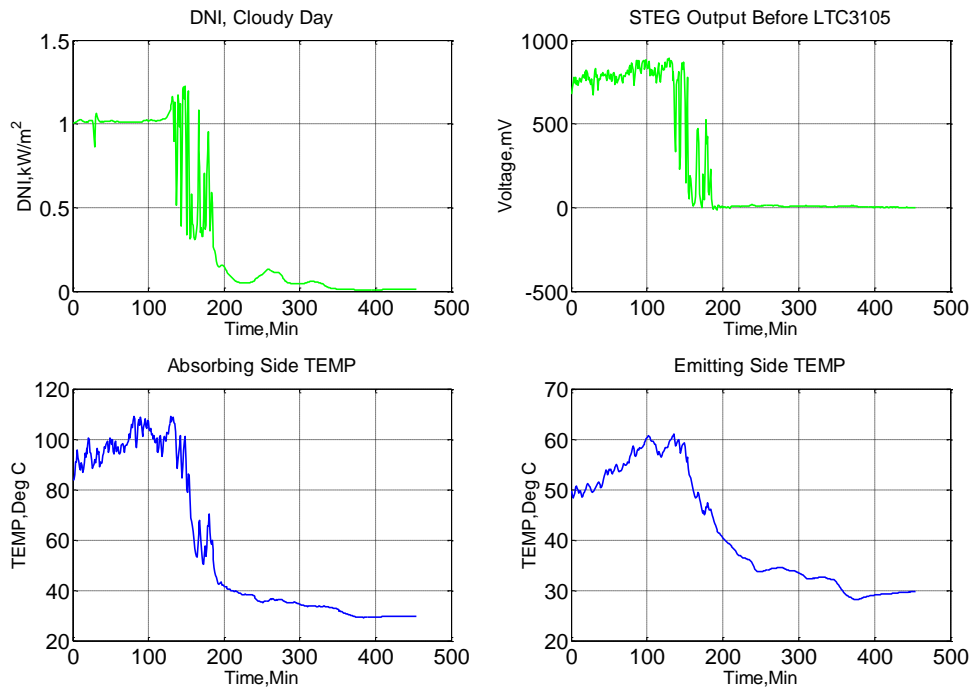
Figure 52 – Related STEG system's variables, Cloudy day

4.2.11.7.1 DNI on a Cloudy Day

Additionally, for clarity, the insolation is separately presented in Figure 53. It can be observed that the changes in the incoming sunlight were instant and abrupt. It changes from high value to low and back again, many times a day. Hence, instead of having a concave-like downward shape, the DNI kept varying from 0.3 to 1.2kW/m^2.
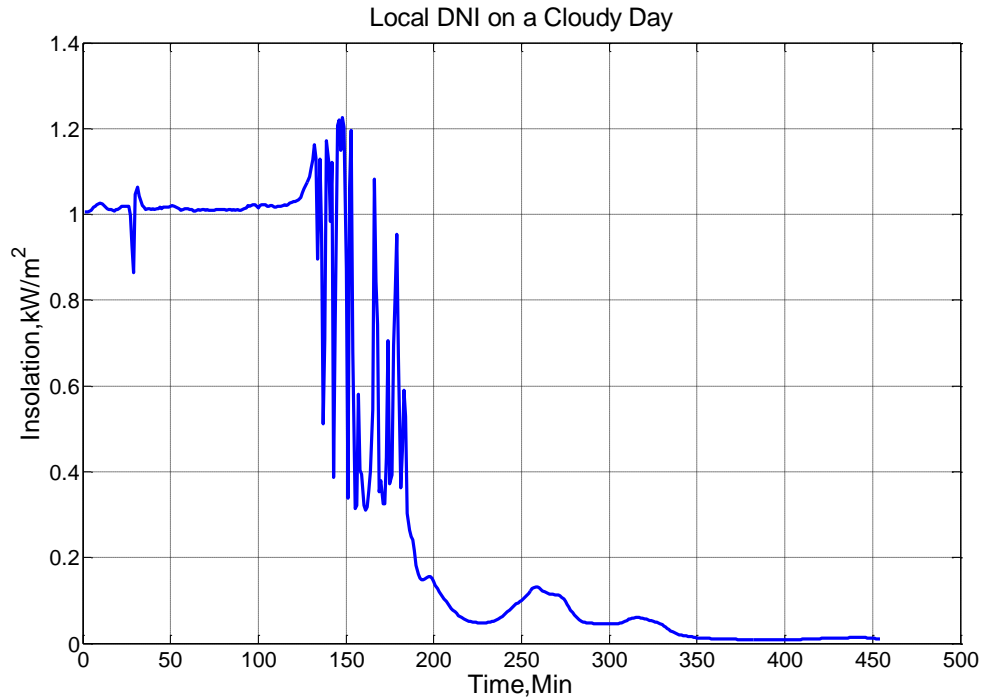
Figure 53 – DNI, Cloudy day (CER)

4.2.11.7.2 Comparative Temperature Profiles, Cloudy Day

Figure 54 compares the three interrelated temperature variables: 1) hot-side temperature (blue); 2) cold-side temperature (green); and 3) temperature differential (red), also known as useful temperature. These three variable parameters were utilized to empirically describe the thermal performance of the STEG system. As can be seen, the temperature differential trends were much more affected by the absorbing side temperature compared to the emitting side temperature. This implies that, since the useful temperature imitates the exact same pattern of the hot side temperature at a lower scale, the thermal inertia across the pile of TEGs had had a lesser effect on it. This can further be interpreted as a good or a bad phenomenon: 1) it is good in the sense that a higher hot side temperature always yields a significant useful temperature, providing a good heat sink is utilized; 2) it is a bad phenomenon in the sense that a lower or intermittent

141

absorbing side temperature results either a much more lower intermittent or a trivial ΔT incapable of generating sufficient voltage through the Seebeck effect.
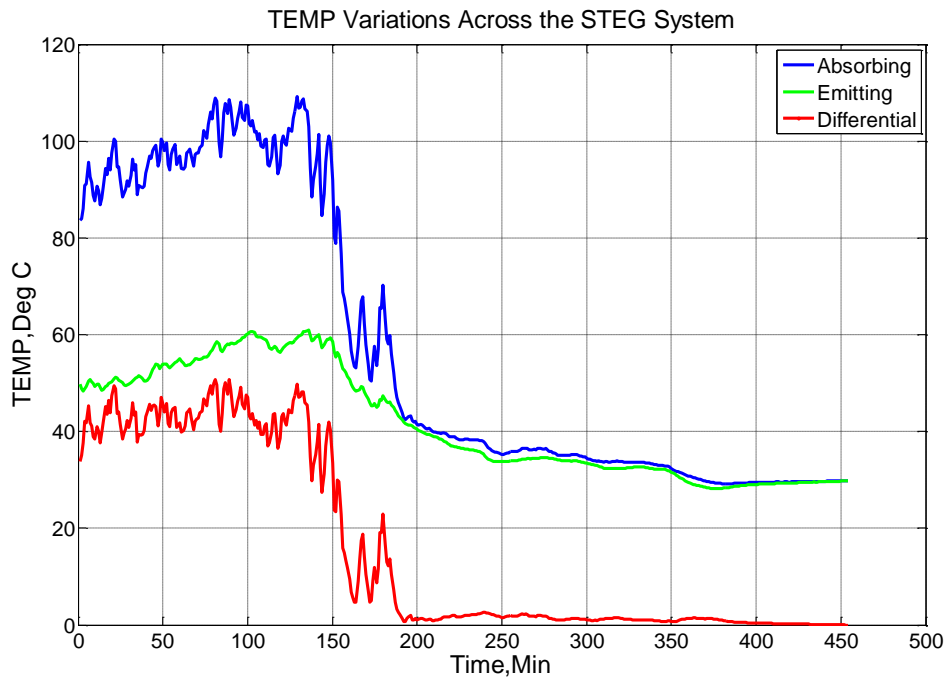
Figure 54 – Comparative Temperatures: Hot side (blue), Cold side (green), and ΔT (red)

4.2.11.7.3 Useful Temperature versus ambient (Cloudy Day)

Figure 55, likewise, illustrates for comparative study demonstration, the temperature differential (red) and the ambient temperature (green). Hence, it important to note that these two variables like the aforementioned parameters were recorded on the same cloudy day. The ambient temperature, as noticed has fewer ripples in it and has stayed in the neighborhood of 33 °C throughout the day. Cloud coverage can be said to have little to no impact on the ambient temperature. This fact contrasts with the effects of cloud coverage on the useful temperature as

viewed from the red curve. However, after sunset, they both converged and adopted the exact same patterns, as the only remaining heat source to the STEG energy-harvesting system was the ambient thermal energy.
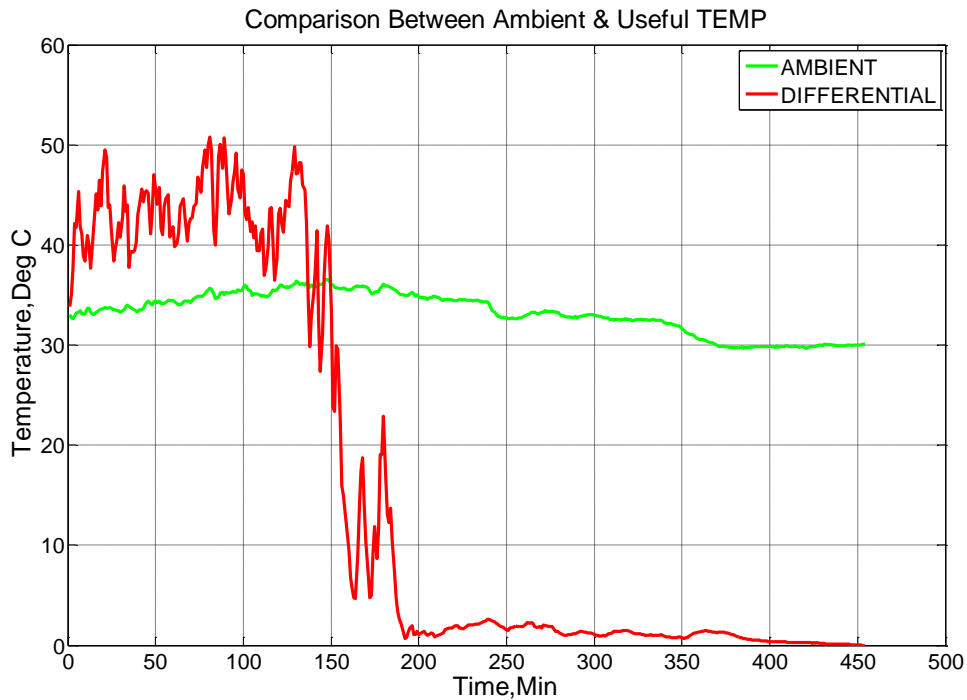
Figure 55 – Ambient (green) and temperature differential (red) trends

4.2.11.7.4   System's output voltage on a cloudy day

Figure 56 portrays the output voltage profile on not only a cloudy day, but also, and importantly, before the consideration of the LTC3105 DC-DC converter in this research. This figure is exclusively added for clarity as a more detailed analysis concerning its matter was covered at the beginning of this section. Nevertheless, it should be noticed that the output voltage

was less than a volt that particular day. Also, the voltage was extremely intermittent throughout the day and the supply was therefore far from being dependable.
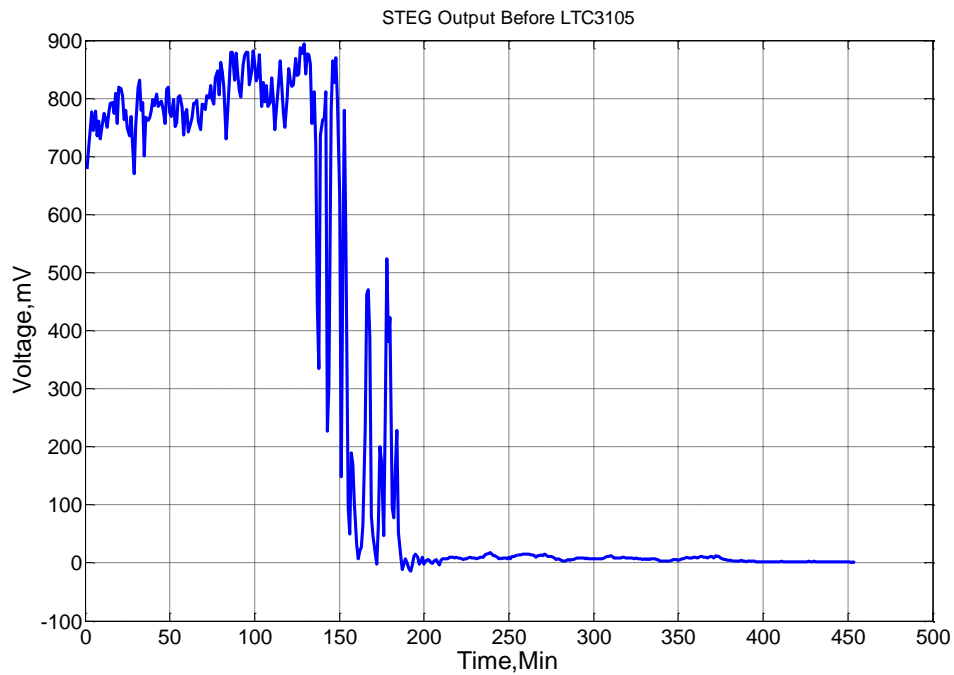
Figure 56 – STEG system's voltage without converter, Cloudy day

4.2.11.8   Normal and Clear Day with the Converter (Real-world)

Figure 56 depicts the results of the STEG energy-harvesting system on a clear day after the LTC3105 DC-DC converter was being added to the generator in order to enhance the overall output. Similar to the investigation performed on the cloudy day, four important variables are presented in this figure, where each one is plotted in its own quadrant by means of a *Matlab* software subplots command. These variable features are, as previously stipulated: 1) the DNI recorded; 2) the resulting hot-side temperature; 3) the resulting cold-side temperatures; and 4)

the converted output voltage. Of these variables, the output voltage has shown some dips although the converter supposedly yields a constant output of 5VDC. Hence, each of these solar energy features is analyzed thoroughly in the subsequent sections.
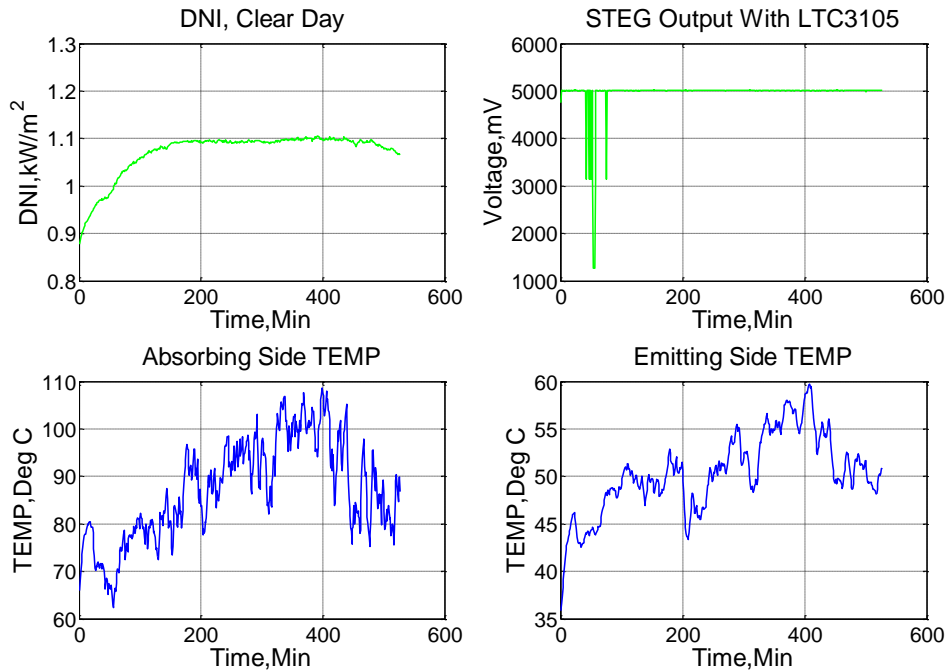
Figure 57 – Related STEG system's variables, Clear day

4.2.11.8.1 DNI on a clear day

Figure 58 illustrates the direct normal insolation recorded at the solar site located at the University of Nevada, Las Vegas (UNLV), where the real-world STEG experiment was conducted. As opposed to Figure 53, the downward concave shape is achievable on this particular clear day. It can be observed that fewer ripples arise in the direct electromagnetic radiation, as the sky was transparent and the day sunny. Because of this, the DNI smoothly

transitioned with a positive slope from about 0.875 to almost 1.10kW/m^2. It stayed at that constant value (*approximation*) the whole day and then completed the concavity by drawing a negative slope. Therefore, the real-environment parameters, such as the absorbing side, emitting side, and useful temperatures exclusively depend on the quality of both the instantaneous and cumulative electromagnetic waves that continuously arrive on the STEG system.
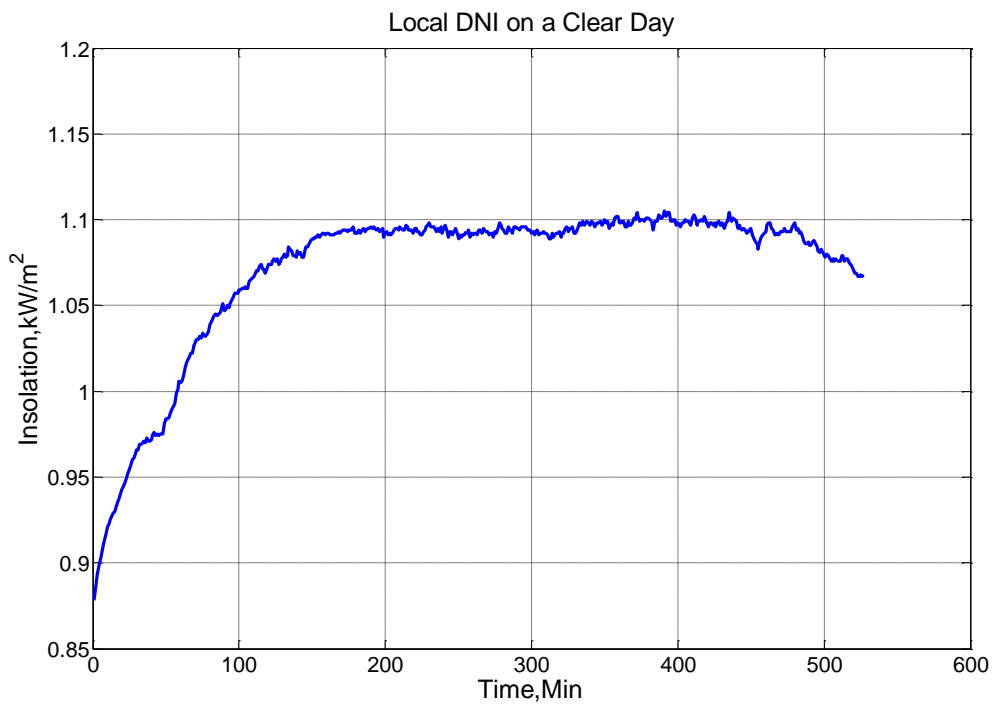
Figure 58 – DNI, Clear day (CER)

4.2.11.8.2   Comparative Temperature Profiles, Clear Day

Figure 59 illustrates the comparative curves of the three interdependent temperature variables. They are, from top to bottom, the absorbing side temperature (blue), the emitting side temperature (green), and the useful temperature (red), as shown in the figure. These parameters,

as previously stated, were utilized to empirically define and investigate the thermal performance of the novel STEG system. The temperature differential trends were tremendously affected by the behavior of the absorbing side temperature. The effect was to the extent that one would undoubtedly think of it as a duplicate, but at a much lower scale. Again, the direct implication is that the thermal inertia across the stack of TEGs had not had as much of an effect on the useful temperature in reference to the emitting side temperature. Furthermore, it can be inferred from these two graphs (blue and green) that a sunny day always yields a significant ΔT which is the sufficient prerequisite for the applicability of the Seebeck theory.

On the contrary, the phenomenon happening on the cold side temperature was totally opposite, but unique in the sense that it stood alone due to the retention of the thermal momentum across the semiconductor pellets.
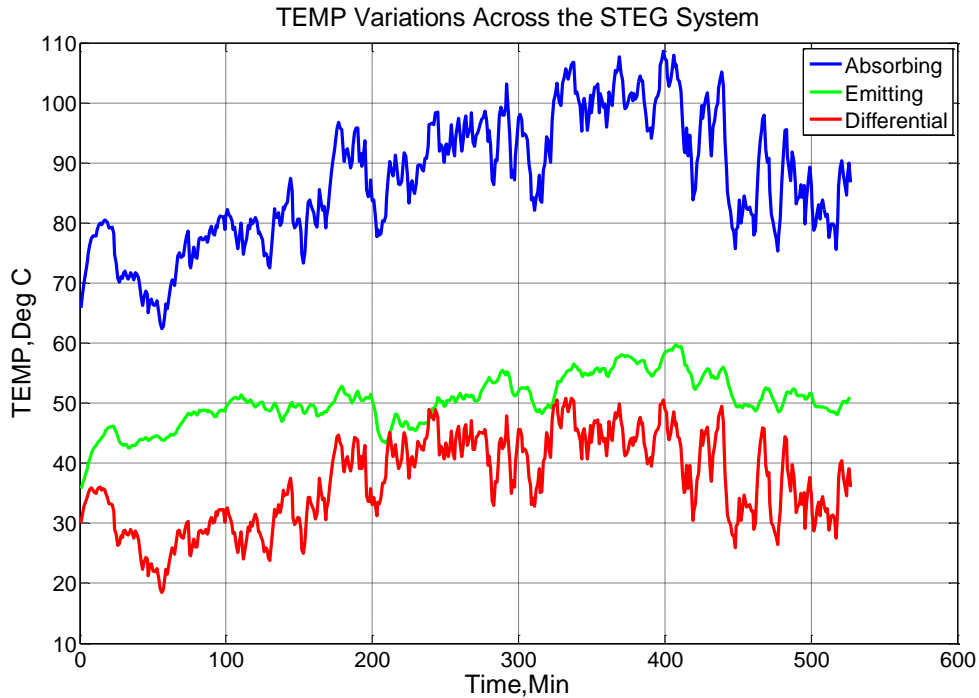
Figure 59 – Temp comparative analysis: Hot side (blue), Cold side (green), and ΔT (red)

4.2.11.8.3   Temperature differential versus ambient (Clear Day)

In light with the same comparative logic approach, Figure 60 purposely compares the temperature differential to the ambient. By extension, it also compares and then contrasts between Figure 60 (Clear day) and Figure 55 (Cloudy Day). As can be seen throughout the day, the *ΔT* rose above the ambient except during some patchy periods. Also, unlike the ambient that was fairly linear, the temperature differential was highly intermittent, although the DNI shown earlier disclosed that the day was clear. Consequently, the *ΔT* is shown to vary between 18 °C to roughly 51 °C through the TEGs. The ambient temperature, as observed, has a distinctive pattern evidently independent of what is happening on either side of the TEGs, as long as the sun shines in the sky.

However, as compared to the previous study done under cloudy day conditions (see Figure 55), after sunset, the ambient as well as the ΔT both have to converge and adopt the same exact patterns. It is worth noting that the only remaining heat source to the whole STEG energy-harvesting system and its surrounding was the ambient thermal energy.
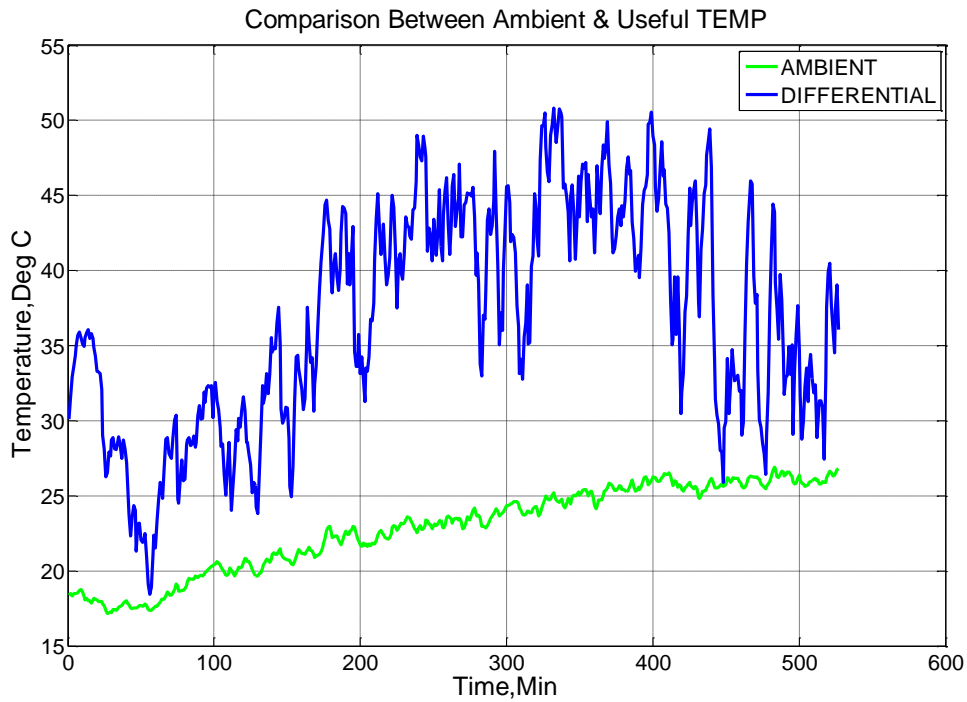
Figure 60 – Comparison: Ambient (green) and differential temperature (blue) trends

4.2.11.8.4   System's output voltage comparison (Cloudy Day with a Converter)

Figure 61 presents the output voltage profiles of the proposed energy-harvesting system in its entirety, including the five TEGs, LTC3105, and K2 battery. It is important to point out that the results shown were recorded on a clear day. Surprisingly, the output of the LTC3105 converter (green) was not constant, as it was disrupted many times. The plausible explanation is

149

that some intermittent phenomena might have taken place either in the circuitry or in the input thermal energy. The occurrence of this weird, but enlightening, phenomenon absolutely shows that a real-world STEG system is far from being safe of frequent transitory behaviors even though the DC-DC converter was utilized.

On the contrary, the safest way to deliver constant and reliable electrical energy to remote residential areas is by utilizing energy storage systems, such as batteries, in conjunction with the STEG system. Therefore, it can be clearly seen that the output of the 3.2V K2 battery remained constant throughout the study period. A significant insinuation is that the proposed system was capable of charging the battery to 3.4 VDC in an efficient manner. It is now an easy practice to connect many of such batteries either in series, and/or in parallel combination, in order to achieve the desired voltage and current levels.
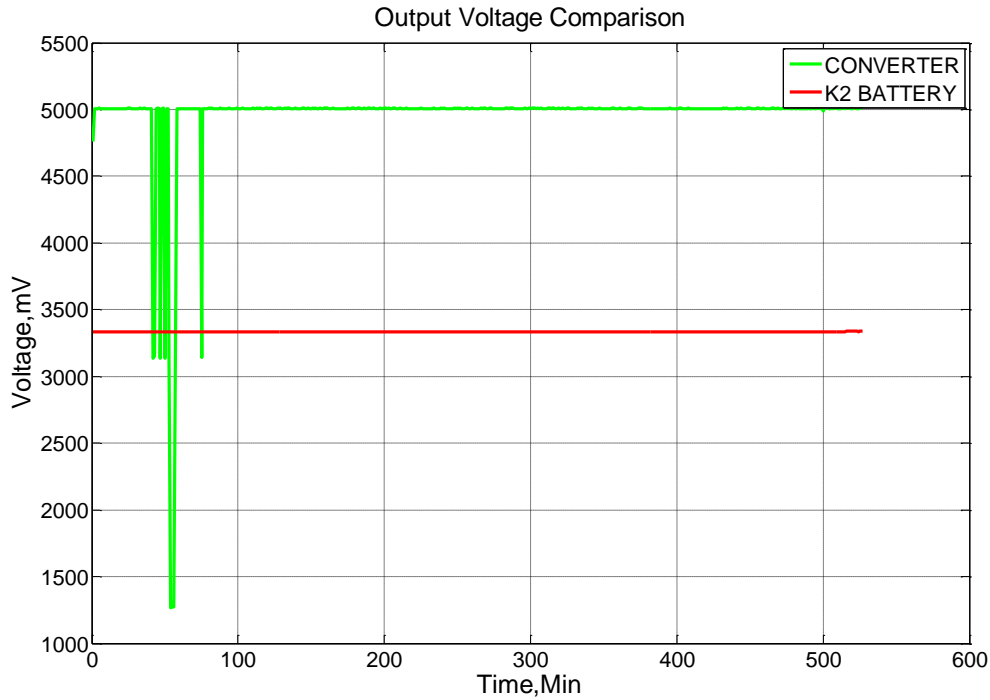
Figure 61 – Comparative STEG system's voltage with converter, Clear day

4.2.11.9 Charge Profiles Analysis

As already mentioned in the previous chapters, solar energy is not available all day long. This fact makes energy storage a suitable technology for remote areas which are far from the grid. K2 batteries, manufactured by a local company were chosen to fit our needs in order to cut down part of upfront costs. A comparative charging analysis was considered and investigated. Figure 62 highlights the various K2 battery charging patterns performed in line with this study. The Maccor 4200 series was used to charge the 3.2V battery in roughly seventeen hours (17 hrs.) in the power laboratory at 1C-rate. After a careful discharge of the battery, the same test stand was re-utilized to recharge the battery at a different C-rate, i.e. ½C, as can be seen in Figure 62. The recharging scenario at ½C-rate was completed at about 33 hours, which almost doubled the charging time at the unit rate capacity (1C-rate).

151

Besides the two different C-rates, other important discoveries made are: 1) achieving the understanding of how the STEG system charges the energy storage system in question and 2) the insight on how real-environment ESS recharge compares to the Lab test. As can be seen from the blue curve, it seemingly takes the real-world system much longer time to charge the battery to the desired level of 3.2 VDC than the Maccor does, irrespective of the C-rates. A more detailed analysis on how the experiment charges the battery is covered in Sec. 4.2.11.9. 2.
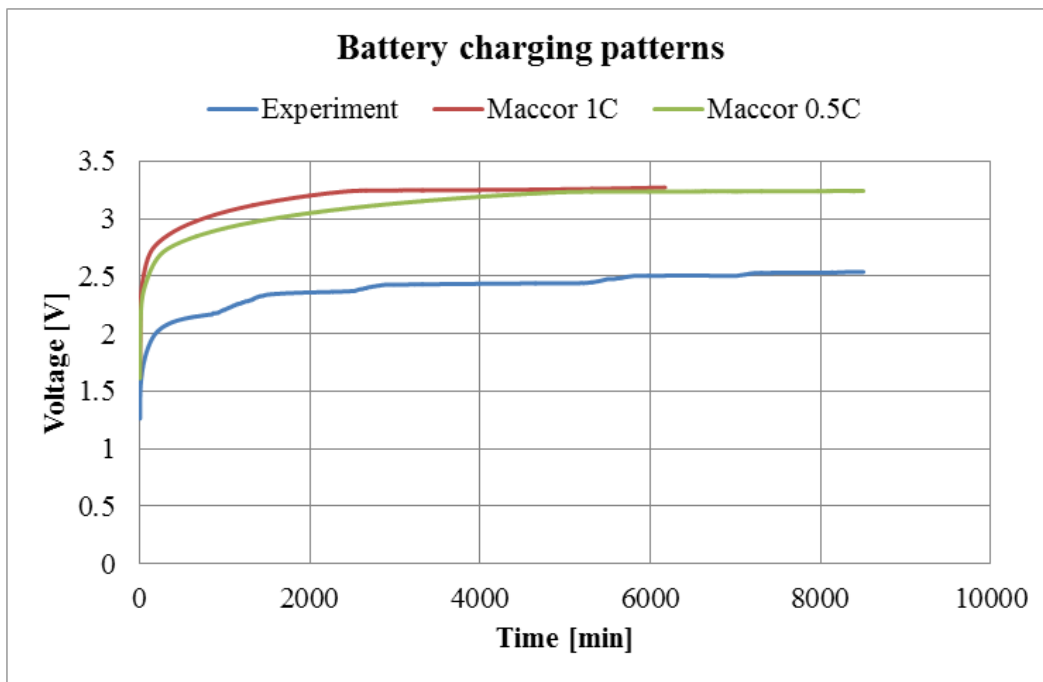
Figure 62 – 3.2V battery charging patterns

4.2.11.9.1   New States Relative to the Old States

Figure 63 presents the various states of charge (SoC) of the LTC3105 converter and compares them to those of the K2 battery. Therefore, in this same graph, four of the important

variable curves were plotted, each in its own quadrant by means of a *Matlab* software subplots command. The two green curves belong to the ESS. The one on the left depicts its *Old SoC* before the discharge event took place, whereas the remaining one on the right hand side (RHS) illustrates the *New SoC* of the battery while it's being continuously charged. Likewise, the two blue curves located at the bottom of Figure 63 portray the O*ld Output* and the *New Output* of the converter, before and during the ESS recharge events correspondingly. The *Old Output* is on the left hand side (LHS) and the *New Output* is illustrated on the RHS. A more in-depth analysis is presented in the two subsequent sections.
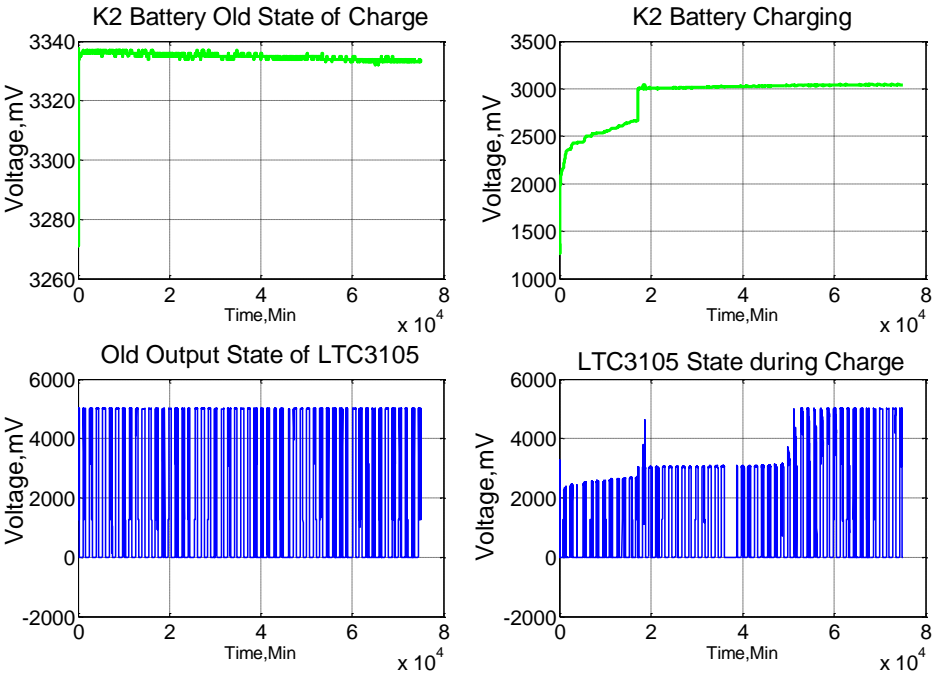
Figure 63 – The states of charge of the K2 ESS and the output of LTC3105 converter

4.2.11.9.2   States of the K2 Battery ESS

Figure 64 shows for comparative purposes the two performance states of charge of the energy storage system under study. As previously stated, the blue curve denotes the *old state* of the battery, whereas the green curve indicates the *new state*. At the very beginning of the investigation, the battery was only utilized as a backup system without any preceding knowledge of how it would actually perform in a real-world scenario in terms of charging and discharging. As can be seen by the blue curve, the battery was not only fully charged but stayed constant at 3.3VDC through the assessment period.

Alternatively, to capture the real charging mechanism of the storage system, the battery was meticulously discharged with the Maccor tester to a safe voltage level of 1.25VDC, as shown by the ordinate axis of Figure 64. The battery was then brought back and hooked up to the STEG energy harvester for real-performance analysis. As shown by the green curve, even after 55 days, the STEG system was unable to recharge the battery to its previous state of charge. This is a great indication that the chemistry of the K2 battery has reached a certain threshold limit beyond which it ceases to convert any of the incoming solar energy into chemical energy. In fact, from the 12th day, the battery has reached its useful limit after the vertical jump from 2.54 VDC to 3.0 VDC in terms of charge retention. Also, beyond that point, the battery was saturated and stayed almost flat for the rest of the 43 days without any significant improvement. Conclusively, the useful and threshold limit of the battery is about 3.0 VDC. Obviously, the Maccor 4200 tester has shown great signs of efficacy compared to the real-world STEG system.
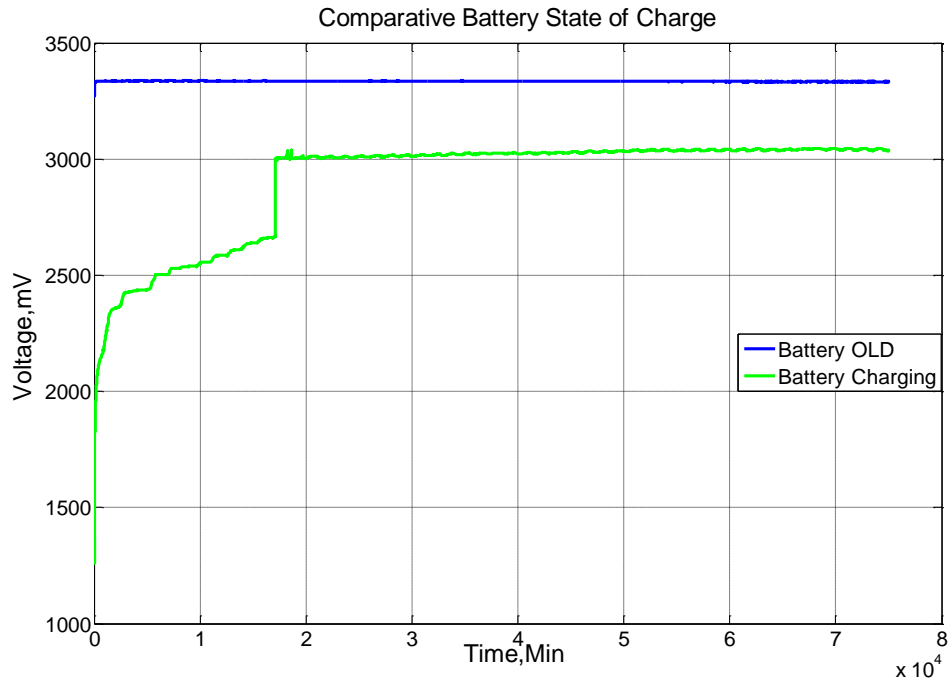
Figure 64 – The old and new states of charge of the battery

As a result, Table 14 recapitulates all the findings discussed above. Irrespective of the battery charger or the value of the C-rates, however, two valuable parameters worthy of consideration for battery performance analysis are: 1) the Time span, t and 2) the Final Voltage, V_F. Therefore, as a quick note, the Maccor 4200 series is a laboratory based battery tester utilized to either charge or discharge any type of battery technology under various conditions, providing the appropriate test procedure is precisely written as discussed in chapter three. Consequently, no additional analysis is required at this stage since these results organized in a tabular format are not only self-explanatory, but are also in favor of the laboratory test stand in terms of both time duration and voltage level.

Table 14 - Summary of K2 charge characteristics

Designations	Maccor 4200 series		STEG
	0.5 C	1C	
Final Voltage (V_F)	3.2 *V*	3.2 *V*	3.0 *V*
Time Span (*t*)	33 *hrs*.	17 *hrs*.	12 *Days*

4.2.11.9.3   States of the LTC3105 Converter

As briefly stated in the introductory discussion of this section, Figure 65 depicts a comparative illustration of the O*ld Output* (blue) and the *New Output* (green) of the converter before and during the K2 battery charging events. Hence, it is worthy of note to point out that this part of the analysis focuses primarily on the whole days as a *SET*, rather than a single day as many events, such as transients and discontinuities, might have happened due to unpredictable or sudden weather changes. Therefore, we are more interested at this stage of the analysis at the global trend of the LTC3105 output voltage over the charge time span. As seen from the blue curve, despite some sporadic voltage dips related to the inherent variability effect of solar energy, the output of the converter can be estimated at 5.0 VDC all day long for the entire 52 days of the test period. This indicates an intimate linear relationship between the battery *Old SoC* and the LTC3105 *Old Output,* as they both stayed constant at their respective values throughout.

In contrast, the green curve reveals three valuable and major findings worthy of discussion: 1) after the addition of the discharged battery, the output of the LTC3105 dropped to 2.4V; 2) the output of the converter has three sections, each carrying a different value and meaning; and 3) the curve also shows a close linear relationship between the battery *New SoC* and the LTC3105 *New Output.*

The overall trend of the green curve is comparable to an N-type doped semiconductor material's carrier density dependence on temperature. The similitude of the first region (*first 12*

days) as compared to the ionization region is termed in this work, the *Initialization region,* where the converter re-adjusts itself to the new environment and then it starts increasing its output voltage as the battery gradually moves to a new *SoC*.
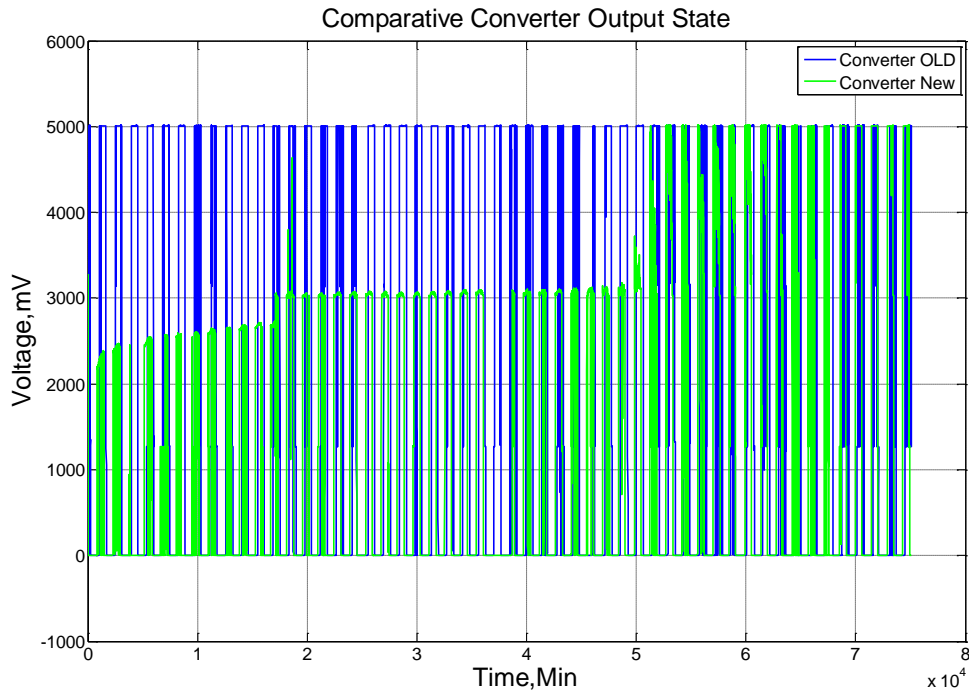
Figure 65 – Comparison between the old and new LTC3105 output

Similarly, the similitude to the extrinsic region is termed here, the *Constant-but-Consistent region,* where the output of the LTC3105 stays flat over a wide range of days. This state is a virtual, but somewhat desired, region of operation. In this region, all the charges are equally split between the converter and the battery where,

$$V_{LTC3105} = 3.0V = V_{K2} \tag{60}$$

157

At this time, any additional thermal energy is regarded as not effective until a new state is reached as days are passing by. The third resemblance has to do with an intrinsic-like region. In this particular similarity, as more and more days were passing by (~24 *days*), the constant region turned into a *Normal-Operation region,* and the output voltage of the LTC3105 exceeds the voltage of the K2 battery. Finally, this analysis by the use of a technique known as *SIMILIE*, strictly applies to the aforementioned *New SoC* of the K2 battery energy-storage system covered in the humidity (RH) on the entire outcome of the STEG system is investigated in this work and then analyzed based of the actual site data. Toward that goal, Figure 66 presents both the RH curve (green) and the useful temperature (blue) retained across the string of TEGs. As can be seen, there is a close correlation between the two variables. The first insight is that these two juxtaposed curves helped to confirm a *FACT*: RH is always higher night time, but obviously lowers during day time due to a high evapotranspiration phenomenon caused by electromagnetic waves. Second insight can be clearly noticed from the 7th column that a higher RH percentage in the air has a strong negative impact on the amount of ΔT that can be achieved. The direct implication of that is, by extension, the Seebeck effect, which is the fundamental TEG working principle, would yield to an insignificant potential difference. Thus, a high RH is irrefutably synonymous of low STEG system performance. The third insight is seemingly at the advantage of any solar energy-harvesting system, such as PV, TEG, and the like. Simply stated, the 9th column of the same comparative graphs reveals that the opposite effect of the above discussion is also correct. Although RH slightly increases the cooling of solar panels which could be of a great benefit in terms of V_{OC}, it does equally demonstrate the tendency to lower the useful temperature of the TEG system in question. In the long run, decreasing ΔT by any means, when it is still

within the manufacturer's specifications is considered as a potential source of negative impact. To sum up, the higher the RH, the lower the inclusive STEG energy generation would be.

In a similar fashion, the wind speed and direction effects on the output of the solar thermoelectric generation system under study can also be analyzed based on real data available to us. For the time being, this phenomenon is overlooked as it is not the focus of this current work.
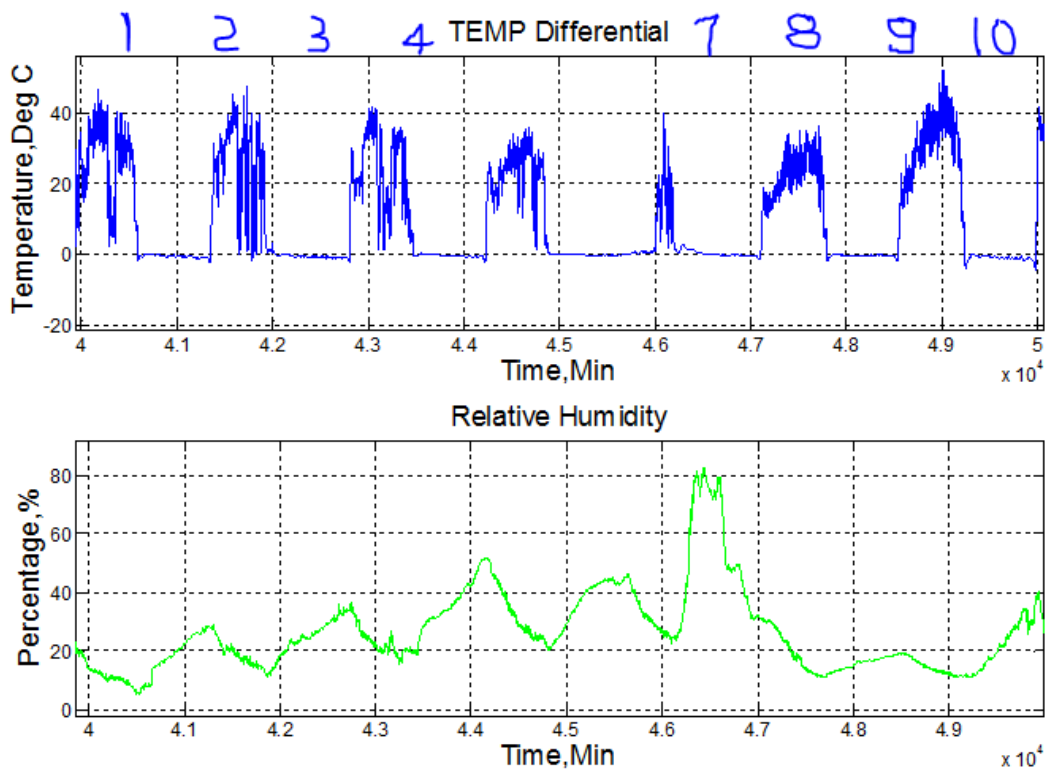
Figure 66 – Local relative humidity vs delta temp (CER)

4.2.12 TEG RC Analogy and Analysis

It has been proven throughout this research that the solar irradiance is directly proportional to the temperature on the hot side of the TEG. So, an impulse of light was organized in a lookup table to simulate the local *DNI* and then fed into the Spice model by means of the built-in LTspice piece wise linear (PWL) command. Hence, *V (Te$_2$)* denoting the temperature on the hot side of each one of the five TEGs, as can be seen in Figure 67, follows the exact same pattern of the impulse light. In the same figure, *V (Ta$_2$)* denotes the temperature on the cold or absorbing side. It is worthy of note to point out that two parameters, *viz.* the internal parasitic capacitance (*C*) and the internal resistance (*R*) of the TEG, turned out to be of great importance in the current study. Figure 45 illustrates a novel way of analyzing an RC circuit as can be seen from R$_{42}$ and R$_{43}$, C$_{29}$ and C$_{30}$ (*5th TEG at upper right of Figure 42*). Further, the impulse-like lookup data were fed through V$_3$ (*low left of Figure 42*). For clarity purposes, the combination of the two resistances is equivalent to the TEG's internal resistor, whereas the summation of the capacitances is referred to as internal parasitic capacitor effects.
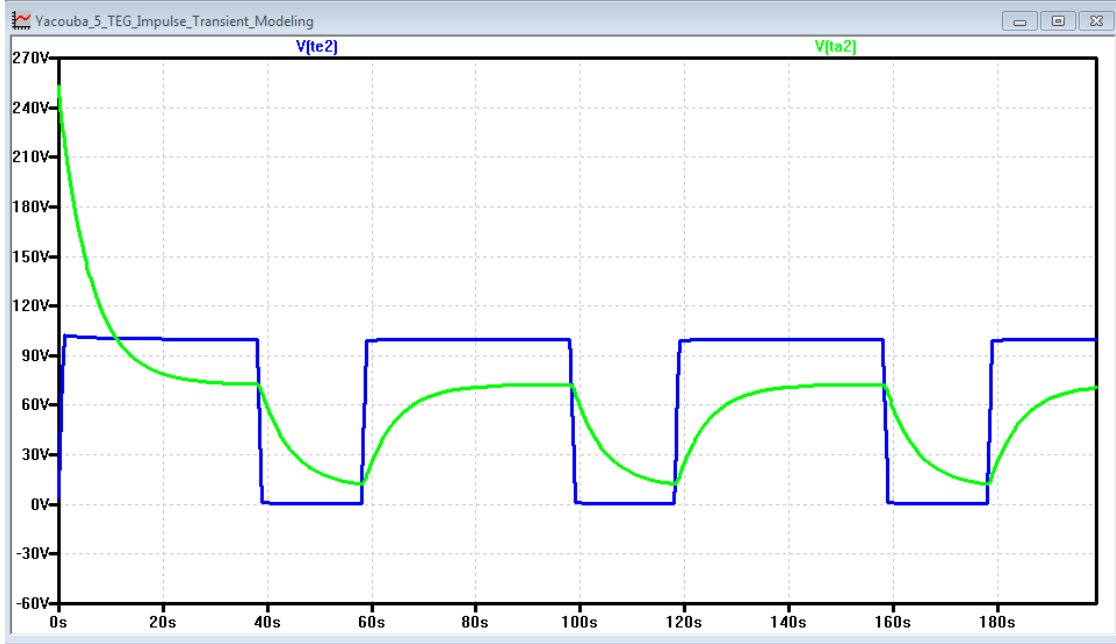
Figure 67 – Ramp rate in an STEG circuit

Therefore, If the input square wave, which is temperature in this study, transitions from 0°C to 100°C (T_{pulse}), then the temperature across the cold side of the TEG is calculated as

$$T_{Cold}(t) = T_{pulse} \cdot \left(1 - (\text{e})^{-\frac{t}{RC}}\right) + T_{Initial} \tag{61}$$

Where, T_{Cold}, T_{pulse}, and t are the temperature on the emitting side, temperature on the absorbing side, and the time variable respectively; $T_{Initial}$ is assumed equal to zero in this case.

Also, it should be mentioned that due to the internal parasitic components effects, such as inductance and capacitance on one hand, and the effect of the heat exchanger on the other hand, the TEG RC analogy is slight different from the conventional *RC* circuit behavior. In essence, the Seebeck theory is only applicable if a certain temperature differential appears across the TEG. So, by virtue of that, when steady state is reached, T_{pulse} and T_{Cold} are quite alike. In

161

addition to that, when the applied pulse goes to zero, $V(Ta_2)$ stays at certain threshold value because of the same aforementioned reasons.

In other words, the time it takes the TEG to reach half of the input pulse, although not similar to the conventional delay time, t_d, can be calculated by

$$\frac{T_{pulse}}{3} = T_{pulse} \cdot (1 - (e)^{-\frac{t}{RC}}) \Rightarrow t_d \approx 0.4 \cdot RC \tag{62}$$

The new RC theory, though has some limitations because it is only applicable to TEGs, needs further explanations. T_{Cold}, as can be seen from Figure 67, begins its ascension at 10% of the applied pulse. It then flattens out at approximately 80% of the latter temperature, which implies that all the computations and the subsequent reasoning would be in the useful range of 0.6 to $0.7 T_{pulse}$.

From the traditional RC circuit theory, the rise time is known to be the time the output pulse takes to go from 10% to 90% of the input pulse. In this particular similitude, we are dealing with temperature rather than voltage. So, in the solar thermoelectric generation RC analogy, it goes from 20% to 60% as can be viewed from Figure 67 and Figure 68. Therefore, the rise time, t_r, in terms of RC time constants is given Eqs. (63) and (64).

$$0.2 \cdot T_{pulse} = T_{pulse} \cdot (1 - (e)^{-\frac{t}{RC}}) \tag{63}$$

and

$$0.6 \cdot T_{pulse} = T_{pulse} \cdot (1 - (e)^{-\frac{t}{RC}}) \tag{64}$$

So, after solving these two equations independently for $t_{0.2}$ and $t_{0.6}$; the results are $0.22RC$ and $0.92RC$ respectively.

Finally, the rise time in question, t_r, of the STEG RC analogy is given by Eq. (65).

$$t_r = t_{0.6} - t_{0.2} = 0.92 \cdot RC - 0.22 \cdot RC = 0.7 \cdot RC \tag{65}$$

In summary, we have demonstrated and developed a novel RC theory applicable only to solar TEG. This new theory explicitly shows not only the implications, but also the effects of internal parasitic elements (R, C, and L) on the inner transient heat transfer occurring in any solar energy-harvesting TEG. Also, for those who are not very familiar with the RC concepts, the t_r found in the current study is the same as t_d found in the conventional RC analysis. The only exception made is that, although they both carry significant meaning, they must be interpreted and understood independently from one another.

Figure 68 illustrates the pulse-like hot side temperature (blue) and how the emitting side temperature rises and falls in response to the applied thermal energy (green). Also, presented in this same graph is the output voltage of the overall energy-harvesting system in red.
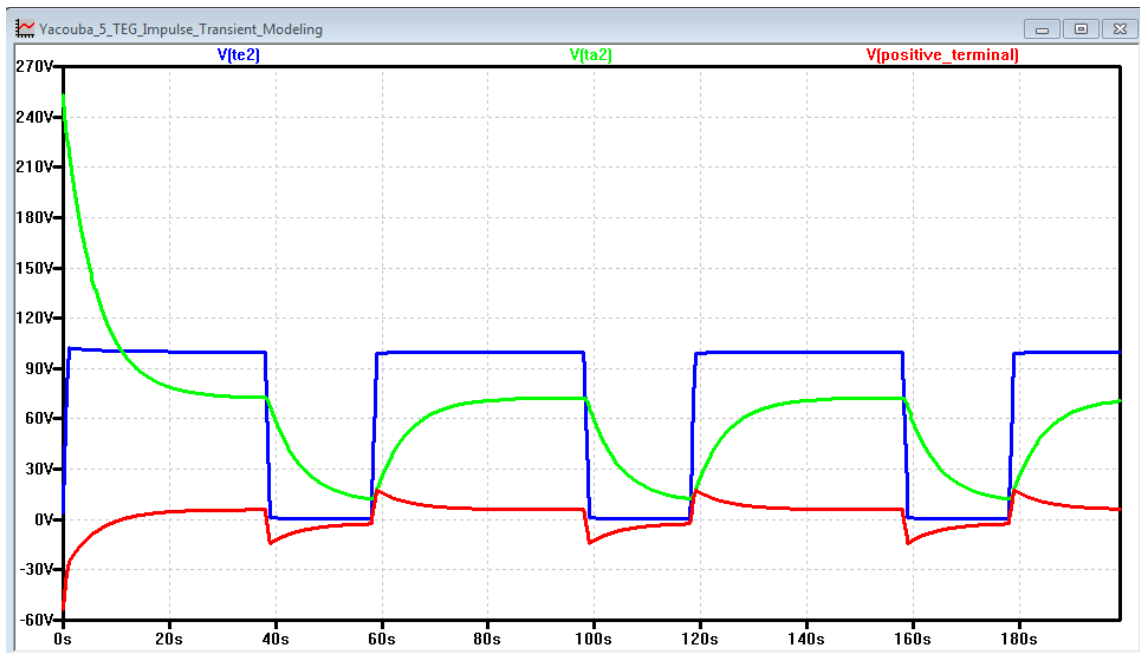
Figure 68 – Spice STEG response to RC analogy

Consequently, the output voltage of the STEG system in response to the applied electromagnetic pulse of light is displayed by itself in Figure 69 for clarity purposes. In like manner, as the pulse like input solar energy was rising, flattening, and then falling sharply, the overall system's output voltage was also varying. It is worth mentioning that when the hot side temperature flattens at 100 °C, the output stabilizes to a certain threshold voltage in the neighborhood of 6V, as can be clearly seen from Figure 69. It then falls with a negative slope and the cycle repeats itself in a periodic fashion. Further, due to the thermal inertia and the way the Seebeck theory works, the voltage continues its negative and abrupt descent until the next thermal pulse kicks in. Hence, this trend once again confirms the need for a DC-DC converter in conjunction with any real-environment STEG energy-harvesting system or it would otherwise be detrimental to costumer sensible electronic appliances. In addition to that, an energy storage system, mainly any of the dominant battery technologies, is highly recommended towards the same goals since solar energy is not only stochastic in nature, but is also absent during night time.
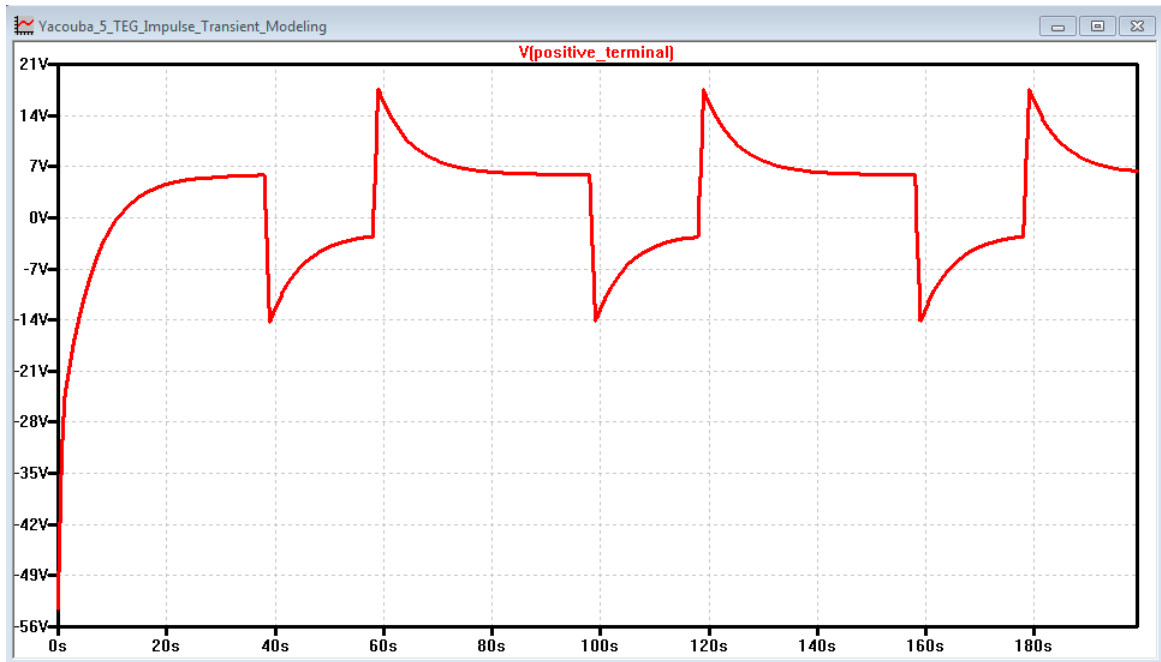
Figure 69 – STEG output voltage in response to light pulse

4.2.13 Summary

A stand-alone and real-world environment solar thermoelectric generator energy-harvesting system was designed, built, and simulated for energy delivery to remote residential areas in developing regions. All the thermal capacitances and resistances of the various physical parts which constitute the system were computed based on the multipart geometries and properties of the device. An LTspice model for the entire system was then developed utilizing the thermal-to-electrical analogy schemes. The internal thermoelectric generators' parasitic inductances and capacitances variations with temperatures were captured in this model for accuracy purposes in the analogy. The local direct normal solar insulation was the only input to the system. Overall, the main objective for energy delivery to off-grid remote and developing regions was positively demonstrated and achieved. Simulated results agreed with the

165

experimental data recorded on site. Any error rate in the model can be explained by either one or both of the following: 1) the internal parasitic components' variation, and 2) the non-homogeneity of the physical blocks that were assumed to be a pure aluminum heat exchanger during the computation of the thermal parameters.

Additionally, this work has introduced a second important and unique analogy. Therefore, this novel RC analogy of the designed solar thermoelectric generator was intended to exclusively estimate the cold side temperature variations of a TEG when an impulse-like electromagnetic wave radiation is applied on the absorbing side of the system. For the time being, this RC analogy is only applicable to a Spice model of any thermoelectric module power generation system or real-world TEG energy-harvesting systems until the theory is widespread.

4.3   Comparative Analysis

Energy researchers have long attempted to convert thermal energy into usable power for daily electrical needs. The sun is the main source of energy on Earth. Several methods have been investigated to harness the tremendous amount of energy that is infinite at a human scale. The conversion of these electromagnetic waves to direct electricity has been dominated to date by solar thermal power generation and photovoltaics. As part of this work, ways were investigated by which TEG systems could, in a near future, compete with solar PV systems, at least for remote off-grid applications in terms of reliability and efficiency. Although this comparative study is not completely conclusive in favor of the solar TEG energy-harvesting systems, the latter affords numerous advantages over PV systems.

4.3.1   Efficiency Comparison

The temperature measurements reveal insufficient temperature difference between absorbing and emitting ceramic plates of the STEG system if compared to the results obtained

166

under standard test conditions. Nevertheless, the average daily temperature efficiency is about 25 percent, but the overall average temperature efficiency over the course of 24 hours is estimated at 14.3 percent. It is worth mentioning that the 25 percent efficiency is more realistic than the latter value due to, again, the nocturnal absence of the sun. Therefore, the temperature efficiency, not to be confused with neither thermal nor electrical efficiency, of this system is evidently higher than that of most PV systems, except the triple junction technology. This previous finding, however, is not meant to obstruct the real electrical efficiency of the STEG system. Thus, the real-world solar thermoelectric generator (STEG) test results show an achievable efficiency of 1.30 percent under arid weather conditions, which is clearly far below the actual solar conversion efficiency of any of the existing PV a technology.

Although the current price of thermoelectric modules is seemingly high, they are extraordinarily small. Therefore, this fact can be viewed as a great advantage for solar projects where space is of a big concern.

Besides, it would have been more convincing to conduct a comprehensive economic analysis to truly disclose the real benefits of TEG without any superficial verdict based on the efficiency alone. This understanding is required to finalize the comparison. Unfortunately for this supplemental study, not only does the comparison require extra time and money, but it is assuredly outside the scope of this research plan.

4.3.2 Reliability Comparison

In contrast to photovoltaic cells, thermoelectric devices can, however, operate anywhere and anytime, day or night, providing there is a significant heat source. Since steam turbines supply around 90 percent of the US daily electrical energy demand, TEGs can be competitively attached to the plants' exhausts to potentially recover waste heat. On the plus side, again, the

167

biggest advantage of thermoelectric generators is that waste heat is freely available and TEG may be the most common way to transform it to usable power.

Conversely, the thermal stability of TEGs is another challenge that has not been totally understood. Additionally, the lifetime of TEG modules is shorter (less than 20 years) as compared to PV, especially when the absorbing side temperature is sufficiently higher to cause permanent damage at the junctions. The projected service life of PV cells is in the neighborhood of three decades.

Chapter 5: Conclusions, Contributions, Discussions, and Suggestions for Future Research

5.1   Overview and Conclusions

This work seeks to investigate ways to deliver renewable energy to remote residential areas in developing regions. Thermoelectric modules that work based on the principles of Seebeck theory were selected for both technical and economic reasons to accomplish the work at hand. A novel transient heat transfer analysis method was introduced, whereby a circuit simulator was proposed rather than the complex analytical heat transfer equations to analyze the experimental system in its entirety. The proposed thermal analysis method is based on the *thermal-to-electrical analogy* schemes. Hence, effects of internal parasitic components, such as inductance and capacitance were estimated and taken into consideration in the current research project. Considering these elements helps to capture the real-world performance of the STEG energy-harvesting system in the LTspice simulation model.

Chapter 1 presents the current situation in emerging economies in terms of access to electricity and how severely the lack of electricity obstructs all sorts of advancements. Additionally, it also highlights the ever-increasing demand for electrical energy on a daily basis with the plethora of electronic gadgets that invade both urban and rural households in developing countries. The chapter, moreover, elaborates on the vivid need for any sovereign country to attain energy independence through not only dependable, but also, and most importantly, renewable sources, such as hydropower, wind power, photovoltaics, solar thermoelectric generators (STEG), and the like, for the sake of global sustainability.

Furthermore, this opening chapter serves as an initial platform where all the important objectives and challenges of the current work are emphasized in a concise manner. Finally, this chapter

covers the motivations and background of the work, and also outlines the dissertation plans in chronological order.

Chapter 2 reviews the literature through identification of the advances accomplished thus far at both academic and industrial levels in the field of thermoelectric devices and systems. The chapter further focuses on categorizing the various areas of thermoelectric modules' applications. Therefore, TEG with DC-DC converter, TEG with energy storage system, Spice modeling of TEGs, and solar TEGs are some of the applications in the literature. Particular emphasis is put on the articles treating the thermal-to-electrical analogy concept, utilizing the family of spice simulator software, as they are the most frequently cited papers throughout this study.

Finally, this literature survey chapter serves as the benchmark to this work because it lays the conceptual foundation for understanding the STEG research and also clarifies the potential research gaps. The chapter is further subdivided into a general and a specific review for clarity purposes, followed by brief concluding remarks.

In **chapter 3**, the proposed energy-harvesting-system methodology and the implementation of the novel thermoelectric LTspice modeling techniques are thoroughly covered. Hence, this project has designed, built, and tested a solar thermoelectric generation system. Investigation of a commercial TEG has been attempted under real conditions similar to arid and harsh weather situations comparable to the Sahel, a unique geographical band located in the northern hemisphere of Africa. Second, and especially worthy of note, electrical parameters have been computed from both a datasheet and the device's geometries and properties.

Additionally, the internal parameters variations with temperatures of the thermoelectric modules have been implemented in the electrical model of the thermal system via the arbitrary behavioral voltage sources (ABVS) command.

In a nutshell, after establishing the basic working theory of TEG modules, the following investigations were performed in a sequential fashion: 1) description of two major LTC DC-DC converters, *viz.* LTC3105 and LTC3525 (although the latter converter has proved not to be applicable to the current STEG system) and ways in which they can enhance the outcome of the study; 2) the performance of the Maccor 4200 series battery tester followed by a rigorous assessment of different battery technologies and some practical sizing scenarios; 3) the simplification of the visual acquisition of the whole system by designing an architectural compact view and energy flow chart; and 4) lastly, a brief cost-effective analysis of a typical rural household's energy storage needs concludes the chapter.

Finally, **chapter 4** presents the experimental verification of the thermo-electricity theory and the results under different scenarios. This chapter is further divided into two separate parts. First, an indoor thermoelectric module performance was investigated; satisfactory results were achieved, compared and then contrasted with the simulated results. It is worth mentioning that the indoor test was conducted for 32 minutes, a relatively short period of time. A relatively significant temperature differential (ΔT) of 13.43°C was achievable.

Second, a real-world-environment solar thermoelectric generator energy harvesting system was designed, built, and simulated for energy delivery to remote residential areas in developing regions. In a like manner, all the physical parts were converted to electrical parameters via the thermal-to-electrical analogy utilizing their various geometries and properties. The circuit model of the thermal system was 75% accurate although the TEGs' internal parasitic

inductance and capacitance variations with temperatures were captured. This error rate in the model can be explained by either one or both of the following: 1) the internal parasitic components' variation and, 2) the heterogeneity of the physical blocks that were assumed to be a pure aluminum heat exchanger during the computation of the thermal parameters.

Interestingly, this work has introduced two novel analogies. To begin with, a novel RC analogy of the solar thermoelectric generator system was introduced to evaluate the emitting side temperature variations when an impulse-like electromagnetic wave is applied on the absorbing side. In contrast to the conventional RC, the rise time was estimated to be 0.7RC. Then the other novel analogy, comparable to an N-type doped semiconductor material's carrier density dependence with temperature, was proposed. In this similitude, we discovered that the converter's new output state has three different regions of operations: 1) *Initialization region,* similar to the ionization region of the N-type carrier density; 2) *Constant-but-Consistent region,* comparable to the carriers' constant region where the output of LTC3105 is equivalent to that of the K2 battery; and 3) *Normal-Operation region,* analogous to the extrinsic region.

5.2   Contributions

A summary of the six major contributions of this research is presented.

5.2.1   Thermal-to-Electrical Conversion Steps

The seven major steps for modeling any thermal system by means of its equivalent electrical analogy were first identified and proposed.

5.2.2   Design and Construction of an Indoor Thermoelectric Cooler

Through reverse polarity techniques, a TEG was demonstrated to function as a heat-removal pump and was proposed to be modeled by LTspice simulator. The device was placed in

an insulated box to avoid any heat exchange with the surroundings. Therefore, this system can be proposed to be utilized for cooling electronic chips.

5.2.3 LTC Circuits

Through an accurate computation of all the physical components that made up the two thermal systems, *viz*. the indoor thermoelectric cooler (TEC) and the real-world solar thermoelectric generation system (STEG), two separate electrical circuits were not only achievable, but also proposed as novel ways to model complex heat-transfer systems. Thus, a much simpler way of investigating transient heat propagation through various media is developed for use by thermal Engineers.

5.2.4 RC Analogy

A novel RC analogy, exclusively applicable, for the time being, to a Spice modeling of any solar thermoelectric generator was investigated and proposed. Through this analogy, we estimated the cold-side temperature variations of a TEG when an impulse-like electromagnetic wave is applied on the absorbing side of the system. The rise time (t_r) is proposed to be equivalent to the delay time (t_d) of the conventional RC analysis.

5.2.5 N-types Semiconductor Temperature Dependence Analogy

Another novel similarity, comparable to an N-type doped semiconductor material's carrier density dependence with temperature, was discovered and then proposed. Through the analysis process, we found that the converter's new output state has three different regions of operations, *viz*. 1) an *Initialization region,* similar to the ionization region of the N-type carrier density; 2) a *Constant-but-Consistent region,* identical to the carriers' constant region where the output of the converter is equal to the output of battery; and 3) a *Normal-Operation region,* analogous to the extrinsic region.

5.2.6 Reliable and Cheap Power Supply

A cheaper and reliable method for energy delivery to remote residential areas is proposed. This system can be used to power households' vital daily energy needs in developing economies in conjunction with the proper energy storage systems. It can also be utilized to power communication devices and bio-sensors, whenever needed, in a dependable manner.

5.3   Suggestions for Future Research

- Similar investigations could be done with different types of TEMs for calibration purposes. Then, the performance of the new set of TEGs with and without a DC-DC converter, and their consequent respective results, should be studied meticulously. This future study should then put a particular emphasis on a comparison of the two STEG energy harvesting systems, for both curves and LTspice equivalent circuits.

- We also propose to further investigate how this solar STEG energy harvesting system will actually perform under different electrical load conditions, i.e. *light*, *normal*, and *heavy loads*.

- Finally, we propose a thorough and systematic cost-effective investigation of the STEG system and then perform a reliability and economic comparison with PV system setup for the same purpose of energy delivery to remote residential regions in developing countries.

5.4   General Conclusion

In the first part, an experimental setup was designed and built to characterize and study the performance of a commercial TEM. One of the main objectives of this part of the work was to develop a solid foundation essential to model thermal systems by an equivalent electrical analogy via LTspice simulator. Through this pilot research, we were able to extract TEM

parameters from manufacturer datasheet and device geometries and properties. These parameters were then utilized to perform the thermal-to-electrical conversion required for the simulation to be as accurate as possible. The module, though manufactured to be operated as a TEG, was run in this setup as a TEC under the technique of the reverse polarity features. Although the indoor test lasted about half an hour, a significant amount of data was recorded. The data were arranged in a lookup table and fed into the SPICE model through the PWL option.

The second part of this work deals with the designing, building, and analysis of a standalone solar thermoelectric generation system for energy delivery to remote residential areas in developing regions. All the thermal capacitances and resistances of the various physical parts, which constitute the system, were computed based on the multipart geometries and properties of the device. An LTspice model for the entire system was then developed by means of thermal-to-electrical analogy schemes. All the internal parasitic components variations with temperatures were incorporated in the model for accuracy purposes. At this stage, the direct solar irradiance was the only input to the system mounted on a double axis solar tracker.

In the third part, three novel and unique analogies were investigated and proposed: 1) an electrical analogy of a thermal system to simulate an indoor as well a real-world solar thermoelectric generation system; 2) a novel RC analogy to estimate the cold side temperature of a TEG when an impulse of light is applied on the hot side; and 3) another analogy, similar to an N-type doped semiconductor material's carrier density dependence with temperature, was also introduced.

Overall, the chief objective for energy delivery to off-grid remote and developing regions was positively demonstrated, achieved, and understood. Simulated results for both the indoor and outdoor were in good agreement with the experimental data recorded in the laboratory and on

site respectively. Any minor offset error is likely the result of internal parasitic effects or the non-homogeneity of the physical blocks that were assumed to be pure aluminum heat sinks during the computation of the thermal parameters.

Conclusively, the real-world STEG system, in conjunction with battery energy storage, can be utilized for all kinds of remote energy applications including domestic, telecommunications, and bio-medical. Overall, the real-environment energy harvesting system is suitable for charging battery cells from 1.2 to 6 volts.

Appendix A
A1 Matlab Codes for Many Days

```
%%
clear all;
close all;
clc;

%%
%----------------Start Input Data for STEG SIM-----------------------
filename = 'STEG_SIM';
a = xlsread(filename);
x = a(:, 1);
BATTERY_OLD = a(:, 2);
BATTERY_CHARGING = a(:, 3);
CONVER_OLD = a(:, 4);
CONVER_During_CHG = a(:, 5);
WIND_SPEED = a(:, 6);
WIND_DIR = a(:, 7);
AMBIENT_TEMP = a(:, 8);
RELATIVE_HUM = a(:, 9);
TEMP_HOT = a(:, 10);
USEFUL_TEMP = a(:, 12);

Etha = (USEFUL_TEMP./TEMP_HOT)*100; % Energy Efficiency Assessment in percent
Average = mean(Etha);
%
figure(01);
subplot(2,2,1)
plot(x,BATTERY_OLD,'g','LineWidth',2)
title('K2 Battery Old State of Charge','fontsize',18)
grid on;
xlabel('Time,Min','fontsize',17);
ylabel('Voltage,mV','fontsize',17);

subplot(2,2,2)
plot(x,BATTERY_CHARGING,'g','LineWidth',2)
title('K2 Battery Charging','fontsize',18)
grid on;
xlabel('Time,Min','fontsize',17);
ylabel('Voltage,mV','fontsize',17);

subplot(2,2,3)
plot(x,CONVER_OLD,'b','LineWidth',2)
title('Old Output State of LTC3105','fontsize',18)
grid on;
xlabel('Time,Min','fontsize',17);
```

```
ylabel('Voltage,mV','fontsize',17);

subplot(2,2,4)
plot(x,CONVER_During_CHG,'b','LineWidth',2)
title('LTC3105 State during Charge','fontsize',18)
grid on;
xlabel('Time,Min','fontsize',17);
ylabel('Voltage,mV','fontsize',17);

%%
figure(02);

plot(x,BATTERY_OLD,'b','LineWidth',3); hold on;
grid on;
plot(x,BATTERY_CHARGING,'g','LineWidth',3);
title('Comparative Battery State of Charge','fontsize',17)
legend ('Battery OLD','Battery Charging');
xlabel('Time,Min','fontsize',17);
ylabel('Voltage,mV','fontsize',17);
hold off

figure(03);
plot(x,CONVER_OLD,'b','LineWidth',3); hold on;
grid on;
plot(x,CONVER_During_CHG,'g','LineWidth',3);
title('Comparative Converter Output State','fontsize',17)
legend ('Converter OLD','Converter New');
xlabel('Time,Min','fontsize',17);
ylabel('Voltage,mV','fontsize',17);
hold off

figure(04);
plot(x,WIND_SPEED,'b','LineWidth',2);
grid on;
title('Wind Speed','fontsize',24)
xlabel('Time,Min','fontsize',24);
ylabel('Speed,m/s','fontsize',24);

figure(05);
plot(x,WIND_DIR,'g','LineWidth',2);
grid on;
title('Wind Direction','fontsize',24)
xlabel('Time,Min','fontsize',24);
ylabel('Direction,degrees','fontsize',24);

figure(06);
```

```
plot(x,RELATIVE_HUM,'k','LineWidth',2);
grid on;
title('Relative Humidity','fontsize',24)
xlabel('Time,Min','fontsize',24);
ylabel('Percentage,%','fontsize',24);

figure(07);
plot(x,AMBIENT_TEMP,'g','LineWidth',2); hold on;
grid on;
plot(x,USEFUL_TEMP,'r','LineWidth',2);
title('Comparison between Ambient vs Useful TEMPs','fontsize',24)
legend ('AMBIENT','DIFFERENTIAL');
xlabel('Time,Min','fontsize',24);
ylabel('Temperature,Deg C','fontsize',24);
hold off

figure(08);
plot(x,Etha,'b','LineWidth',2);
grid on;
title('Energy Efficiency','fontsize',24)
xlabel('Time,Min','fontsize',24);
ylabel('Percentage,%','fontsize',24);

figure(09);
plot(x,RELATIVE_HUM,'g','LineWidth',2); hold on;
grid on;
plot(x,USEFUL_TEMP,'b','LineWidth',2);
title('Comparison between Relative humidity and Useful TEMP','fontsize',24)
legend ('RH','DELTA TEMP');
xlabel('Time,Min','fontsize',24);
ylabel('Temperature,Deg C','fontsize',24);
hold off

%%
subplot(2,1,1); plot(USEFUL_TEMP)
title('TEMP Differential','fontsize',24);
xlabel('Time,Min','fontsize',24);
ylabel('Temperature,Deg C','fontsize',24);

subplot(2,1,2); plot(RELATIVE_HUM)
title('Relative Humidity','fontsize',24);
xlabel('Time,Min','fontsize',24);
ylabel('Percentage,%','fontsize',24);
%%%%
figure % new figure
[hAx,hLine1,hLine2] = plotyy(x,RELATIVE_HUM,x,USEFUL_TEMP,'plot'); hold on;
```

```
grid on;
title('Comparison between Relative humidity and Useful TEMP','fontsize',24)
legend ('RH','DELTA TEMP');
xlabel('Time,Min','fontsize',24);
ylabel(hAx(1),'Percentage,%','fontsize',24); % left y-axis
ylabel(hAx(2),'Temperature,Deg C','fontsize',24); % right y-axis
hold off
```

A2 Clear Day Matlab Codes

```
%%
clear all;
close all;
clc;

%%
%----------------Start Input Data for STEG SIM on Clear Day-------------
filename = 'Clear Day';
a = xlsread(filename);
x = a(:, 1);
IRRADIANCE = a(:, 2);
HOT_TEMP = a(:, 3);
COLD_TEMP = a(:, 4);
DIFF_TEMP = a(:, 5);
AMBIENT = a(:,6);
VOLTAGE_LTC3105 = a(:, 7);
VOLTAGE_K2 = a(:, 8);
%
figure(01);
subplot(2,2,1)
plot(x,IRRADIANCE,'g','LineWidth',2)
title('Direct Normal Insolation, Clear Day','fontsize',24)
grid on;
xlabel('Time,Min','fontsize',24);
ylabel('DNI,kW/m^2','fontsize',24);

subplot(2,2,2)
plot(x,VOLTAGE_LTC3105,'g','LineWidth',2)
title('STEG Output With LTC3105','fontsize',24)
grid on;
xlabel('Time,Min','fontsize',24);
ylabel('Voltage,mV','fontsize',24);

subplot(2,2,3)
plot(x,HOT_TEMP,'b','LineWidth',2)
title('Absorbing Side TEMP','fontsize',24)
grid on;
```

```
xlabel('Time,Min','fontsize',24);
ylabel('TEMP,Deg C','fontsize',24);

subplot(2,2,4)
plot(x,COLD_TEMP,'b','LineWidth',2)
title('Emitting Side TEMP','fontsize',24)
grid on;
xlabel('Time,Min','fontsize',24);
ylabel('TEMP,Deg C','fontsize',24);

%%
figure(02);

plot(x,IRRADIANCE,'b','LineWidth',3);
grid on;
title('Local DNI on Clear Day','fontsize',24)
xlabel('Time,Min','fontsize',24);
ylabel('Insolation,kW/m^2','fontsize',24);

figure(03);
plot(x,HOT_TEMP,'b','LineWidth',3); hold on;
grid on;
plot(x,COLD_TEMP,'g','LineWidth',3);
plot(x,DIFF_TEMP,'r','LineWidth',3);
title('TEMP Variations Across the STEG System','fontsize',24)
legend ('Absorbing','Emitting','Differential');
xlabel('Time,Min','fontsize',24);
ylabel('TEMP,Deg C','fontsize',24);
hold off

figure(04);
plot(x,AMBIENT,'g','LineWidth',3); hold on;
grid on;
plot(x,DIFF_TEMP,'b','LineWidth',3);
title('Comparison Between Ambient & Useful TEMP','fontsize',24)
legend ('AMBIENT','DIFFERENTIAL');
xlabel('Time,Min','fontsize',24);
ylabel('Temperature,Deg C','fontsize',24);
hold off

figure(05);
plot(x,VOLTAGE_LTC3105,'g','LineWidth',3); hold on;
grid on;
plot(x,VOLTAGE_K2,'r','LineWidth',3);
title('Output Voltage Comparison','fontsize',24)
legend ('CONVERTER','K2 BATTERY');
```

```matlab
xlabel('Time,Min','fontsize',24);
ylabel('Voltage,mV','fontsize',24);
hold off
```

A3 Cloudy Day Matlab Codes
```matlab
%%
clear all;
close all;
clc;

%%
%----------------Start Input Data for STEG SIM on Cloudy Day-------------
filename = 'Cloudy Day';
a = xlsread(filename);
x = a(:, 1);
IRRADIANCE = a(:, 2);
VOLTAGE = a(:, 3);
HOT_TEMP = a(:, 4);
COLD_TEMP = a(:, 5);
DIFF_TEMP = a(:, 6);
AMBIENT = a(:, 7);
USEFUL_TEMP = HOT_TEMP-COLD_TEMP;
%
figure(01);
subplot(2,2,1)
plot(x,IRRADIANCE,'g','LineWidth',2)
title('Direct Normal Insolation, Cloudy','fontsize',18)
grid on;
xlabel('Time,Min','fontsize',17);
ylabel('DNI,kW/m^2','fontsize',17);

subplot(2,2,2)
plot(x,VOLTAGE,'g','LineWidth',2)
title('STEG Output before LTC3105','fontsize',18)
grid on;
xlabel('Time,Min','fontsize',17);
ylabel('Voltage,mV','fontsize',17);

subplot(2,2,3)
plot(x,HOT_TEMP,'b','LineWidth',2)
title('Absorbing Side TEMP','fontsize',18)
grid on;
xlabel('Time,Min','fontsize',17);
ylabel('TEMP,Deg C','fontsize',17);

subplot(2,2,4)
```

```matlab
plot(x,COLD_TEMP,'b','LineWidth',2)
title('Emitting Side TEMP','fontsize',18)
grid on;
xlabel('Time,Min','fontsize',17);
ylabel('TEMP,Deg C','fontsize',17);

%%
figure(02);

plot(x,IRRADIANCE,'b','LineWidth',3);
grid on;
title('Local DNI on Cloudy Day','fontsize',24)
xlabel('Time,Min','fontsize',24);
ylabel('Insolation,kW/m^2','fontsize',24);

figure(03);
plot(x,HOT_TEMP,'b','LineWidth',3); hold on;
grid on;
plot(x,COLD_TEMP,'g','LineWidth',3);
plot(x,DIFF_TEMP,':r','LineWidth',3);
title('TEMP Variations Across the STEG System','fontsize',24)
legend ('Absorbing','Emitting','Differential');
xlabel('Time,Min','fontsize',24);
ylabel('TEMP,Deg C','fontsize',24);
hold off

figure(04);
plot(x,AMBIENT,'g','LineWidth',3); hold on;
grid on;
plot(x,USEFUL_TEMP,'r','LineWidth',3);
title('Comparison Between Ambient & Useful TEMP','fontsize',24)
legend ('AMBIENT','DIFFERENTIAL');
xlabel('Time,Min','fontsize',24);
ylabel('Temperature,Deg C','fontsize',24);
hold off
figure(05);
plot(x,VOLTAGE,'g','LineWidth',2)
title('STEG Output before LTC3105','fontsize',18)
grid on;
xlabel('Time,Min','fontsize',17);
ylabel('Voltage,mV','fontsize',17);
```

Appendix B

Color-code based wiring diagram

CR1000 Wiring Diagram for Yacouba.SCW

LI200 Pyranometer — CR1000
Wire	Terminal
Red	1H
Black	1L
White	⏚ (Ground)
Clear	⏚ (Ground)

03001 Wind Speed & Direction Sensor — CR1000
Wire	Terminal
Anemometer, White	⏚ (Ground)
Anemometer, Clear	⏚ (Ground)
Vane, Clear	⏚ (Ground)
Vane, White	⏚ (Ground)
Vane, Red	4H
Vane, Black	EX1
Anemometer, Black	P1

HMP45C (6-wire, panel switched power) — CR1000
Wire	Terminal
White	⏚ (Ground)
Black	⏚ (Ground)
Clear	⏚ (Ground)
Yellow	4L
Blue	5H
Red	SW-12

Differential Voltage (1) — CR1000
Wire	Terminal
Shield	⏚ (Ground)
High	6H
Low	6L

Differential Voltage (2) — CR1000
Wire	Terminal
Shield	⏚ (Ground)
High	7H
Low	7L

Differential Voltage (3) — CR1000
Wire	Terminal
Shield	⏚ (Ground)
High	8H
Low	8L

Type K (chromel-alumel) Thermocouple (1) — CR1000
Wire	Terminal
Yellow	2H
Red	2L

Type K (chromel-alumel) Thermocouple (2) — CR1000
Wire	Terminal
Yellow	3H
Red	3L

Page 1

Appendix C

YACOUBA MOUMOUNI
ELECTRICAL AND COMPUTER ENGINEERING
UNIVERSITY OF NEVADA, LAS VEGAS
TOPIC: THERMOELECTRIC GENERATOR TESTING AND OPTIMIZATION
PROGRAMMING CODES FOR DATALOGGER

```
CR1000
'Created by Short Cut (2.5)

'Declare Variables and Units
Public Batt_Volt
Public SlrkW
Public SlrkJ
Public WS_ms
Public WindDir
Public AirTC
Public RH
Public DiffVolt
Public DiffVol_2
Public PTemp_C
Public DiffVol_3
Public Temp_C
Public Temp_C_2

Units Batt_Volt=Volts
Units SlrkW=kW/m²
Units SlrkJ=kJ/m²
Units WS_ms=meters/second
Units WindDir=Degrees
Units AirTC=Deg C
Units RH=%
Units DiffVolt=mV
Units DiffVol_2=mV
Units PTemp_C=Deg C
Units DiffVol_3=mV
Units Temp_C=Deg C
Units Temp_C_2=Deg C

'Define Data Tables
DataTable(Table1,True,-1)
```

```
        DataInterval(0,1,Min,10)
        Average(1,Batt_Volt,FP2,False)
        Average(1,SlrkW,FP2,False)
        Average(1,WS_ms,FP2,False)
        Sample(1,WindDir,FP2)
        Average(1,AirTC,FP2,False)
        Sample(1,RH,FP2)
        Average(1,DiffVolt,FP2,False)
        Average(1,DiffVol_2,FP2,False)
        Average(1,DiffVol_3,FP2,False)
        Average(1,Temp_C,FP2,False)
        Average(1,Temp_C_2,FP2,False)
EndTable

DataTable(Table2,True,-1)
        DataInterval(0,1440,Min,10)
        Minimum(1,Batt_Volt,FP2,False,False)
EndTable

'Main Program
BeginProg
        Scan(30,Sec,1,0)
                'Default Datalogger Battery Voltage measurement Batt_Volt: THIS IS
NECESSARY FOR THE OPERATION OF THE DATALOGGER.
                Battery(Batt_Volt)
                'LI200X Pyranometer measurements WITH THE UNITS OF THE INSOLATION
SET IN S.I UNIT (kW). THIS RECORDS EVERY MINUTE THE AMOUNT OF ENERGY
HITING THE RELFECTORS.
                VoltDiff(SlrkW,1,mV7_5,1,True,0,_60Hz,1,0)
                If SlrkW<0 Then SlrkW=0
                SlrkJ=SlrkW*6.0
                SlrkW=SlrkW*0.2
                '03001 Wind Speed & Direction Sensor measurements WS_ms and WindDir.
THESE TWO COMPONENTS AFFECT THE AMOUNT OF ENERGY BEING
CONVERTED:
                PulseCount(WS_ms,1,1,1,1,0.75,0.2)
                If WS_ms<0.21 Then WS_ms=0
                BrHalf(WindDir,1,mV2500,7,1,1,2500,True,0,_60Hz,355,0)
                If WindDir>=360 Then WindDir=0
```

'HMP45C (6-wire) Temperature & Relative Humidity Sensor measurements
AirTC and RH. SIMILAR TO THE ABOVE, THE HUMIDITY WILL ALSO AFFECT THE
CONVERSION:

        PortSet(9,1)
        Delay(0,150,mSec)
        VoltSE(AirTC,1,mV2500,8,0,0,_60Hz,0.1,-40.0)
        VoltSE(RH,1,mV2500,9,0,0,_60Hz,0.1,0)
        PortSet(9,0)
        If RH>100 And RH<108 Then RH=100
        'THE Differential Voltage 1 MEASURES THE VOLTAGE ACROSS THE
DIVIDER EVERY MINUTE. IT DOESN'T REPRESENT THE TOTAL VOLTAGE
GENERATED BY THE TEGS:

        VoltDiff(DiffVolt,1,mV5000,6,True,0,_60Hz,1.0,0.0)
        'THE Differential Voltage 2 MEASURESS THE VOLTAGE ACROSS THE
SHUNT RESISTOR (R=0.003 OHM) WHICH WILL HELP TO DETERMINE THE
CURRENT PRODUCED BY THE TEGS:

        VoltDiff(DiffVol_2,1,mV5000,7,True,0,_60Hz,0.330,0.0)
        'Wiring Panel Temperature measurement PTemp_C:
        PanelTemp(PTemp_C,_60Hz)
        'THE Differential Voltage 3 MEASURES THE DIFF VOLTAGE GENERATED
BY THE SOLAR FLUX SENSOR. THE ACTUAL VALUE WILL BE DTERMINE BY
UTILIZING THE MULTIPLIER:

        VoltDiff(DiffVol_3,1,mV5000,8,True,0,_60Hz,1.0,0.0)
        'Type K (chromel-alumel) Thermocouple MEASURES THE TEMPERATURES
ACROSS THE HOT SIDE OF THE TEGS IN DEGREES C:

        TCDiff(Temp_C,1,mV7_5C,2,TypeK,PTemp_C,True,0,_60Hz,1,0)
        'Type K (chromel-alumel) Thermocouple MEASURES THE TEMPERATURES
ACROSS THE COLD SIDE OF THE TEGS IN DEGREES C:

        TCDiff(Temp_C_2,1,mV7_5C,3,TypeK,PTemp_C,True,0,_60Hz,1,0)
        'Call Data Tables and Store Data
        CallTable(Table1)
        CallTable(Table2)
    NextScan
EndProg

References

[1]   R. Jones, "Energy Poverty: How to make modern energy access universal?," *Spec. early excerpt World Energy Outlook*, no. September, p. 52, 2010.

[2]   R. J. B. Y. Moumouni, A. Sajjad, "A System Dynamics Model for Energy Planning in Niger," *Int. J. Energy Power Eng.*, vol. 3, no. 6, p. 308, 2014.

[3]   W. Li, Z. Zhang, and M. Wei, "Forecast on Hebei energy consumption based on system dynamics," *Cross Strait Quad-Regional Radio …*, pp. 1541–1543, 2011.

[4]   S. L. Koh and Y. S. Lim, "Meeting energy demand in a developing economy without damaging the environment—A case study in Sabah, Malaysia, from technical, environmental and economic perspectives," *Energy Policy*, vol. 38, no. 8, pp. 4719–4728, Aug. 2010.

[5]   H. A. and S. Bandol, "Economic Analysis of," *IEEE Trans. Power …*, vol. 1, pp. 654–658, 2007.

[6]   P. M. Costa and M. a. Matos, "Economic analysis of microgrids including reliability aspects," *2006 9th Int. Conf. Probabilistic Methods Appl. to Power Syst. PMAPS*, pp. 1–8, 2006.

[7]   a. B. Sebitosi, P. Pillay, and M. a. Khan, "An analysis of off grid electrical systems in rural Sub-Saharan Africa," *Energy Convers. Manag.*, vol. 47, no. 9–10, pp. 1113–1123, 2006.

[8]   C. Bobean and V. Pavel, "The study and modeling of a thermoelectric generator module," *2013 8Th Int. Symp. Adv. Top. Electr. Eng.*, pp. 1–4, May 2013.

[9]   S. Bensaid, M. Brignone, A. Ziggiotti, and S. Specchia, "High efficiency Thermo-Electric power generator," *Int. J. Hydrogen Energy*, vol. 37, no. 2, pp. 1385–1398, Jan. 2012.

[10]   M. Hodes, "Optimal pellet geometries for thermoelectric power generation," *IEEE Trans. Components Packag. Technol.*, vol. 33, no. 2, pp. 307–318, 2010.

[11]   M. G. Molina, L. E. Juanicó, and G. F. Rinalde, "Design of innovative power conditioning system for the grid integration of thermoelectric generators," *Int. J. Hydrogen Energy*, vol. 37, no. 13, pp. 10057–10063, Jul. 2012.

[12]   A. Gontean and M. O. Cernaianu, "High-accuracy thermoelectrical module model for energy-harvesting systems," *IET Circuits, Devices Syst.*, vol. 7, no. 3, pp. 114–123, May 2013.

[13]   M. Chen, L. A. Rosendahl, I. Bach, T. Condra, and J. K. Pedersen, "Transient Behavior Study of Thermoelectric Generator through SPICE Electro-thermal model," *… , 2006. ICT'06. 25th …*, 2006.

[14]   S. Lineykin and S. Ben-Yaakov, "Modeling and Analysis of Thermoelectric Modules," *IEEE Trans. Ind. Appl.*, vol. 43, no. 2, pp. 505–512, 2007.

[15]   US department of the Interior Bureau of Reclamation Power Resources office, "Reclamation: managing water for the west," *Hydroelectr. Power*, 2005.

[16]   J. Tsao, N. Lewis, and G. Crabtree, "Solar FAQs," *US Dep. Energy*, pp. 1–24, 2006.

[17]   G. W. Crabtree and N. S. Lewis, "Solar energy conversion," *Phys. Today*, vol. 60, no. 3, pp. 37–42, 2007.

[18]   P. C. Loh, L. Zhang, S. He, and F. Gao, "Compact integrated solar energy generation systems," *2010 IEEE Energy Convers. Congr. Expo.*, pp. 350–356, 2010.

[19]   Y. Moumouni, Y. Baghzouz, and R. F. Boehm, "Power 'smoothing' of a commercial-size photovoltaic system by an energy storage system," in *Proceedings of International Conference on Harmonics and Quality of Power, ICHQP*, 2014.

[20] R. Y. Nuwayhid, A. Shihadeh, and N. Ghaddar, "Development and testing of a domestic woodstove thermoelectric generator with natural convection cooling," *Energy Convers. Manag.*, vol. 46, no. 9–10, pp. 1631–1643, Jun. 2005.

[21] V. Leonov, T. Torfs, P. Fiorini, and C. Van Hoof, "Thermoelectric Converters of Human Warmth for Self-Powered Wireless Sensor Nodes," *IEEE Sens. J.*, vol. 7, no. 5, pp. 650–657, May 2007.

[22] J. Lofy and L. E. Bell, "Thermoelectrics for environmental control in automobiles," *Twenty-First Int. Conf. Thermoelectr. 2002. Proc. ICT '02.*, pp. 471–476, 2002.

[23] L. Chen, D. Cao, Y. Huang, and F. Z. Peng, "Modeling and power conditioning for thermoelectric generation," *PESC Rec. - IEEE Annu. Power Electron. Spec. Conf.*, pp. 1098–1103, Jun. 2008.

[24] J. P. Ploteau, P. Glouannec, and H. Noel, "Conception of thermoelectric flux meters for infrared radiation measurements in industrial furnaces," *Appl. Therm. Eng.*, vol. 27, no. 2–3, pp. 674–681, 2007.

[25] K. Matsubara, "Development of a high efficient thermoelectric stack for a waste exhaust heat recovery of vehicles," *Twenty-First Int. Conf. Thermoelectr. 2002. Proc. ICT '02.*, pp. 418–423, 2002.

[26] J. a. Paradiso and T. Starner, "Energy scavenging for mobile and wireless electronics," *IEEE Pervasive Comput.*, vol. 4, no. 1, pp. 18–27, 2005.

[27] S. . Riffat and X. Ma, "Thermoelectrics: a review of present and potential applications," *Appl. Therm. Eng.*, vol. 23, no. 8, pp. 913–935, Jun. 2003.

[28] D. M. Rowe, "Thermoelectrics, An Environmentally-Friendly Electrical Power," *Renew. Energy*, vol. 16, pp. 1251–1256, 1999.

[29] D. M. Rowe, "Thermoelectric harvesting of low temperature natural/waste heat," *AIP Conf. Proc.*, vol. 485, pp. 485–492, 2012.

[30] X. F. Zheng, C. X. Liu, Y. Y. Yan, and Q. Wang, "A review of thermoelectrics research – Recent developments and potentials for sustainable and renewable energy applications," *Renew. Sustain. Energy Rev.*, vol. 32, pp. 486–503, Apr. 2014.

[31] G. F. Rinalde, L. E. Juanicó, E. Taglialavore, S. Gortari, and M. G. Molina, "Development of thermoelectric generators for electrification of isolated rural homes," *Int. J. Hydrogen Energy*, vol. 35, no. 11, pp. 5818–5822, Jun. 2010.

[32] M. Eswaramoorthy and S. Shanmugam, "Techno-economic Analysis of a Solar Thermoelectric Power Generator for a Rural Residential House," vol. 4, no. 10, pp. 1911–1919, 2009.

[33] D. Champier, J. P. Bedecarrats, M. Rivaletto, and F. Strub, "Thermoelectric power generation from biomass cook stoves," *Energy*, vol. 35, no. 2, pp. 935–942, Feb. 2010.

[34] D. Champier, J. P. Bédécarrats, T. Kousksou, M. Rivaletto, F. Strub, and P. Pignolet, "Study of a TE (thermoelectric) generator incorporated in a multifunction wood stove," *Energy*, vol. 36, no. 3, pp. 1518–1526, Mar. 2011.

[35] A. Gontean and M. O. Cernaianu, "Parasitic elements modelling in thermoelectric modules," *IET Circuits, Devices Syst.*, vol. 7, no. 4, pp. 177–184, Jul. 2013.

[36] C. M. University, "The Sun & its Energy," *http://environ.andrew.cmu.edu/m3/s2/02sun.shtml*, 2003. [Online]. Available: http://environ.andrew.cmu.edu/m3/s2/02sun.shtml. [Accessed: 20-Jan-2015].

[37] D. Lashof and S. Yeh, "Cleaner and Cheaper: Using the Clean Air Act to Sharply Reduce Carbon Pollution from Existing Power Plants, Delivering Health, Environmental, and

Economic Benefits," *http://www.nrdc.org/air/pollution-standards/*, 2014. [Online]. Available: http://www.nrdc.org/air/pollution-standards/. [Accessed: 20-Jan-2015].

[38] A. Date, A. Date, C. Dixon, and A. Akbarzadeh, "Progress of thermoelectric power generation systems: Prospect for small to medium scale power generation," *Renew. Sustain. Energy Rev.*, vol. 33, pp. 371–381, May 2014.

[39] K.-H. Wu and C.-I. Hung, "Effect of substrate on the spatial resolution of Seebeck coefficient measured on thermoelectric films," *Int. J. Therm. Sci.*, vol. 49, no. 12, pp. 2299–2308, Dec. 2010.

[40] R. McCarty, "Thermoelectric Power Generator Design for Maximum Power: It's All About ZT," *J. Electron. Mater.*, vol. 42, no. 7, pp. 1504–1508, Oct. 2012.

[41] M. Zebarjadi and G. Chen, "Recent advances in thermoelectrics," *2011 Int. Electron Devices Meet.*, no. 2, pp. 10.1.1–10.1.4, Dec. 2011.

[42] M. Telkes, "Solar Thermoelectric Generators," *J. Appl. Phys.*, vol. 25, no. 6, p. 765, 1954.

[43] K. P. Suleebka, "High temperature solar thermoelectric generator," *Appl. Energy*, vol. 5, no. 1, pp. 53–59, Jan. 1979.

[44] D. M. Rowe, "A high performance thermoelectric solar powered generator," *Appl. Energy*, vol. 8, pp. 269–273, 1981.

[45] D. Rowe and G. Min, "Evaluation of thermoelectric modules for power generation," *J. Power Sources*, no. November 1997, 1998.

[46] S. Maneewan, J. Khedari, B. Zeghmati, and J. Hirunlabh, "Investigation on generated power of thermoelectric roof solar collector," vol. 29, pp. 743–752, 2004.

[47] N. Vatcharasathien, J. Hirunlabh, J. Khedari, and M. Daguenet, "Design and analysis of solar thermoelectric power generation system," *Int. J. Sustain. Energy*, vol. 24, no. 3, pp. 115–127, Sep. 2005.

[48] B. Poudel, Q. Hao, Y. Ma, Y. Lan, A. Minnich, B. Yu, X. Yan, D. Wang, A. Muto, D. Vashaee, X. Chen, J. Liu, M. S. Dresselhaus, G. Chen, and Z. Ren, "High-thermoelectric performance of nanostructured bismuth antimony telluride bulk alloys.," *Science*, vol. 320, no. May, pp. 634–638, 2008.

[49] L. Juanicó and G. Rinalde, "Comparative analysis of photovoltaic and thermoelectric panels for powering isolated homes," *J. Renew. Sustain. ...*, 2009.

[50] R. Amatya and R. J. Ram, "Solar Thermoelectric Generator for Micropower Applications," *J. Electron. Mater.*, vol. 39, no. 9, pp. 1735–1740, Apr. 2010.

[51] Q. Zhang, A. Agbossou, Z. Feng, and M. Cosnier, "Solar micro-energy harvesting based on thermoelectric and latent heat effects. Part II: Experimental analysis," *Sensors Actuators A Phys.*, vol. 163, no. 1, pp. 284–290, Sep. 2010.

[52] D. Kraemer, B. Poudel, H.-P. Feng, J. C. Caylor, B. Yu, X. Yan, Y. Ma, X. Wang, D. Wang, A. Muto, K. McEnaney, M. Chiesa, Z. Ren, and G. Chen, "High-performance flat-panel solar thermoelectric generators with high thermal concentration.," *Nat. Mater.*, vol. 10, no. 7, pp. 532–8, Jul. 2011.

[53] F. Meng, L. Chen, and F. Sun, "A numerical model and comparative investigation of a thermoelectric generator with multi-irreversibilities," *Energy*, vol. 36, no. 5, pp. 3513–3522, May 2011.

[54] C. Alaoui, "Peltier thermoelectric modules modeling and evaluation," *Int. J. Eng.*, no. 5, pp. 114–121, 2011.

[55] J. Chavez and J. Ortega, "SPICE model of thermoelectric elements including thermal effects," *... , 2000. IMTC 2000. ...*, 2000.

[56]   S. Lineykin and S. Ben-Yaakov, "SPICE compatible equivalent circuit of the energy conversion processes in thermoelectric modules," *2004 23rd IEEE Conv. Electr. Electron. Eng. Isr.*, pp. 346–349, 2004.

[57]   S. Lineykin and S. Ben-yaakov, "Modeling and Analysis of Thermoelectric Modules," *IEEE Trans. Ind. Electron.*, pp. 2019–2023, 2005.

[58]   M. Cernaianu and A. Cernaianu, "Thermo electrical generator improved model," *Int. Conf. Power ...*, vol. 13, pp. 343–348, 2012.

[59]   Mihail Cernaianu, "Dissertation TEG modeling in LTspice," 2012.

[60]   A. Mirocha and P. Dziurdzia, "Improved Electrothermal Model of the Thermoe- lectric Generator Implemented in SPICE," pp. 317–320, 2008.

[61]   M. Cernaianu, "Thermoelectrical energy harvesting system: Modelling, simulation and implementation," *... (ISETC), 2012 10th ...*, pp. 2–5, 2012.

[62]   F. S. Inc., "Thermal Analysis of Semiconductor Systems," *White Pap.*, 2008.

[63]   Y. and Moumouni and R. J. Baker, "Improved SPICE Modeling and Analysis of a Thermoelectric Module," *IEEE 58th Int. Midwest Symp.*, no. 1, pp. 1–4, 2015.

[64]   J. L. M. Hensen and A. E. Nakhi, "Fourier and Biot numbers and the accuracy of conduction modelling," 1992.

[65]   A. Laprade, S. Pearson, and S. Benczkowski, "Application Note 7532 A New PSPICE Electro-Thermal Subcircuit For Power MOSFETs," *Fairchild Semicond. Appl. Note 7534*, no. July, pp. 1–16, 2004.

[66]   "http://www.customthermoelectric.com/MaterialProperties.htm," 2014. [Online]. Available: http://www.customthermoelectric.com/MaterialProperties.htm. [Accessed: 29-Jul-2014].

[67]   N. Gorbachuk and V. Sidorko, "Heat capacity and enthalpy of Bi2Si3 and Bi2Te3 in the temperature range 58-1012 K," *Powder Metall. Met. Ceram.*, vol. 43, no. 437, pp. 284–290, 2004.

[68]   "Bismuth telluride Bismuth telluride," 2014. [Online]. Available: http://www.chemspider.com/Chemical-Structure.11278988.html. [Accessed: 29-Jul-2014].

[69]   M. Li, "Thermoelectric-generator-Based DC DC Conversion Network for Automotive Applications," 2011.

[70]   Y. Moumouni and R. F. Boehm, "Utilization of Energy Storage to Buffer PV Output during Cloud Transients," *Appl. Mech. Mater.*, vol. 705, pp. 295–304, 2014.

[71]   I. Buchmann, "What ' s the best battery ?," *http://batteryuniversity.com/*, 2009. [Online]. Available: http://batteryuniversity.com/learn/article/whats_the_best_battery. [Accessed: 04-Sep-2015].

[72]   N. Singamsetti and S. Tosunoglu, "A Review of Rechargeable Battery Technologies," p. 6, 2012.

[73]   I. Hadjipaschalis, A. Poullikkas, and V. Efthimiou, "Overview of current and future energy storage technologies for electric power applications," *Renew. Sustain. Energy Rev.*, vol. 13, no. 6–7, pp. 1513–1522, 2009.

[74]   H. Chen, T. N. Cong, W. Yang, C. Tan, Y. Li, and Y. Ding, "Progress in electrical energy storage system: A critical review," *Prog. Nat. Sci.*, vol. 19, no. 3, pp. 291–312, 2009.

[75]   A. Stan, M. Swierczynski, D. Stroe, R. Teodorescu, S. J. Andreasen, and K. Moth, "A Comparative Study of Lithium Ion to Lead Acid Batteries for use in UPS Applications," 2014.

[76] G. Zanei, E. Cevenini, H. Ruff, and O. Ulibas, "Integrated systems for UPS New solutions in the power quality chain.pdf," pp. 582–586, 2007.

[77] A.-I. Stan, M. Swierczynski, D.-I. Stroe, R. Teodorescu, and S. J. Andreasen, "Lithium ion battery chemistries from renewable energy storage to automotive and back-up power applications — An overview," pp. 713–720, 2014.

[78] M. Ceylan, T. Sarikurt, and A. Balikci, "A Novel Lithium-Ion-Polymer Battery Model for Hybrid / Electric Vehicles," *IEEE Int. Symp. Ind. Electron. ISIE*, pp. 366–369, 2014.

[79] L. W. Hruska, "Smart batteries and lithium ion voltage profiles," *Twelfth Annu. Batter. Conf. Appl. Adv.*, pp. 205–210, 1997.

[80] D. Stolitzka and W. S. Dawson, "When is it intelligent to use a smart battery?," *Proc. 9th Annu. Batter. Conf. Appl. Adv.*, pp. 173–178, 1994.

[81] Y. Moumouni and R J. Baker, "Buffer Sizing of Concentrated Photovoltaic Batteries : An Economic Analysis," in *IEEE 58th International Midwest Symposi*, 2015, pp. 704–707.

[82] P. Meier, V. Tuntivate, D. Barnes, S. Bogach, and D. Farchy, "Peru: National survey of rural household energy use," *Spec. Rep.*, no. August, 2010.

[83] E. Cready, J. Lippert, J. Pihl, I. Weinstock, P. Symons, and R. G. Jungst, "Final Report Technical and Economic Feasibility of Applying Used EV Batteries in Stationary Applications A Study for the DOE Energy Storage Systems Program," *Sandia Natl. Lab.*, no. March, 2003.

[84] S. E. Nicholson, "Sahel, West Africa," *Encyclopedia of Environmental Biology*. pp. 261–275, 1995.

[85] C. Brown, "How to Size a Deep Cycle Battery Bank," *http://www.btekenergy.com/documents/215.html*, 2015. [Online]. Available: www.btekenergy.com/documents/215.html.

[86] J. VENTRE, *Photovoltaic systems engineering*, Second. Boca Raton London New York Washington, D.C: CRC Press, 2004.

[87] Ieee, *IEEE Recommended Practice for Maintenance , Testing , and Replacement of Valve-Regulated Lead- Acid (VRLA) Batteries for*, vol. 2005, no. February. 2006.

[88] B. Nykvist and M. Nilsson, "Rapidly falling costs of battery packs for electric vehicles," *Nat. Clim. Chang.*, vol. 5, no. April, pp. 100–103, 2015.

[89] G. Albright, J. Edie, and S. Al-Hallaj, "A Comparison of Lead Acid to Lithium-ion in Stationary Storage Applications," *AllCell Technol. LLC*, no. March, 2012.

[90] C. C. & M. Clark, "The Difference Between Lead Acid and Lithium EV Batteries," 2000. [Online]. Available: http://www.electriccarinternational.com/media/The-Difference-Between-Lead-Acid-and-Lithium-EV-Batteries.pdf. [Accessed: 10-Sep-2015].

[91] Y. Moumouni and R J. Baker, "Concise Thermal to Electrical Parameters Extraction of Thermoelectric Generator for Spice Modeling," in *IEEE 58th International Midwest Symposi*, 2015.

[92] G. Alonso, "What ' s New with LTspice IV ?," 2011. [Online]. Available: http://www.linear.com/. [Accessed: 31-Jul-2014].

[93] D. Mastbergen and B. Willson, "Generating Light from Stoves Using a Thermoelectric Generator," *ETHOS Int. Stove Res. Conf.*, 2005.

[94] P. Dziurdzia, "Modeling and simulation of thermoelectric energy harvesting processes," *... Energy Harvest. Technol. Present ...*, 2011.

[95]   C. Q. Choi, "NASA Discovers New Radiation Belt Around Earth," 2012. [Online]. Available: http://www.space.com/20004-earth-radiation-belt-discovery.html. [Accessed: 04-Jun-2015].

[96]   P. R. Epstein and C. Rogers, "Inside the Greenhouse the Impacts of Co2 and Climate Change on Public Health in the Inner City," 2004.

[97]   Robert T. Watson, "Climate change 2001: synthesis report," 2001.

[98]   U. Nations, "Promotion of new and renewable sources of energy," Johannesburg, SA, 2011.

[99]   D. Wolpert and P. Ampadu, "Managing Temperature Effects in Nanoscale Adaptive Systems," *... Temp. Eff. Nanoscale Adapt. ...*, no. 0, pp. 15–34, 2012.

[100]   S. Lee, "How to select a heat sink," *Adv. Therm. Eng. Aavid Therm. Technol. Inc.*

[101]   O. Loebel, "Thermal insulation materials made of rigid polyurethane foam," *http://www.excellence-in-insulation.eu/*, vol. 1, no. October 06, pp. 1–33, 2012.

[102]   Engineering Tool Box, "Air properties." [Online]. Available: http://www.engineeringtoolbox.com/air-properties-d_156.html. [Accessed: 01-Jun-2015].

[103]   D. Salerno, "Ultralow Voltage Energy Harvester Uses Thermoelectric Generator for Battery-Free Wireless Sensors In this issue ...," *Linear Technol. Analog Innov.*, vol. 20, no. 3, pp. 2–11, 2010.

Curriculum Vitae

Graduate College
University of Nevada, Las Vegas
Electrical and Computer Engineering

Yacouba Moumouni
Degrees:
Bachelor of Engineering, Electrical Engineering, 2002
Federal University of Technology, Minna, Nigeria
Senior Design Project Title: Design and Construction of an Automatic Door Control

Masters of Science, Mechanical Engineering, 2012
University of Nevada, Las Vegas
Thesis Title: Buffering PV Output during Cloud Transients with Energy Storage

Doctor of Philosophy (Ph.D.), Electrical Engineering, 2015
University of Nevada, Las Vegas
Dissertation Title: Designing, Building and Testing a Solar Thermoelectric Generation, STEG, for Energy Delivery to Remote Residential Areas in Developing Regions
Selected Publications:

- LTspice Model of a Solar Thermoelectric Generation System, submitted at the *IEEE 8th Clemson University Power System Conference 2016.*
- Analysis of a Residential 5kW Grid-tied Photovoltaic System, submitted at the *IEEE 8th Clemson University Power System Conference 2016.*
- Concise Thermal to Electrical Paramters Extraction of Thermoeleectric Generator for Spice Modeling, *IEEE 58th MWSCAS, Fort Collins Colorado 2015.*
- Improved SPICE Modeling and Analysis of a Thermoelectric Module, *IEEE 58th MWSCAS, Fort Collins Colorado 2015.*
- Application of Used Electric Vehicle Batteries to Buffer PV Output Transients, *IEEE 58th MWSCAS, Fort Collins Colorado 2015.*
- CPV Battery Buffer Sizing and Economic Analysis, *IEEE 58th MWSCAS, Fort Collins Colorado 2015.*
- Evaluation of the impact of Partial Shading on the Performance of a Grid-Tied PV system, *IEEE 5th International Conference on Clean Electrical Power, Italy 2015.*
- Utilization of Energy Storage to Buffer PV Output during Cloud Transients; *International Conference on Renewable Energy Technologies, ICRET, Hong Kong 2014.*
- Power "Smoothing" of a Commercial-Size Photovoltaic System by an Energy Storage System, *IEEE Power & Energy Society, ICHQP, Romania 2014.*

Dissertation Examination Committee:
Chairperson and Academic Advisor, R. Jacob Baker, Ph.D.
Committee Member, Yahia Baghzouz, Ph. D.
Committee Member, Rama Venkat, Ph. D.
Graduate Faculty Representative, Robert F. Boehm, Ph. D.